REPORT DOCUMENTATION PAGE

Form Approved
OMB No. 0704-0188

1. REPORT DATE *(DD-MM-YYYY)*	**2. REPORT TYPE**	**3. DATES COVERED** *(From - To)*
05-07-2009		

4. TITLE AND SUBTITLE

Monitoring Cosmic Radiation Risk: Comparisons Between Observations and Predictive Codes for Naval Aviation

5a. CONTRACT NUMBER

5b. GRANT NUMBER

5c. PROGRAM ELEMENT NUMBER

6. AUTHOR(S)

Dobisesky, Jacob P. (Jacob Paul) , 1987-

5d. PROJECT NUMBER

5e. TASK NUMBER

5f. WORK UNIT NUMBER

7. PERFORMING ORGANIZATION NAME(S) AND ADDRESS(ES)

8. PERFORMING ORGANIZATION REPORT NUMBER

9. SPONSORING / MONITORING AGENCY NAME(S) AND ADDRESS(ES)

U.S. Naval Academy
Annapolis, MD 21402

10. SPONSOR/MONITOR'S ACRONYM(S)

11. SPONSOR/MONITOR'S REPORT NUMBER(S)

Trident Scholar Project Report no. 377 (2009)

12. DISTRIBUTION / AVAILABILITY STATEMENT

This document has been approved for public release; its distribution is UNLIMITED

13. SUPPLEMENTARY NOTES

14. ABSTRACT

Utilizing a unique, Far West Technology Tissue Equivalent Proportional Counter (TEPC)-based system called the HAWK, the atmospheric radiation exposures of commercial air travelers and naval personnel were compared to the quantity predicted by commercially available radiation codes. The HAWK simulates a two micron-diameter somatic cell, measuring the lineal energy, absorbed dose, and dose equivalent based on the International Commission on Radiological Protection (ICRP)-60 recommendations. Prior to the flights, the HAWK detector response was modeled with MCNP5 and GEANT4. Later, the data were analyzed both to produce a dose rate as well as a total dose for the flight's duration.

15. SUBJECT TERMS

TEPC, HAWK detector, tissue equivalent proportional counter, radiation codes, cosmic radiation risk

16. SECURITY CLASSIFICATION OF:			**17. LIMITATION OF ABSTRACT**	**18. NUMBER OF PAGES**	**19a. NAME OF RESPONSIBLE PERSON**
a. REPORT	**b. ABSTRACT**	**c. THIS PAGE**		88	**19b. TELEPHONE NUMBER** *(include area code)*

U.S.N.A. --- Trident Scholar project report; no. 377 (2009)

Monitoring Cosmic Radiation Risk:
Comparisons between Observations and Predictive Codes for Naval Aviation

by

Midshipman 1/c Jacob P. Dobisesky
United States Naval Academy
Annapolis, Maryland

_____
(signature)

Certification of Adviser(s) Approval

Professor Martin N. Nelson
Mechanical Engineering Department

_____
(signature)

_____
(date)

Vincent L. Pisacane
Aerospace Engineering Department

_____
(signature)

_____
(date)

CAPT John W. Nicholson, USN
Weapons and Systems Engineering Department

_____
(signature)

_____
(date)

Acceptance for the Trident Scholar Committee

Professor Carl E. Wick
Associate Director of Midshipman Research

_____
(signature)

_____
(date)

USNA-1531-2

Abstract

Monitoring Cosmic Radiation Risk: Comparisons between Observations and Predictive Codes for Naval Aviation

Jacob Dobisesky, Midshipman
M. Nelson, Professor Mechanical Engineering
CAPT J. Nicholson, Professor Weapons and Systems Engineering
V.L. Pisacane, Professor Aerospace Engineering
United States Naval Academy
Annapolis, Maryland

Utilizing a unique, Far West Technology Tissue Equivalent Proportional Counter (TEPC)-based system called the HAWK, the atmospheric radiation exposures of commercial air travelers and naval personnel were compared to the quantity predicted by commercially available radiation codes. The HAWK simulates a two micron-diameter somatic cell, measuring the lineal energy, absorbed dose, and dose equivalent based on the International Commission on Radiological Protection (ICRP)-60 recommendations. Prior to the flights, the HAWK detector response was modeled with MCNP5 and GEANT4. Later, the data were analyzed both to produce a dose rate as well as a total dose for the flight's duration.

Over 40 hours of flight data was obtained on commercial aircraft in addition to several experiments on military and private aircraft. Flights were conducted across the continental United States, from Massachusetts to California. The military flights were conducted on an EA-6B Prowler from the Navy's VX-23 Squadron in Patuxent River, Maryland. Commercial aircraft altitudes reached a ceiling of approximately 38,000 feet while typical military operations were around 25,000 feet. During the flight, data including dose and dose equivalent rates were collected along with corresponding GPS data such as geodetic latitude, longitude, and altitude. The GPS data were then utilized as inputs for several commercially available radiation codes for assessing atmospheric radiation risk. These codes included CARI-6, developed by the US Federal Aviation Administration (FAA), EPCARD developed by Germany's GSF – National Research Center for Environment and Health, and EXPACS, developed by Japan's Atomic Energy Agency. Analysis of the code outputs yielded several conclusions. First, EXPACS predicts radiation doses very close to CARI-6 and could be developed into a more user-friendly and adaptable code for the Navy given its EXCEL-based platform and multiple input variables. Second, radiation dose predictions on the EA-6B Prowler and commercial aircraft at altitudes below 15,000 feet begin to break down and the codes no longer accurately predict radiation. In addition, pilots, aircrew, and frequent fliers may exceed the one milli-Sievert per year limit for the general public depending on their destinations and duration at high altitudes. Finally, these commercial codes provide a conservative, accurate method to predict and estimate the radiation risk of naval pilots and aircrew.

Acknowledgements

Traveling to over 14 states and collecting more than 40 hours of radiation measurements on commercial, private, and military flights required the motivation and support of a great team of advisors – Dr. Nelson, Dr. Pisacane, CAPT Nicholson, and Mr. Delikat, the Nucleonics Lab Technician. Their humor and common sense approach kept me on track throughout the year and my eye "on the prize."

In addition, several outside researchers contributed greatly to my understanding of radiation health, nuclear physics, and the TEPC: Dr. Esch and Dr. Tovesson at Los Alamos National Laboratory, CDR Benevides for making the LANL Internship possible, Dr. Conroy, the creator of the TEPC, Dr. Lewis and Dr. Bennett, at the Royal Military College, CDR Millett, USNA Professor, and the code developers, Dr. Mares (EPCARD), Dr. Friedberg (CARI-6), and Dr. Tatsuhiko (EXPACS). A special thanks also goes to Admiral Stiedle of the Aerospace department at the Naval Academy for arranging my military flights with the VX-23 Squadron at Patuxent River Naval Air Station and Midshipman 1/C James Haley for piloting my low altitude flights. And finally, I would like to thank everyone at VX-23 for allowing me to visit often and understanding when I would attempt to throw the detector in the back of the plane when no one was looking.

TABLE OF CONTENTS

List of Symbols and Abbreviations

$\frac{dE}{dx}$	Stopping Power
$\bar{l}$	mean chord length
ALARA	As Low As Reasonably Achievable
BEIR	Biological Effects of Ionizing Radiation
CARI	CARI
cm	centimeter
csv	comma-separated value
$D_{T,R}$	absorbed dose D (in grays) to tissue T from radiation R
D	absorbed dose
d	day
DNA	Deoxyribonucleic Acid
E	Effective Dose
e	electron
e+ or β+	positron
EPCARD	European Program for the Calculation of Aviation Route Dose
ER	Electromagnetic Radiation
EURADOS	European Radiation Dosimetry Group
EXPACS	Excel-Based Program for calculating Atmospheric Cosmic Ray Spectrum
FAA	Federal Aviation Administration
g	gas
GCR	Galactic Cosmic Rays
GEANT	GEometry ANd Tracking
GeV	10^9 electron-volts

gm	gram
Gy	gray
h	hour
H*(10)	Ambient Dose Equivalent, defined as a dose at a depth of 10 mm in the ICRU sphere
HAWK	Far West Technology Tissue Equivalent Proportional Counter
H_T	tissue equivalent dose given by HAWK, W_R x $D_{T,R}$
ICRP	International Commission on Radiological Protection
ICRU	International Commission on Radiation Units
ICRU Sphere	A 30 cm diameter sphere of unit density tissue and composition as specified by ICRU (H, 10.1%; C, 11.1%; N, 2.6%; O, 76.2%; where %-compositions are given by weight)
IGRF	International Geomagnetic Reference Field
kg	kilogram
LET	Linear Energy Transfer or Lineal Energy Transfer
m	mass
m	minutes
MCA	Multi-Channel Analyzer
MCNP	Monte Carlo N-Particle Transport Code
MeV	10^6 electron-volts
mrem	milli-rem
MULASSIS	Multi-layered Shielding Simulation Software
n	neutron
NCRP	National Commission on Radiological Protection (United States)
NIST	National Institute of Standards and Technology
O	Oxy Radical

OH	Hydroxide Radical
p	proton
PARMA	PHITS-based Analytical Radiation Model in the Atmosphere
PCAIRE	Predictive Code for Aircrew Radiation Exposure
PHITS	Particle and Heavy Ion Transport code System
Q	Quality Factor
R	Roentgen
Rad	radiation absorbed
Rem	roentgen equivalent in man
s	second
S	surface area
SPE	Solar Particle Event
SPENVIS	Space Environment Information System
SRIM	Stopping Range of Ions in Matter
Sv	sievert
t	tissue
V	volt
W_R	radiation weighting factor
y	lineal energy
z	specific energy
α	alpha particle
β	beta particle
γ	gamma/photon/x-ray
μ	muon
μCi	micro-Curie

μm	micrometer
ν	neutrino
π	pion
ρ	density

List of Figures

List of Tables

Chapter I: Introduction

In 2006, the Biological Effects of Ionizing Radiation (BEIR) VII report, sponsored primarily by the Department of Defense and U.S. Nuclear Regulatory Commission, stated an increase in the likelihood of cancer development from low levels of *ionizing* radiation, defined as 0 to approximately 100 millisievert (mSv) [1]. More specifically, the report refers to the low-dose, low - "linear energy transfer" (LET) that may be energetic enough to break biomolecular bonds and lead to DNA changes, initiating cancer development. It stated that approximately one individual in 1000 would develop cancer from an exposure to 10 mSv.

Currently, the United States Navy has two major documents concerning radiation exposure limits and procedures. These are the NAVMED P-5055, Radiation Health Protection Manual [2] and NAVSEA SO420-AA-RAD-010, or simply referred to as the RAD-010 [3]. In the NAVMED P-5055, the limit set for the general public is not more than 0.02 mSv (2 mrem) per hour or 1 mSv (100 mrem) per year. Classified by the Navy as non-radiation workers, naval aviators are limited to 5 mSv per year if the radiation experienced in the atmosphere is considered "radioactive material" [2]. If not, as in most cases, naval aviators fall under the general public limit of 1 mSv per year. In the RAD-010, the philosophy of As Low As Reasonably Achievable (ALARA) is addressed in addition to stating that "this requirement is intended not to preclude personnel exceeding 0.5 rem per year, but to provide an administrative review point of individual and command work practices and personnel exposure trends before authorization for individuals to exceed the control level is granted" [3]. As a result, naval officers are not monitored for operating aircraft at various altitudes in the atmosphere, an environment conducive for additional radiation exposure.

Radiation sources at flight altitudes consist of galactic cosmic rays and solar particle events. Galactic Cosmic Rays (GCRs) travel within our galaxy and incessantly bombard our solar system. Like the ocean's tide against a beach, GCRs gently envelope the heliosphere, moving through periods of high and low intensity in a fairly predictable fashion. Solar Particle Events (SPEs) are spontaneous emissions of high energy radiation from the Sun leading to additional radiation exposure at the higher altitudes in the atmosphere or at the higher latitudes, near the poles. Several factors like the solar cycle, atmospheric depth, and magnetosphere help protect life on earth, but not all the radiation can be blocked. With the increase in duration, frequency, and altitude of airplane travel around the world, exposure to GCRs and Solar Particle Events (SPEs) has also begun to rise. Specifically, pilots, aircrew, and frequent-fliers have been society's most susceptible members to this fairly well-documented radiation.

In the United States, the Federal Aviation Administration issued an Advisory Circular in 1990 acknowledging the presence of a cosmic and terrestrial radiation capable of producing dose rates on the average of 6 μSv/hr (0.6 mrem/hr), but so far, has instituted no regulations for in-flight exposure [4]. Currently, the Nuclear Regulatory Commission NUREG/BR-0322 limits the general public to less than 1 mSv/yr (0.1 rem/yr) [5]. This is similar to the International Commission on Radiological Protection (ICRP) that recognizes the occupational exposure of aircrew to cosmic radiation. In fact, a recommendation was made to lower the occupational exposure from 50 to 20 mSv/yr (5 to 2 rem/yr) averaged over 5 years, as well as a reduction in the general population exposure from 5 to 1 mSv/yr (0.5 to 0.1 rem/yr) which was also accepted as the limit for the general public [6]. European countries have already begun to enforce laws requiring the monitoring of aircrew and pilots while the United States Navy and commercial airlines have no such policy.

Several years of research have already been conducted around the world on the topic of atmospheric radiation exposure. At the Royal Military College in Canada, Dr. Lewis and Dr. Bennett analyzed over 160 flights to compile data utilized to create a Predictive Code for Aircrew Radiation Exposure, also known as PCAIRE [7]. In Germany, another researcher led to the development of EPCARD, a program used to calculate the radiation dose obtained along any aviation flight altitude between 5000 meters, or 16,000 feet, and 25,000 meters, or 82,000 feet. An Excel-based Program for calculating Atmospheric Cosmic-ray Spectrum, abbreviated as EXPACS was developed in Japan [8]. Within the United States, the Federal Aviation Administration developed the CARI code, providing predictions for radiation dose exposure to aircraft [9]. This research investigated these codes by comparing their dose equivalent rates per minute to the measured values recorded on private, military, and primarily commercial flights. By quantifying several unique mixed radiation fields at various altitudes where naval aviators and aircrew typically work, the risk for harmful biological effects associated with radiation environments inside the aircraft was assessed.

CHAPTER II: Radiobiology

A. Radiation Units

Current regulatory policies established for occupations dealing with radioactive materials utilize units unique to the nuclear science and engineering field. This chapter will address the commonly used radiation units and conversion factors. Throughout this project, radiation will be reported and described in terms of exposed dose, absorbed dose, and dose equivalent. A summary of the radiobiology units is given in Table II.1. Exposed dose is measured in roentgens (R) and is defined as that quantity of radiation that produces $2.58x10^4$ coulombs of charge per kilogram of dry air. Absorbed dose is measured in grays and corresponds to the energy deposited per mass, or 1 joule per kilogram of material. Since different types and energies of radiation affect a human cell in various ways, a non-dimensional radiation weighting factor called the quality factor (Q) is utilized to normalize the damage to human tissue by multiplying it by the absorbed dose in grays (Gy), producing the dose equivalent (H) in units of sieverts.

Table II.1 - Radiobiology Units [9]

Quantity	SI Units	Common Units	Conversions
Exposure	*roentgen (R)* 1R of X-rays or γ-rays produce 2.58x10-4 coulombs of charge per kilogram of dry air.	N/A	1 R = 88 rads from X-ray or gamma radiation in human tissue
Absorbed Dose	*gray (Gy)* 1 Joule of energy being deposited by the radiation per kg of material	*Radiation absorbed dose (rad)* Radiation energy absorbed in units of 100 ergs/g of material	1 rad = 0.01 Gy
Effective Dose & Dose Equivalent	*sievert (Sv)* Relates absorbed dose to effective biological damage	*roentgen equivalent man (rem)* Relates absorbed dose to effective biological damage	1 rem = 0.01 Sv

B. Sievert Quantities

Two additional quantities commonly found in the field of radiation protection are the dose equivalent, H, used primarily in radiation protection, and the ambient dose equivalent H*(10), a quantity predicted by the commercial codes [10]. Both of these quantities have units of sieverts. The dose equivalent H in tissue takes into account the biological damage caused by the radiation and is equal to the absorbed dose times a quality factor. H*(10) represents the radiation 10 mm deep into a tissue equivalent phantom of 30 cm diameter. The TEPC produces the dose equivalent related specifically to a two-micron cell of tissue. For this project, it was assumed that the dose equivalent, H, measured by the TEPC was approximately equal to the ambient dose equivalent, H*(10), predicted by the codes. This equivalence is based on two assumptions. First, the backscatter of the aircraft is close to that from the 30 cm phantom, and second, the attenuation of the aluminum case, propane sphere, and A150 wall was very close to the attenuation of 10 mm of equivalent tissue. With these assumptions in place, the ambient dose equivalent from the commercial codes was assumed to be equal to the dose equivalent H given by the TEPC.

C. Quality Factor

As a unitless quantity responsible for converting an absorbed dose in Grays to a dose equivalent in sieverts, the quality factor exerts tremendous influence on the overall dose experienced by radiation workers. Based on the quality factor, two types of linear energy transfer (LET) have been established, referred to as high and low LET. A particle with high LET typically deposits more than 10 keV/micron when traversing a micron-sized somatic cell [11]. At ground level, the radiation received typically falls into the low LET spectrum, usually less than 1 keV/micron. Figure II.1 shows the quality factor for linear energy, based on ICRP-40 and ICRP-60 recommendations, respectively.

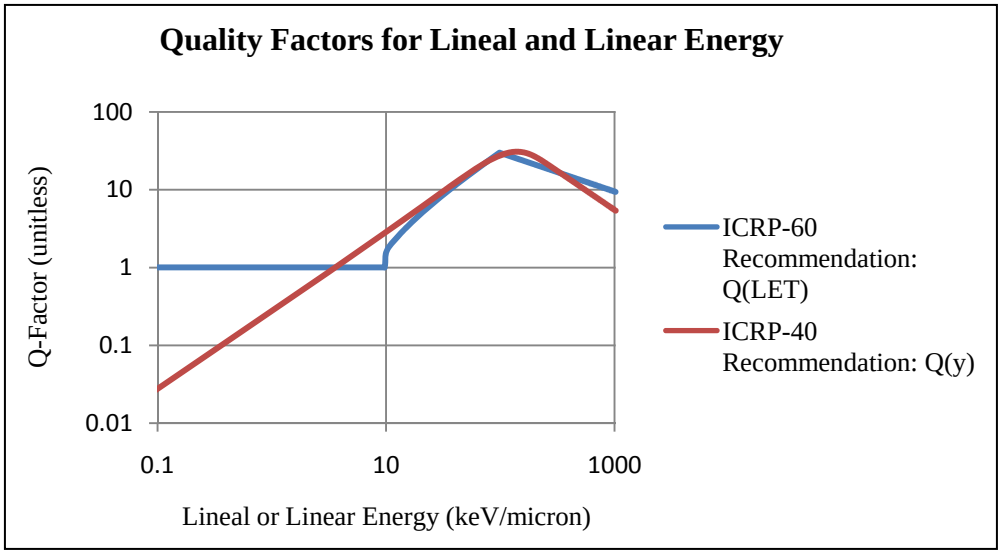

Figure II.1 – Differences in quality factor values

Figure II.1 emphasizes the differences in the ICRP-40 recommendation that the quality factor be related to linear energy whereas the ICRP-60 recommendations require the relation to occur with the linear energy transfer of a particle [11]. An important subtlety lies in the description of lineal and linear energy which will be addressed in the next section.

D. Linear vs. *Lineal* Energy Transfer

To simplify radiation protection calculations, an unrestricted linear energy transfer produces the quality factor, neglecting energy transfers from secondary particle "delta rays." Delta rays refer to fast electrons produced by ionizing collisions. The relationship between the quality factor and LET is not fundamental, but rather based upon empirical radiobiological data. When measuring the radiation deposited in very small volumes, like two micrometer somatic cells, the *lineal* energy, *y*, takes delta rays, variations of the intercepted trajectory length, changes in LET during traversal, finite track length, and track curvature and straggling into account. In addition, the LET is not a stochastic quantity, subject to an energy cut-off where the *lineal* energy is stochastic and is subject to geometric cutoff values through the utilization of a "mean chord length" approximation discussed in more detail in Appendix E. In this case, the mean

chord length was determined from the sphere of propane inside the detector which be discussed in greater detail in Chapter IV. The *lineal* energy relation to the quality factor expressed in Figure II.1 is mathematically described below [13]:

$$Q(y) = \frac{a_1}{y}\left[1 - \exp\left(-a_2 y^2 - a_3 y^3\right)\right] \qquad \text{(II.1)}$$

Where:

$Q(y)$ = quality factor, unitless
y = lineal energy, keV/μm
$a_1 = 5510$ keV/μm
$a_2 = 5 \cdot 10^5$ μm^2/keV^2
$a_3 = 2 \cdot 10^{-7}$ μm^3/keV^3

In addition, when working with a spherical detector geometry, the lineal energy was taken to equal 3/2 times the linear energy.

E. The Human Cell

The fundamentals of radiation health studies and the units associated with such science become most apparent with an understanding of a typical somatic (non-sex) cell. From a general, macroscopic viewpoint, radiation health studies are attempting to assess the total amount of damage done to the body by individual cellular mutations. More specifically, these studies focus on the probability that an individual radiation particle disrupts an important function of a cell that causes it to die or mutate. In this project, references to a "human cell" refer to a typical two-micrometer somatic cell for the basis of observed and recorded radiation doses.

In the human body, cells are divided into gametes and somatic cells. The gametes' only function is for reproduction whereas the large division of somatic cells refers to cells with different functions and characteristics, like a 3 foot-long nerve cell, or much smaller brain cell. There are approximately 4 x 10^{13} cells in the average adult person [9] with varying purposes.

Within the cell, various organelles perform functions similar to our body's organs to help sustain the cell's life. They are suspended in cytoplasm, a transparent, dilute mixture of water and various molecules and electrolytes that comprises the bulk of the cell volume. Because of the large amount of cytoplasm in the cell, a common practice in microdosimetry is to assume a material density of water, 1 gm·cm^{-3} [14]. Within the center of the cell is the nucleus, containing the chromatin and strains of DNA that act as the instructions for proper cell division. Damage to the chromatin can lead to serious consequences for the cell, such as improper cell division that may create a mutated cell. When cells begin to mutate, they may lose their ability to properly function, but still keep their ability to divide, creating more useless or destructive, mutated cells in the body. In medicine, this is commonly referred to as cancer, and most of radiation health deals with the probabilities associated with receiving a certain amount of radiation and the likelihood of cancer development. The mutations that occur from radiation are no different than the mutations that naturally occur throughout our body on a daily basis.

There are two basic methods by which radiation particles may interfere with the life of a cell. First, the ionizing particles may break molecular bonds of important organelles or DNA in the cell, known as the "direct effect of radiation" [14]. Second, the deposition of energy from ionizing particles may result in the production of new chemicals, such as the highly reactive oxy

(O) and hydroxyl (OH) radicals, which then interact chemically within the cell, known as the "indirect effect of radiation" [14].

Cell death is a common occurrence in the body and through evolution, the body has developed natural repair mechanisms to combat the death of its cells from natural forces and unforeseen trauma, such as running a marathon. Both high and low LET radiation cause cellular damage and by analyzing survival curves for cells exposed to acute doses of radiation, like Figure II.2, the differences between the two types of radiation become apparent. High LET leads to cellular death much faster than Low LET and the knee of the Low LET curve seems to indicate a threshold at which the body can recover successfully from the damage inflicted on it from low LET radiation. This area of research is still very controversial and inconclusive. For the most part, the dose pilots usually experience falls within the unknown health effects region – the knee of low LET [14].

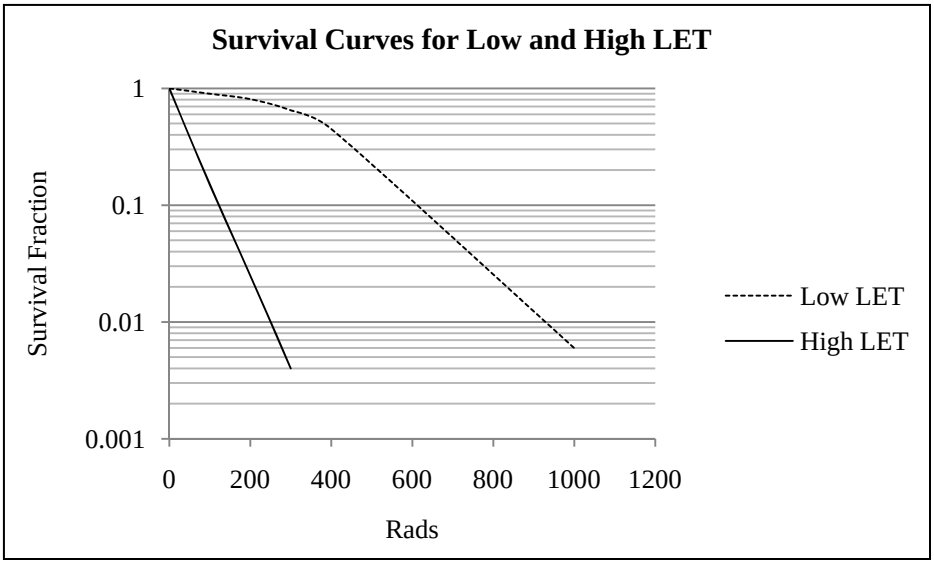

Figure II.2 – Survival Curves for Cells Exposed to Acute Doses of Radiation

F. Health Effects of Radiation Exposure

Little information exists for the study of low-dose, chronic exposure to radiation, like the kind affecting pilots and radiation workers. There are two reasons for this: 1) the root causes for symptoms and cancer rates found in society become hard to decipher between other naturally occurring sources and 2) there is no long-term information to analyze like that for large acute doses with the studies of the casualties and survivors of World War II. Regardless, for completeness in addressing the issue of radiation health effects, Table II.2 depicts the early effects which may be seen from large acute doses. Table II.3 is a more appropriate source of information for the dose expected in this project.

Table II.2 – Probably Health Effects of Large, Acute Doses [14]

Acute Dose (rems)	Probably Observed Effect
5 to 75	Chromosomal aberrations and temporary depression of white blood cell levels in some individuals. No other observable effects.
75 to 200	Vomitting in 5 to 50% of exposed individuals within a few hours, with fatigue and loss of appetite. Moderate blood changes. Recovery within a few weeks for most symptoms.
200 to 600	For doses of 300 rems or more, all exposed individuals will exhibit vomiting within 2 horus. Severe blood changes, with hemorrhage and increased susceptibility to infection, particularly at the higher doses. Loss of hair after 2 weeks for doses over 300 rems. Recovery from 1 month to a year for most individuals at the lower end of the dose range; only 20% survive at the upper end of the range.
600 to 1,000	Vomiting within 1 hour. Severe blood changes, hemorrhage, infection, and loss of hair. From 80% to 100% of exposed individuals will succumb within 2 months; those who survive will be convalescent over a long period.

Table II.3 – Average Annual Individual Doses in mrems from Natural and Man-made Radiation Sources [14]

Source	Exposed Group	Number Exposed	Body Portion Exposed	Dose (mrem)
		Natural Radiation		
Cosmic Rays	Total Population	226×10^6	Whole Body	28
Terrestrial γ-rays	Total Population	226×10^6	Whole Body	26
		Internal Sources		
^{40}K	Total Population	226×10^6	Gonads, bone	19, 15
^{222}Rn	Total Population	226×10^6	Lungs, bone	200, 0.6
		Man-made Radiation		
Medical x-rays	Adult Patients	105×10^6	Bone	103
	Medical personnel	195,000	Whole Body	300-350
Nuclear weapon	Total population	226×10^6	Whole Body	4-5
Air Travel	Passengers	35×10^6	Whole Body	3
	Crew	40,000	Whole Body	160
Tobacco	Smokers	50×10^6	Bronchial epithelium	8,000

Chapter III: Atmospheric Particle Characteristics and Interactions

Measuring the "mixed" radiation field environment of naval aviators and aircrew requires a familiarity with a variety of different subatomic particles, particularly neutrons, protons, and electrons. Along with other subatomic particles in the atmosphere, these build the foundation for various types of interactions leading to energy deposition in a human cell. The Tissue Equivalent Proportional Counter attempts to account for these types of radiation by measuring the lineal energy deposited by each particle, previously discussed in Chapter II. Understanding the characteristics and formation of different types of radiation, shown in Figure III.1, helps decipher the radiation field at various altitudes in the atmosphere. The following sections describe the characteristics and interactions anticipated at various altitudes in the atmosphere.

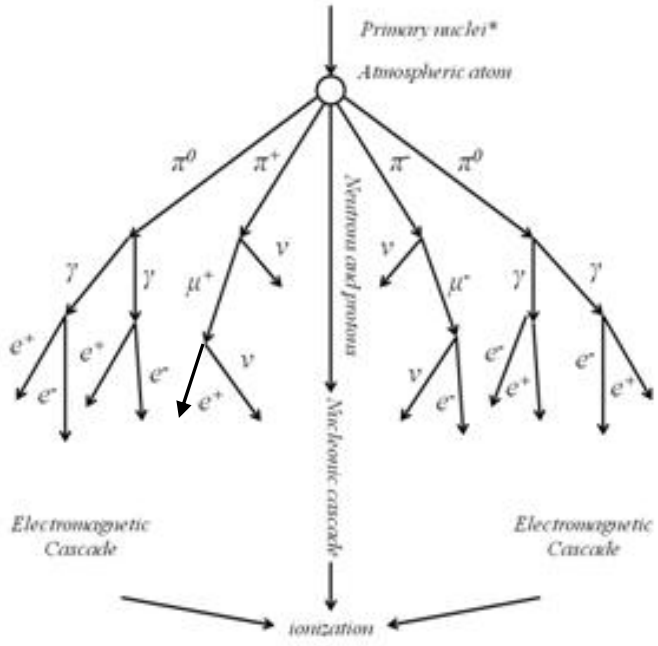

Figure III.1: Cosmic Ray Spectrum [15]

A. Alpha Particles

These are helium nuclei, capable of interacting strongly with matter and heavily ionizing cells. Fortunately, they have a low penetrating power and travel in straight lines until they lose most of their kinetic energy. Certain alpha particles also have a distinct lineal energy distribution, making them ideal for calibration purposes. The HAWK utilizes an internal Curium-244 alpha source to ensure the detector's proper calibration. Further details about this alpha source can be found in Chapter VI.

In regards to radiation safety, the pilot will be protected from alphas created in the atmosphere by the airplane's aluminum skin. As a result, a very negligible dose is expected from alpha particles during flight. Typical alpha particle energy is 5 MeV with a typical range of 50 millimeters in air [16].

B. Beta Particles, Electrons, and Positrons

Beta particles are electrons created by nuclear decay, possessing the same mass and charge as an electron. A positron is similar to a beta but holds a positive charge. They travel very fast, near the speed of light, which does not allow for a great amount of radiation to be deposited in a mass. They are considered to be low LET radiation [16].

These particles have a small mass and cause ionization by displacing electrons from their orbits. Their range in air is about 10 feet per MeV, which can lead to long ranges for betas produced in the atmosphere at energies around 1 GeV. However, the plane's aluminum skin and honeycomb internal structure will remove almost all beta and positron radiation, except for those produced inside the plane.

C. Photons as Gamma Rays and X-rays

These particles are very prevalent in the atmosphere and are lightly ionizing and highly penetrating. A gamma ray is formed from a nuclear interaction whereas an X-ray originates from an interaction with the electron cloud. X-rays are considered a type of long-wavelength electromagnetic radiation (ER) while the gamma ray is short wavelength ER [16]. Both particles are considered photons and have zero rest mass.

There are three main gamma ray interactions: Compton scattering, the photoelectric effect, and pair production, which affect the dose a human cell receives. Compton scattering is the most common method to produce a measureable energy deposition. In this interaction, a photon collides with an electron and conserves both energy and momentum. If the electron is struck with enough energy, it recoils and flies in another direction. This produces a scattered gamma and a newly released electron free to collide with other particles, or in the electron's case, generate a moving charge, or current, in the detector. Another reaction is the photoelectric effect. This occurs when an initial gamma ray or "photon" interacts with the entire atom and is absorbed, causing an electron to be released with energy equal to the difference of the incident photon and ionization energy. This is a rare occurrence within the detector and unlike Compton scattering, the initial particle disappears, so there is only one electron left to add to the dose the detector records. Pair production is the final and most unlikely process to lead to energy deposition. It requires at least a 1.02 MeV gamma to occur and when it does, a positron and an electron are created which then interact with the electron cloud causing a decrease in their kinetic energy. The positron combines with an electron in an annihilation reaction that produces two photons [14].

D. Neutrons

As a nuclear particle with no charge and approximately the same mass of a proton, the neutron becomes a very damaging particle. Hydrogenous material, or a composition with a high amount of hydrogen atoms, helps slow these particles down. Several different interactions take place with neutrons that are very important for understanding the mixed radiation field at various altitudes in the atmosphere given their high probability of occurrence. Neutrons most commonly undergo elastic and inelastic scattering reactions. Given their large size in relation to other atomic particles and their neutral charge, they are most likely to collide with a nucleus and produce heavy ion recoils which lead to an increased energy deposition in a given mass.

They may also have an ionizing effect by colliding with electrons that make up the molecules within the A-150 Tissue Equivalent plastic wall in the HAWK. An absorption reaction may also occur (n, γ) [9]. During this interaction, a nucleus captures a neutron and releases a characteristic gamma-ray which increases the probability of an electron entering the propane detecting sphere and depositing energy. There are also charged-particle reactions, (n, p) and (n, α), but they are endothermic and do not occur below some threshold energy [14]. Thermal neutrons have kinetic energies less than 1 electron volt and fast neutrons are greater than 100 keV. Water is a very effective shield for neutrons, while the water vapor within the atmosphere is not dense enough to considerably affect the dose produced from neutron interactions [10].

E. Protons

Identical to the nucleus of a hydrogen atom, the proton carries a positive charge of one unit. Its mass is 1800 times the electron and consequently, is more difficult to deflect with a range in aluminum only several micrometers long at energies in the MeV range. Ranges of protons in various materials can be found by use of the SRIM code [17].

F. Pions/Muons

The pion, originally referred to as the π meson, was one of the earliest elementary particles discovered in research with cosmic rays and photographic emulsion plates. There are three variations of the pion: π^0, π^+, π^-. These are the lightest mesons and have a very short half-life. In atmospheric interactions, they help produce muons and neutrinos [17]. The π^+ is composed of an up quark and anti-down quark. Its antiparticle is the π^- while the π^0 is its own antiparticle. The most common decay mode is: $\pi^+ \rightarrow \mu^+ + \nu_\mu$ and this occurs more than 99% of the time. Its mass is about 200 times greater than the electron and it has the ability to interact with any particles, including nuclei. Once the pion decays into a muon, the particle quickly deposits its energy in the TEPC, leading to very low doses of LET, but still worthy of mentioning.

The muon is most commonly created from decay of a cosmic ray pion. They are heavier than the electron and neutrinos but lighter than all other matter particles. Muon detectors around the world constantly monitor the muon flux reaching ground level.

G. Neutrinos

These elementary particles travel near the speed of light and can pass though almost any matter undisturbed. Neutrinos are extremely hard to detect but they are believed to have a very small, non-negligible mass. There are three flavors of neutrinos: electron, muon, tau that are formed from different particle decays. Their contribution to the dose experienced by pilots and aircrew is negligible but their presence should be acknowledged and understood as a by-product of cosmic ray interactions in the atmosphere. Every second, over 400 billion neutrinos from the Sun pass through the human body [18].

Table III.1 – Summary of the Particles Discussed in Sections III.A-G

Particle	Class	Symbol	Charge	Typical Lineal Energy Range in Tissue	LET	Mean-life
Alpha	Hadrons	α	+2	<350 keV/micron	High	Varies
Beta/ Electron/ Positron	Leptons	β e^- e^+	+1, -1, 0	<20 keV/micron	Low	Varies
Gamma (Photon)/ X-ray (Photon)	Bosons	γ	0	<10 keV/micron	Low	Varies
Neutron	Hadrons	n	0	N/A	N/A	Varies
Proton	Hadrons	p	+1	<100 keV/micron	High	Varies
Pions	Mesons	π^0 π^+ π^-	$\pi^{+,-}$: +-e π^0 : 0	<10 keV/micron	Low	$\pi^{+,-}$: 2.6×10^{-8} π^0 : 0.84×10^{-16}
Muons	Leptons	μ^- μ^+	+1, -1	<10 keV/micron	Low	2.2 μsec
Neutrino	Lepton	ν_e ν_μ ν_τ	0	N/A	N/A	Varies

Chapter IV: Tissue Equivalent Proportional Counter

In order to quantify the effects of a mixed radiation field at high altitudes on a normal tissue cell, a tissue equivalent proportional counter can be used. As mentioned earlier, this type of radiation detector simulates the size of a typical somatic cell two microns in diameter. In this project, the Far West Technology Hawk Tissue Equivalent Proportional Counter (HAWK) was utilized for dose and dose rate measurements in the atmosphere. Researchers around the world have previously flown this type detector on commercial flights around the world [11], but little research has occurred on currently-commissioned military aircraft.

A. Physical Dimensions

The initial areas of concern when inserting the TEPC into the cockpit of an aircraft were the size and weight restrictions. On commercial and private aircraft, this was not a problem and the device was carried on in the container every flight. The carrying case with the detector weighed approximately 10 kilograms and was 35 x 65 x 30 centimeters. Without the carrying case, the detector weighed 4 kilograms. For military aircraft, special flight clearances and flight plans had to be created to accommodate a foreign electronic device being placed next to the electronics of the aircraft.

The detector's cylindrical construction is divided in two parts: a detecting sphere and electronics. Within the electronics exists a pre-amplifier, amplifier, and multi-channel analyzer, along with a GPS system that was not used during this experiment. Very low pressure propane (7 Torr) made up the 12.57 cm (inside) diameter detecting sphere, which was also surrounded by a 0.21 cm layer of A150 Conducting Tissue Equivalent Plastic that functioned to simulate the tissue cell membrane as a result of its similar composition to a somatic cell [19]. A mathematical proof of the proportionality can be seen in Appendix E. In Table IV.1, values from NIST are utilized to show the comparison of TEPC materials to soft tissue. Protecting the electronics and detecting sphere was a Type 302 Stainless Steel case. The composition of Type 302 Stainless Steel is given below in Table IV.2.

Table IV.1 – Comparisons of Chemical Composition of TEPC Materials to Soft Tissue

	Hydrogen	Carbon	Nitrogen	Oxygen	Fluorine	Calcium
Soft Tissue (ICRU 4-Component)	10.1172 %	11.1000 %	2.6000 %	76.1828 %		
A-150 Tissue Equivalent Plastic	10.1327 %	77.5501 %	3.5057 %	5.2316 %	1.7422 %	1.8378 %
Tissue-Equivalent Gas (propane-based)	10.2672 %	56.8940 %	3.5022 %	29.3366 %		
Propane	18.2855 %	81.7145 %				

Table IV.2 – Chemical Composition of Type 302 Stainless Steel [20]

Type 302 Stainless Steel	
Atomic Number	Fraction by Weight
6 (Carbon)	0.001500
14 (Nitrogen)	0.010000
16 (Oxygen)	0.002900
24 (Chromium)	0.180000
25 (Manganese)	0.020000
26 (Iron)	0.695600
28(Nickel)	0.090000

B. General Operation Theory

Proportional counters were first introduced in the late 1940s as a way to measure radiation too small for detection by an ion chamber. The HAWK's basic function is to passively collect charge with an anode running through the middle of the detecting sphere at a voltage typically around 700 V. An electric field is created that induces the electrons to move toward the anode, forming the link between particle activity and energy deposition to a measurable electronic signal. As various particles of different energies enter the sphere, they deposit energy by freeing charges which are detected after migrating toward the anode/cathode. This energy deposition is referred to as the stopping power of a radiation particle.

As the anode receives the small current peaks, a preamplifier is utilized to enhance the signal and then bin the voltages developed with a multi-channel analyzer, creating a histogram of lineal energy. Specifically, the linear stopping power, "S," is defined as the differential energy loss for a particular particle within a material divided by the corresponding differential path length in Equation IV.1 [21].

$$S = -\frac{dE}{dx} \tag{IV.1}$$

The stopping power is closely related to the linear and lineal energy transfer described in Chapter II through Equation IV.2 found in the ICRP-26 recommendations [22]:

$$\text{Lineal Energy} = \frac{3}{2} \cdot \frac{dE}{dx} \tag{IV.2}$$

The value along a particle track is also referred to as a specific energy loss or a "rate" of energy loss. As the particle velocity decreases, the stopping power increases. For a nonrelativistic particle, dE/dx varies inversely with particle energy $1/v^2$, where "v" is velocity. This is a result of the charged nature of a particle which can be seen in the Bethe formula [21].

(IV.3)

(IV.4)

Where:

e = electronic charge
z = charge of primary particle
v = velocity of primary particle
m_0 = electron rest mass
I = average excitation and ionization potential of absorbers
N = number density
Z = atomic number
c = speed of light

When the particle slows down, it spends a greater amount of time near any given electron, feeling the electron's impulse and transferring the largest amount of energy. Comparing particles of identical velocity reveals that only the z^2 term, charge of the primary particle, affects the stopping power. Thus, alpha particles will lose energy at a rate greater than protons of the same velocity, but less than that of more highly charged materials.

The Bragg Curve is a key concept in the utilization of a TEPC as well as in radiation measurements. It is the graphical representation of specific energy loss, or stopping power, along a charged particle's track [21]. Stopping power can further be divided into energy loss by bremsstrahlung radiation and energy loss by collisions. As mass and charge of a moving particle increases, the magnitude of LET increases rapidly. Thus, alpha particles again have a considerably larger LET than electrons for the same energy. Alpha particles and other heavy ions are referred to as high LET radiation and electrons are considered low LET radiation. The classification of particles into high or low LET regions is important for considering the biological consequences of certain types of radiation. The LET values of uncharged neutrons and gamma-rays can also be determined from the secondary interactions these particles generate, especially since LET is usually a measure of subsequent energy deposition after the first interaction in a material [14]. Figure IV.1 depicts LET of alpha particles and protons in the three main components of the TEPC theory, tissue equivalent gas (propane-based), A-150 plastic, and adipose, or fat tissue, using the Stopping Range of Ions in Matter (SRIM) program [17].

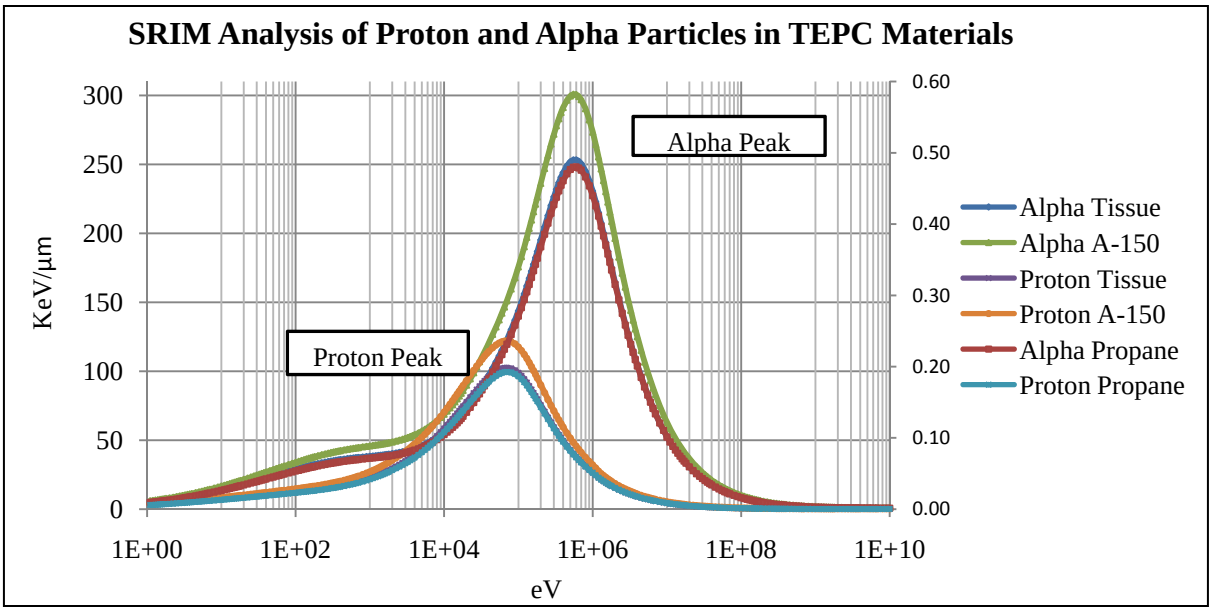

Figure IV.1 - SRIM Analysis of Proton and Alpha Particles in Pertinent Materials (Proton Propane overlaps Proton Tissue, Alpha Propane overlaps Alpha Tissue)

In Figure IV.1, it becomes apparent that the TEPC is a very effective device in calculating a dose for a radiation field of various particles with varying ionization characteristics. The overlapping curves show the ability of propane at 0.0092 atmosphere to simulate the amount of energy that may also be deposited in an equivalent sphere of tissue. Unfortunately, SRIM cannot calculate the Stopping Power of electrons, pions, or muons. In Chapter V, Monte Carlo simulation codes will be used to test the detector's response to these types of particles.

C. TEPC Data Analysis Programs

There are several programs utilized to analyze the data generated from the TEPC during flights and experimental runs. These include SEE2, CONDEQU2 [19], Hawk020 and SPECT2. SEE2 and CONDEQU2 are very similar to each other and involve the recording of dose measurements every 4 seconds within each 1 minute interval. An example of SEE2 and CONDEQU2 can be found in Appendix A and Appendix B, respectively. They contain a great deal of information that is easily displayed using the macro Hawk020. This macro takes the information in CONDEQU2 and separates it into an organized comma-separated value (csv) Excel spreadsheet for further evaluation. An example of this output can be found in Appendix C. The SPECT2 program creates a lineal energy spectrum with total counts in each bin for a designated time period. This output file is utilized to generate a microdosimetric spectrum and calculate the dose and dose equivalent rates. An example of SPECT2 can be seen in Appendix D. A derivation performed by Dr. Lewis at the Royal Military Concern can be used to compare the measured values of the TEPC with by-hand calculations. Both methods are fairly accurate and the derivation can be found in Appendix E with further discussion of its utilization in this report in Section VIII.C.

Chapter V: Simulating TEPC Response and the Canopy Experiment

A. Cobalt-60 Gamma Response

In order to validate the TEPC's dose calculation and calibration before the in-flight experiments, an experiment was run with stacked cobalt-60 sources and then compared to the output of several simulations. The physical experiment was performed in the Rickover Hall Nucleonics Laboratory and involved stacking six individual, one micro-Curie cobalt-60 sources into one tall, cylindrical source placed ten centimeters from the TEPC. By stacking the sources, the activity, also known as disintegrations per second, was increased, reducing the amount of time needed to measure dose and dose rates. The area around the TEPC and source was cleared of obstructions for a three meter radius in order to reduce the complexity of the environment for the Monte Carlo N Particle (MCNP) simulation.

The MCNP5 transport code, developed at Los Alamos National Laboratory [23], was chosen in this experiment since it models the probabilities and interactions of gamma rays with the environment very well. In nuclear engineering, it is utilized as a tool to simulate the mean flight paths and interactions particles may take in a well-defined environment. The code structure and language of MCNP5 is very similar to FORTRAN. An example of the MCNP5 source code for a cobalt experiment can be found in Appendix F. The experiment required one input, or source file, that when executed, established the desired environment, type of source, geometry of detector, and other pertinent information like elemental compositions of various materials in the HAWK. The cobalt experiment took more than 24 hours of continuous calculation to generate an output file with a 3.40 GHz Intel Pentium(R) D processor. The main reason for the long computation time is the execution of random sampling throughout the particle's life in the simulation. When a source is placed in an environment, it gives off its own characteristic decay particles at distinct energies. Once released from the source, these decaying products are now free to interact with the world in a variety of ways. For cobalt-60's decay, two photons, or gamma rays at 1.37 and 1.17 MeV are released from the decay process. As a result, MCNP5 mathematically determines the probability that each particle would have interacted with the world in a specific fashion. With gamma rays, some examples of interactions simulated by MCNP are Compton scattering, pair production, and the photo-electric effect.

After analyzing the MCNP5 model, several adjustments were made to the spectrum for a direct comparison to the output of the TEPC. For instance, the normalized distribution was multiplied by an integer constant in order to scale the curve on the y-axis and appropriately fit the HAWK response curve to the MCNP5 simulation. As shown in Figure V.1, this analysis reveals the effect of gas multiplication, a theory critical in the operation of most TEPCs. The initial energy deposition of an individual particle alone is usually not great enough to overcome the electrical noise of the system. However, with a propane-filled sensing sphere, the number of ions created in the initial event are amplified with secondary ionizations, causing the amount of energy to pass the threshold level for detection. This multiplication must take place in the electric field, large enough to sustain a chain of secondary ionizations, referred to as an avalanche. In order to determine the characteristics of the electric field, both the composition of the detecting gas and geometry of the device must be considered [24].

As stated in the HAWK user manual, the TEPC operates at a gas multiplicative factor around 200 and 400 for voltages of 600 to 900. While simulating the TEPC gamma response curve, the gas multiplicative factor was found through simulation with MCNP5. Originally, the

detector was modeled simply as a sphere of propane gas encased by a concentric shell of A-150 tissue equivalent plastic. But later, the model became more sophisticated with the addition of a concentric cylinder of stainless steel around the propane and A-150 spheres. Once these geometry definitions and the environment was created, the way in which the output file would be written had to be considered. In MCNP, the "tally" function controls the type of data that is recorded and printed out to the screen. In this case, the *F8 and F6 tallies were used to record the net and total amount of energy deposited in the mass of proscribed cells, respectively. Next, a spectrum was produced as shown in Table V.1 below. The shaded area represents "trash bins" which collected energy too small to produce a noticeable affect on a somatic cell. Since both the energy bin and counts were normalized to each particle and minute, the spectrum was multiplied by the gas multiplication factor for the TEPC. Using Equation V.1, the normalized counts were multiplied by an arbitrary number, in this case, 10^7, allowing the MCNP LET spectrum to be compared to the low LET spectrum of the HAWK. As can be seen in Figure V.1 below, there is a strong correlation between both curves, with an error in dose through simulation to the TEPC less than 10%. Figure V.1 shows that the gas multiplication for the HAWK is 400, because the MCNP5 output when multiplied by this factor agrees with the normal HAWK output.

Table V.1 - MCNP5 Output Spectrum of Cobalt-60 Experiment

Energy Deposited (MeV)	Normalized Counts
0.00E+00	7.99E-06
1.00E-06	1.10E-01
2.93E-03	1.32E-03
5.86E-03	3.55E-05
8.79E-03	9.63E-06
1.17E-02	4.64E-06
1.46E-02	2.12E-06
1.76E-02	6.36E-07
2.05E-02	1.49E-07
2.34E-02	4.00E-08
2.64E-02	1.06E-08
2.93E-02	2.50E-09
3.22E-02	1.25E-09
3.52E-02	0.00E+00
3.81E-02	0.00E+00
4.10E-02	0.00E+00

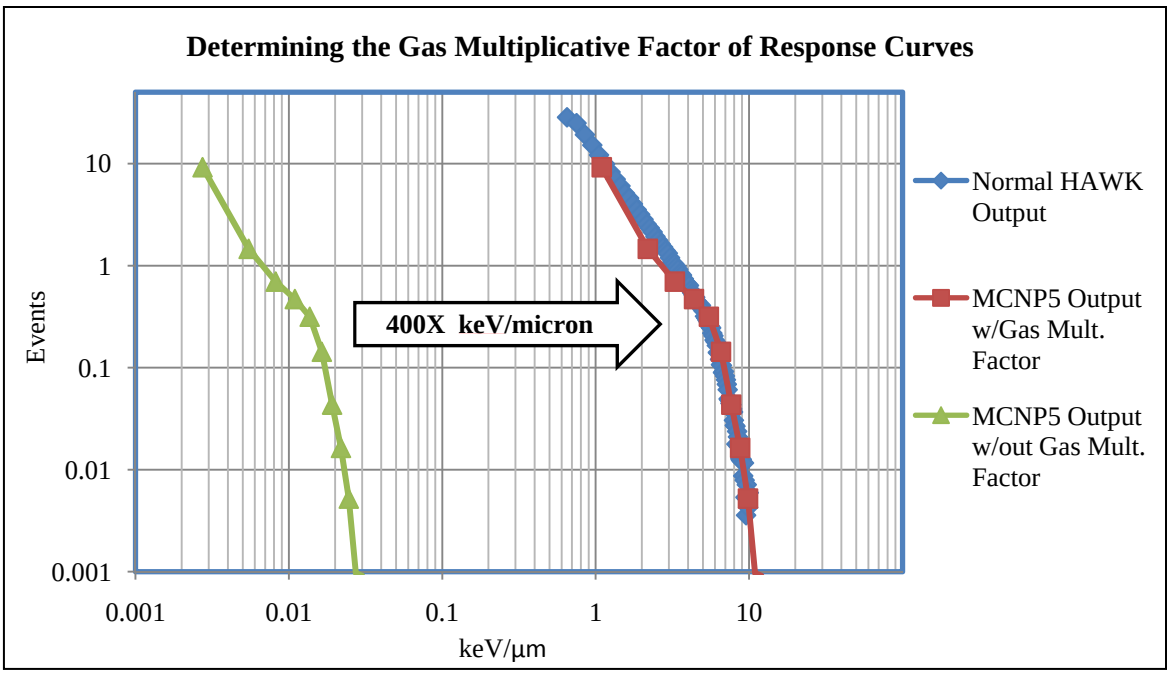

Figure V.1 - MCNP5 Cobalt-60 Response Curve Compared to HAWK Response Curve

B. Curium-244 Alpha Source Response

Before the TEPC is sent away from the manufacturer, each device is calibrated with a curium-244 source. During the project, this calibration process was modeled with SPENVIS [25], a user-friendly interface that simplifies simulations done by MULASSIS, which simulated the energy deposition within various materials utilizing GEANT4 code [26]. Several inputs were utilized to simulate a sphere of propane, the technical specifications of the source and the main geometry of the simulation. Utilizing SRIM to create a table of stopping ranges for different isotopes, the maximum values were determined.

In addition to creating an output text file, a virtual reality file is created which can be used to double check the experiment's geometry and ion scattering. In Figure V.2, the red lines can be seen as ionization trails of alpha rays colliding with electrons and nuclei during the experiment. Both of these experiments were simulated with 100,000 alpha particles. An example of the output spectrum from the HAWK compared to the GEANT prediction for propane is shown in Figure V.3, revealing a calibration peak at the expected value of 155 keV/micron for Curium-244 alpha particles. In GEANT, the source was defined to have a collimation angle of 10 degrees, directly influencing the width of the simulated peak shown in Figure V.3. By decreasing the collimation angle, the simulation should produce a more well-defined peak.

Figure V.2 – GEANT4 .wrl Visualization: Output of Propane Sphere (left), Output of Adipose Tissue (right)

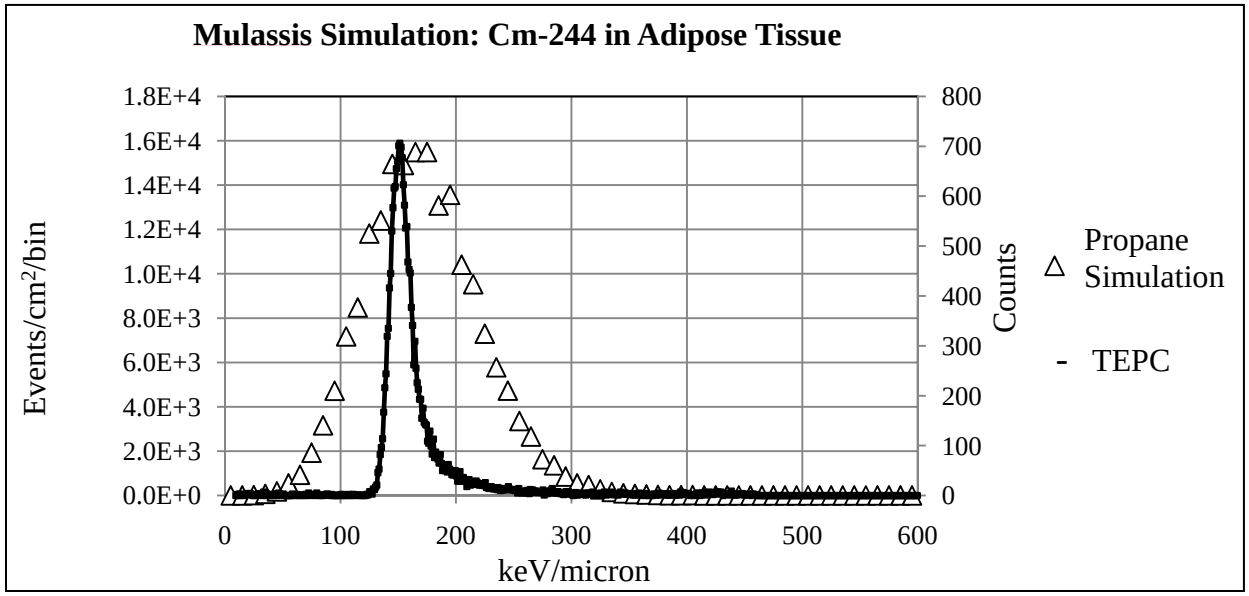

Figure V.3 GEANT4 Alpha Calibration Comparison with HAWK Output

C. Canopy Experiment

At Los Alamos National Laboratory during the Summer of 2008, several experiments were carried out with actual samples of canopy from the EA-6B Prowler. In naval aviation, no other airplane has a canopy like the EA-6B prowler, and when evaluating the different structures of aircraft, this was a major issue with calculating dose. Since the primary mission of an EA-6B is to perform electronic countermeasures, the gold-lined canopy was suppose to act like a Faraday cage, blocking the majority of harmful electromagnetic radiation from the crew. However, very little information existed describing the interaction between very high energy particles and the gold annealed in the EA-6B canopy. Three 5” x 5” canopy samples were obtained from the manufacturer in Jacksonville, Florida with the help of Mr. Howard Royce. Once these samples were obtained, they were irradiated in between a fission chamber and the TEPC. This allowed the difference in dose rates to be measured both before and after the high energy neutrons, from a 10 GeV polyenergetic neutron source passed through the canopy samples. The basic dose attenuation equation was utilized below:

$$D = D_o e^{-\mu x} \quad \text{(V.1)}$$

Where:

D = Dose Rate with Target
D_o = Dose Rate with no Target
μ = Dose attenuation coefficient, cm^{-1}
x = 0.700 cm, thickness of canopy

During one experiment, the dose attenuation coefficient, μ, was found to be 0.01, revealing a negligible shielding effect from the canopy. With limited time to experiment with the canopy samples, enough data was obtained to draw preliminary conclusions that the canopy would not protect the pilot and aircrew from galactic cosmic rays and solar particle events. When comparing the dose equivalent rates measured on the EA-6B Prowler to commercial aircraft, there should be little deviation seen at similar altitudes as a result of aircraft structure.

Chapter VI: Experimental Flights

A. Aircraft Platforms

Experiments with the TEPC were conducted on private, commercial, and military aircraft. Each plane had significant variation in its structure, typical operational altitude, and mass. The variations between the commercial aircraft were considered to be negligible and for ease of calculation, only one type of commercial plane was considered – the Boeing 767-400ER. Below, Table VI.1 describes a few of the key characteristics of the three air platforms. A Cessna is shown in Figure VI.1. This type of aircraft was piloted by a fellow classmate for the low altitude flights in the project. As can be expected, private aircraft have the least amount of shielding among the other two platforms and travel, on average, at a slower speed and at a lower altitude. In Figure VI.2, a typical Boeing model is shown to represent all the different commercial planes encountered during the experimentation phase of this project. While the shielding varies slightly between the different commercial aircraft, as was shown with the EA-6B Prowler canopy, very few materials in the hull of aircraft will be able to stop the most biologically destructive radiation in the atmosphere. Compared to the commercial and private aircraft, the EA-6B Prowler shown in Figure VI.3 can fly faster, higher, and more aggressively. And after showing the negligible effect of the Prowler canopy, speed and structural shielding was found to be of very little concern in altering the dose rate experienced during typical operations.

Table VI.1 – Aircraft Characteristics

	Private [27]	Commercial [28]	Military [29]
Name	1978 Cessna Model 152	Boeing 767-400ER	EA-6B Prowler
Maximum Altitude	~ 13,500 feet	~ 40,000 feet	~ 50,000 feet
Maximum Speed	126 mph (110 knots)	530 mph (461 knots)	651 mph (566 knots)
Maximum Weight	1241 lbs	450,000 lbs	65,000 lbs
Wingspan	33 ft 4 in (10.2 meters)	170 ft 4 in (51.9 m)	53 ft (15.9 m)

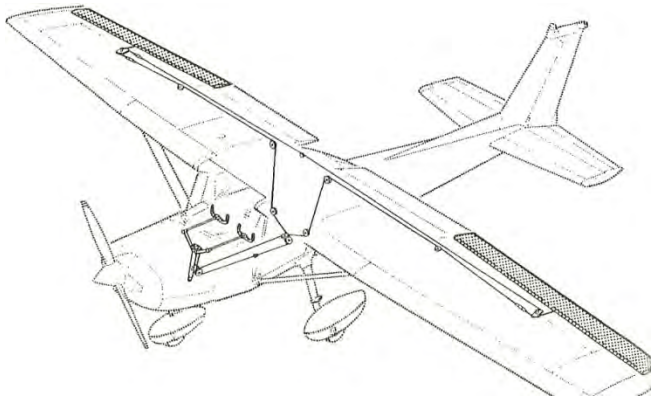

Figure VI.1 – Schematic of 1978 Cessna Model 152 [27]

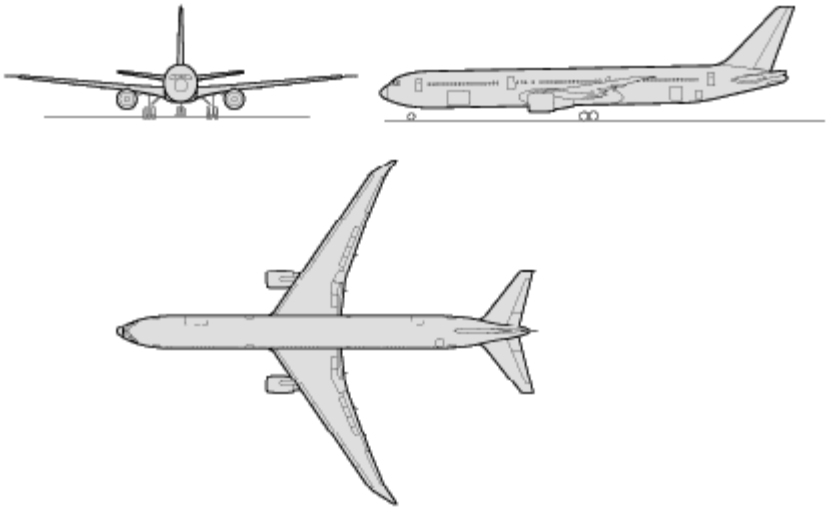

Figure VI.2 – Schematic of a Boeing 767-400ER [30]

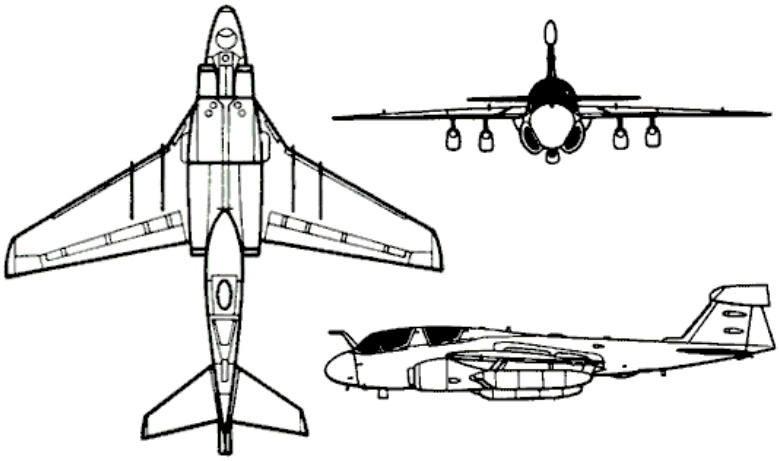

Figure VI.3 – Schematic of an EA-6B Prowler [31]

On each aircraft, the placement of the TEPC varied slightly. With the private aircraft, the device was situated directly behind the pilot and co-pilot seats. In the military flights, the TEPC was positioned next to the seat of the pilot. On the commercial flights, the TEPC was placed in the overhead storage compartment or in the storage area underneath the seat. The vast differences between these three platforms allowed inter-comparisons to be made later which would assess the effect of aircraft structure on the high energy particles present in the atmosphere.

The first experiments conducted were on private aircraft, piloted by a first-class, Naval Academy midshipman. A maximum altitude of 13,000 feet was reached over the Annapolis/Bay Bridge area. These flights lasted approximately two hours and encountered no turbulence or external disturbances which could have affected the TEPC's measurements. If placed in a highly turbulent environment and the device was not properly stowed, violent collisions inside the cockpit could generate spurious counts. The purpose of these flights was to become acclimated

with the operation of the GPS equipment and TEPC interface. Through these flights, it quickly became apparent that the TEPC's internal GPS system was not working properly, and as a result, an external Garmin GPS system was utilized which recorded the latitude, longitude, and altitude to a DATALOGGER. Eventually data from the DATALOGGER were downloaded to the computer and later correlated with the TEPC measurements in Zulu Time. Another important observation from the low-altitude flights was the necessity for more background information. As a result, the TEPC was always powered on for at least one hour before and after subsequent flights. The first two flights in Table VI.2 were the low-altitude flights.

With the TEPC and GPS system fully operational, two flights were conducted on the EA-6B Prowler with the VX-23 squadron at Patuxent River Naval Air Station. These flights were much shorter and at lower altitudes than initially expected. Unfortunately, after three flights were flown successfully with the TEPC, operational maintenance and personnel issues did not allow the device to be flown again. With less than two hours of data from the Prowler flights, it is very difficult to draw adequate conclusions for this research. Regardless, the two Prowler flights help complete the project's dataset and will hopefully allow for future comparisons to be made to atmospheric radiation measurements on other military aircraft as well.

B. Flight Data

The majority of data collected in this project occurred on commercial aircraft. In fact, over 40 hours of in-flight data were collected in flights across the continental United States. The detector has traveled to 14 states, with the specific destinations listed in Table VI.2. As mentioned earlier, most of the commercial aircraft flights were on a platform very similar to the Boeing 767 aircraft, especially for flights of a longer duration. The detector took measurements on flights during the day and night and in various weather conditions. Since the cockpit and crew cabin spaces were heated, the environment temperature was not a concern in the proper operation of the TEPC. Table VI.3 includes the entire inventory of flights conducted during this research project. The last three columns from the right represent the ambient dose equivalent value in micro-Sieverts, H*(10), predicted by two commercial codes and the TEPC. The H*(10) measurements do not exist for EPCARD because Table VI.3 shows the dose expected for the entire flight, even for altitudes below 16,400 feet, EPCARD cannot determine. Where "No GPS" is listed, there was a malfunction with the GPS system and no data could be obtained. In this situation, dose information was still collected from the TEPC, but it could not be compared to the predictive codes since they required geographic information as the primary input in calculating dose.

Table VI.2 – List of Airports and Locations of Flights

Abbreviation	Airport Name	State
BBA	Bay Bridge Airport	Maryland
ANN	Annapolis	Maryland
PAX	Patuxent River Naval Air Station	Maryland
BWI	Baltimore Washington-International Airport	Maryland
ATL	William B Hartsfield International Airport	Georgia
ABQ	Albuquerque International Sunport Airport	New Mexico
SLC	Salt Lake City International Airport	Utah
OKC	Will Rogers World Airport	Oklahoma
DFW	Dallas Fort-Worth International Airport	Texas
DTW	Detroit-Metro Airport	Michigan
CLT	Charlotte Douglas International Airport	North Carolina
GNV	Gainesville Regional Airport	Florida
BOS	Logan International Airport	Massachusetts
ORD	Chicago O'Hare International Airport	Illinois
IND	Indianapolis International Airport	Indiana
SFO	San Francisco International Airport	California
PHX	Phoenix Sky Harbor International Airport	Arizona

Table VI.3 – Flight Inventory: Private, Military, and Commercial Included

Flight Departure	Flight Destination	Take-off Date	Start Time (Zulu)	End Time (Zulu)	Duration (minutes)	Average Cruising Altitude (ft)	TEPC H_T Total (uSv)	EXPACS H*(10) Total (uSv)	CARI-6M H*(10) Total (uSv)
BBA	ANN	14MAY08	0713	0848	95	No GPS	0.481	-	-
BBA	ANN	18SEP08	1251	1451	120	12748/41	0.816	0.409	0.470
PAX	PAX	16OCT08	1547	1636	49	19649/14	0.549	0.402	0.376
PAX	PAX	23OCT08	1644	1750	67	No GPS	0.342	-	-
BWI	ATL	21DEC08	1454	1639	105	33522/58	4.65	5.79	5.76
ATL	ABQ	21DEC08	2209	0125	196	No GPS	10.5	-	-
ABQ	SLC	22DEC08	1419	1551	92	30035/46	2.57	3.33	3.18
SLC	BWI	22DEC08	1748	2103	195	36225/146	14.6	17.9	18.5
BWI	OKC	12FEB09	2230	0152	202	33057/166	10.7	14.6	14.7
OKC	DFW	13FEB09	0218	0254	36	17951/10	0.221	0.242	0.207
DFW	DTW	16FEB09	2238	0037	119	33254/80	7.03	7.62	7.68
DTW	BWI	17FEB09	0259	0402	63	29337/18	1.72	1.67	1.64
BWI	CLT	19FEB09	1205	1305	60	27202/23	1.56	1.59	1.62
CLT	GNV	19FEB09	1449	1556	67	32105/23	1.76	2.34	2.35
GNV	CLT	21FEB09	1958	2058	60	29004/26	1.09	1.75	1.72
CLT	BWI	21FEB09	2311	0006	55	No GPS	0.909	-	-
BWI	BOS	01MAR09	1753	1918	85	21435/29	1.81	1.60	1.55
BOS	BWI	03MAR09	2233	2331	58	33106/16	2.17	1.90	1.97
BWI	DTW	05MAR09	2035	2150	75	31298/29	2.88	3.18	3.02
DTW	BWI	07MAR09	2338	0035	57	33267/23	1.78	2.71	2.61
BWI	IND	08MAR09	1606	1840	154	38415/42	10.7	13.5	13.3
IND	ORD	08MAR09	2051	2154	63	0.391/12	0.982	0.675	0.582
ORD	SFO	09MAR09	0020	0432	252	37733/206	18.2	25.9	25.7
SFO	PHX	10MAR09	1302	1430	88	39244/21	3.95	3.91	3.85
PHX	BWI	10MAR09	1557	1943	226	39720/100	14.9	20.1	19.8
Total:	**25 flights**		**Total:**	2639 mins	(~44 hours)				

Chapter VII: Predictive Codes

Commercial, predictive codes for calculating radiation exposure provide a valuable and practical application to this research project. By utilizing the aircraft's geographic position and time of flight as inputs into these programs, a dose equivalent rate per hour may be output for further analysis. As mentioned earlier, various European institutions have already adopted EPCARD as their official predictive tool to monitor the radiation exposure of their commercial pilots [11]. In this research, EXPACS became the central focus since very little research compared this code to already established and certified predictive codes. The following sections describe the capabilities and critical differences in the predictive code calculations.

A. CARI-6 Description

Created by Dr. Friedberg at the Federal Aviation Administration, CARI-6 is the United States' predictive code for determining atmospheric radiation exposure. The program calculates an effective and H*(10) dose of galactic cosmic radiation received by an individual along a user-entered flight profile [32]. Flight data may also be entered as waypoints of latitude, longitude, and altitude ranging from 0 to 60,000 feet. The code accounts for dose fluctuations as a result of changes in altitude, geographic location, and date. This is done by choosing the correct vertical cut-off factor from the IGRF95 reference table which relates to the aircraft's current latitude, longitude, and altitude [32]. Additional information including the month and year of the flight also allows the appropriate heliocentric potential to be selected from an adjustable database. These heliocentric potentials, in Megavolts, relate to the sun's solar activity calculated from ground level neutron measurements provided by Dr. Eduard Vashenyuk of the Apatity Cosmic Ray Station of the Polar Geophysical Institute in Russia [32]. It is also "the result of a steady-state solution to the diffusion equation of cosmic rays through the solar wind" [33]. A high heliocentric potential relates to reduced cosmic ray dose rates, and a low heliocentric potential leads to increased cosmic ray dose rates. These codes are updated by the user inputting these solar activity values for each new month in the database.

In addition, a radiation transport code called LUIN2000 is utilized to generate a flux for individual particles in the atmosphere. It uses "a superposition approximation to handle alpha particles and heavier ions present in the primary galactic cosmic ray flux at the top of the atmosphere. The approximation becomes less accurate as altitude increases" [32]. Table VII.1 shows the radiation quality factors utilized by CARI-6 and the other predictive codes.

Table VII.1 – Radiation Weighting Factors in CARI-6

Radiation Weighting Factors	
Type and Energy Range	Radiation Quality Factor, w_R
Photons, all energies	1
Electrons and muons, all energies[1]	1
Neutrons, energy < 10 keV	5
10 keV to 100 keV	10
> 100 keV to 2 MeV	20
> 2 MeV to 20 MeV	10
> 20 MeV	5
Protons, other than recoil protons, energy > 2 MeV	2
Alpha particles, fission fragments, heavy nuclei	20

[1]Excluding Auger electrons emitted from nuclei bound to DNA

In Table VII.2, a few values were chosen from the heliocentric potential database stored in CARI-6. These values allow the program to adjust for changes in galactic radiation levels that occur with changes in solar activity. As can be seen in Table VII.2, these values have been consistently decreasing since the beginning of the research project, indicating an overall minimum in solar activity compared to past years. In Figure VII.1, a screenshot of CARI-6 reveals that the program was operated under a Microsoft Windows operating system in this research project. Unfortunately, permission to gain access to the source code was denied, so only the features available when the program was run with MS-DOS were utilized.

Table VII.2 – Selected Values of Heliocentric Potentials from CARI-6 Database

Months ('08-'09)	Heliocentric Potential
May '08	321
June '08	323
July '08	319
August '08	305
September '08	276
October '08	285
November '08	270
December '08	266
January '09	256
February '09	252
March '09	238

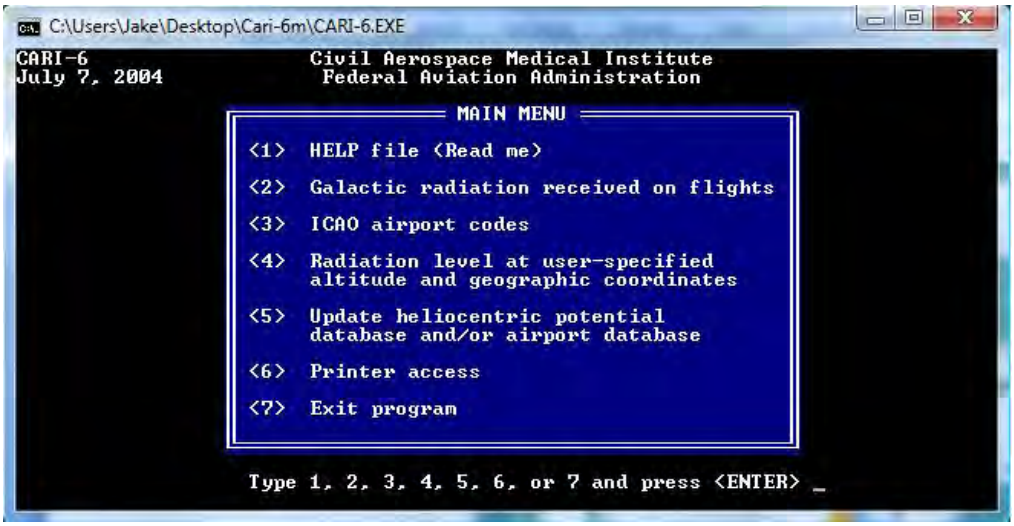

Figure VII.1 – Screenshot of CARI-6

B. EPCARD Description

In Germany, EPCARD has become the predictive code established by law to help regulate the amount of radiation exposure EU aircrews and pilots receive [34]. Similar to CARI-6, flight data may be entered as waypoints of latitude, longitude, and altitude. The program calculates vertical cut-off rigidity from previous research conducted by Dr. Shea and Dr. Smart. Vertical cut-off rigidity can be described as a value that sets the minimum energy needed by a particle to penetrate the Earth's atmosphere at certain altitudes. The acceptable input altitudes for EPCARD are between 16,404 feet and 82,021 feet. It uses the results of FLUKA [35],

similar to LUIN2000 in CARI-6, a Monte Carlo radiation transport code which also takes into account the most recent cross section data. Where CARI-6 utilizes a heliocentric potential, derived from the result of a steady-state solution to the diffusion equation of cosmic rays through the solar wind, EPCARD uses a "solar deceleration" to account for the variations in solar activity. Figure VII.2 depicts the operation of EPCARD in a flow chart found in the User's Manual [35]. EPCARD produces an effective dose at any position, like CARI-6, in micro-sieverts per hour and can also produce an ambient dose-equivalent rate in micro-sieverts per hour. In order to obtain these values, EPCARD utilized fluence, the number of particles that entered a sphere divided by the cross-sectional area of the sphere, to dose coefficients, shown in Table VII.3, leading to the calculation of the ambient dose equivalent from the output of FLUKA.

Table VII.3 – Fluence to Dose Coefficients for EPCARD [35]

Particle	$H^*(10)/\varphi$ (pSv cm^2)[1]	E_{iso}/φ (pSv cm^2)[1]
Neutrons	242	207
Protons	919	3000
Charged Pions	799	1043
Electrons	249	116
Photons	2.70	6.02
Muons	328	338

[1]The uncertainties of the conversion coefficients are estimated to ±10%

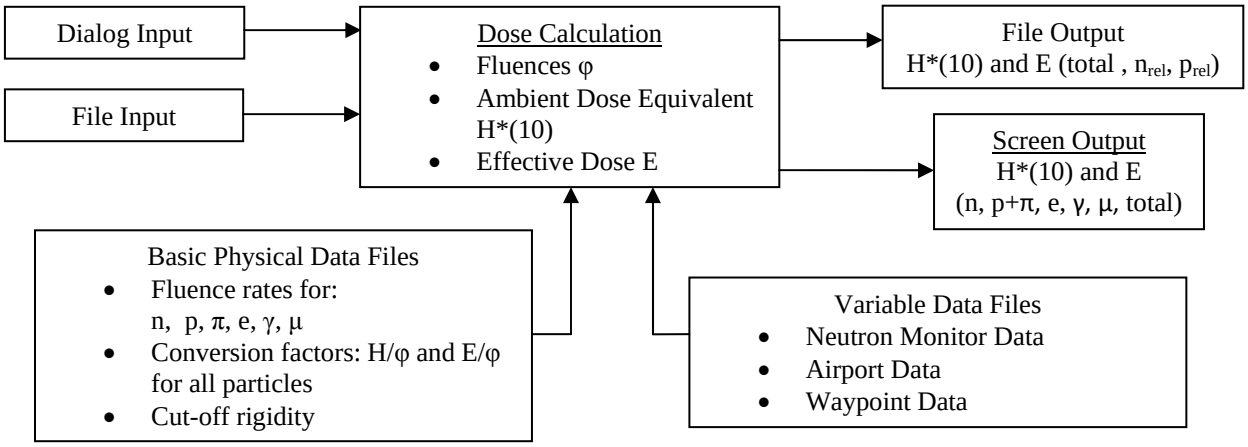

Figure VII.2 – Flow Chart from User Manual Demonstrating EPCARD Processes [35]

Unlike CARI-6 and EXPACS, EPCARD came on a CD-ROM with a very sophisticated User's Manual and license agreement. Since EPCARD has already been adopted in the European Union as the official software to be utilized to track radiation exposure for commercial pilots and aircrew, the package was much more developed and geared toward airport-to-airport flight patterns. Figure VII.3 shows the small script that was utilized within the program to calculate the dose rate at each geographic position, much like in CARI-6.

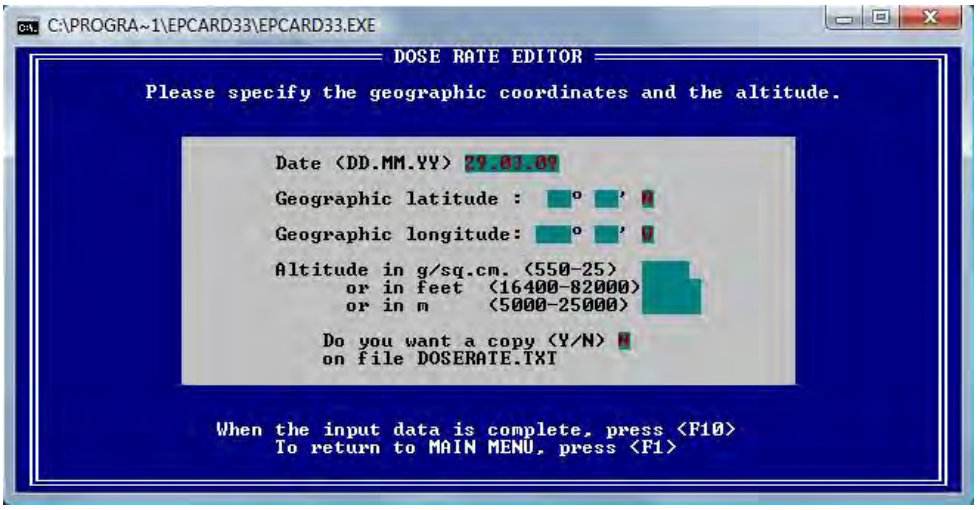

Figure VII.3 – Screenshot of EPCARD

C. EXPACS Description

EXPACS was originally developed in Japan by the Japan Atomic Energy Agency. Flight data is entered into an Excel-Based Spreadsheet as waypoints of latitude, longitude, and altitude. The program calculates vertical cut-off rigidity at the point of interest from a database built by "magnetocosmics." The day, month, and year are entered to calculate the "force field potential" (FFP), an index of solar activity based on the count rates of several ground-level Thule neutron monitors [36] which can be thought of as similar to the heliocentric potential and solar deceleration value described earlier. Its minimum and maximum periods are approximately 400 and 1200 MV, respectively. A special input is required (mass of aircraft) called the "surrounding environment and local effect parameter" – used for neutron spectra in aircraft. The radiation transport code utilized is called PARMA (PHITS based Analytical Radiation Model in the Atmosphere) [36]. The particle fluxes calculated from the input condition can be seen, unlike CARI-6M and EPCARD. An effective dose for the isotropic irradiation geometry is then calculated through dose conversion coefficients from ICRP60 and ICRP74. A summary of these coefficients are shown in Table VII.4. In this table, "protons, other than recoil protons with energies greater than 2 MeV" have a radiation quality factor of 2, leading EXPACS to under-estimate doses in comparison to EPCARD [37]. Figure VII.4 shows a partial screenshot of EXPACS in excel, the most compelling feature being the particle flux to energy graphs which are recalculated for each change of individual input variables.

Table VII.4 – Radiation Factors in EXPACS from ICRP 74 Recommendation [37]

Radiation Quality Factors[1]	
Type and Energy Range	Radiation Quality Factor, w_R
Photons, all energies	1
Electrons and muons, all energies[2]	1
Neutrons, energy < 10 keV	5
10 keV to 100 keV	10
> 100 keV to 2 MeV	20
> 2 MeV to 20 MeV	10
> 20 MeV	5
Protons, other than recoil protons, energy > 2 MeV	2
Alpha particles, fission fragments, heavy nuclei	20

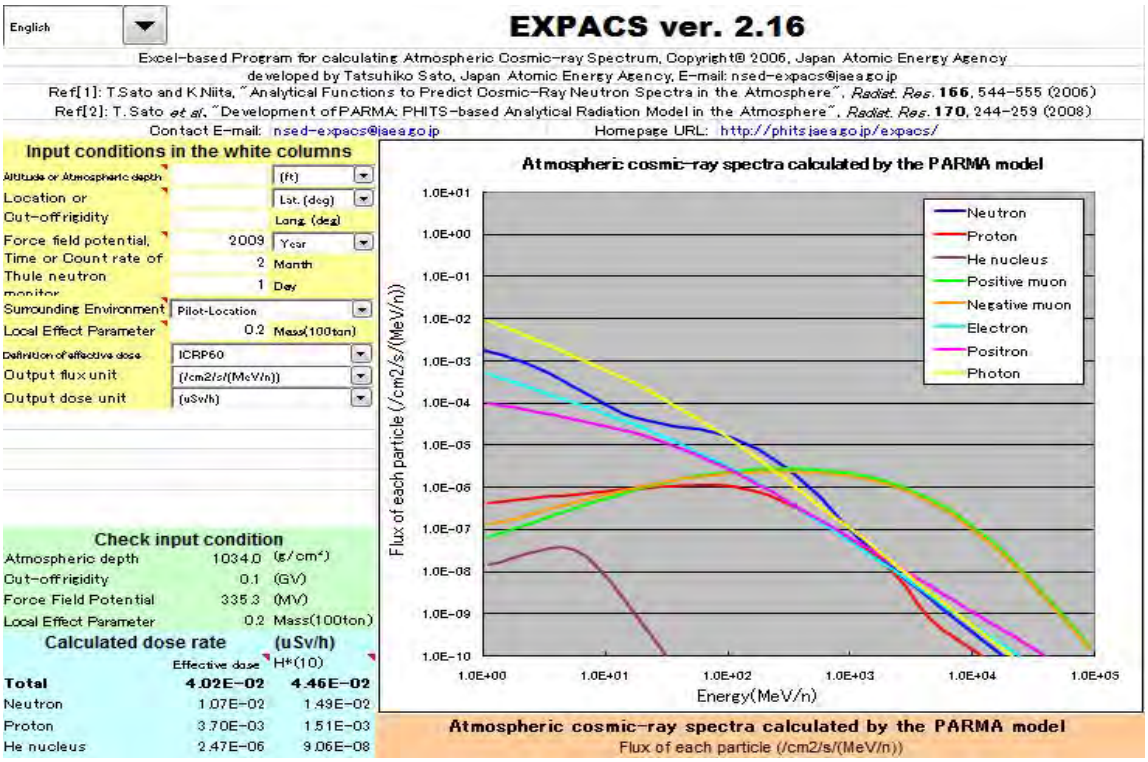

Figure VII.4 – A Partial Screenshot of EXPACS Program

After studying each individual commercial code, Table VII.5 summarizes the differences below. While the names for different sub-codes and values might change in the codes, they all still have the same structure: a transport code, a solar activity value, and a way to convert particle fluxes or fluences to a dose equivalent rate.

Table VII.5 – Summary of Predictive Code Characteristics

Predictive Code	Altitudes (feet)	Transport Code	Solar Activity Value	Input	Accounted Particles	Output
CARI-6	0-60,000	LUIN99	Heliocentric Potential	Lat, Long, Alt, Date	N,p,π,e,μ,γ, α, heavy ions	1. H_T 2. H*(10)
EPCARD	16,404-82,021	FLUKA	Solar Deceleration	Lat, Long, Alt, Date	N,p,π,e,μ,γ	1. H_T 2. H*(10)
EXPACS	0-65,617	PARMA	Force Field Protection	Lat, Long, Alt, Date, aircraft mass	N,p,α,π,e,μ,γ	1. H_T 2. H*(10)

Chapter VIII: Code Analysis and Comparisons

With over 40 hours of flight data, several important relationships of dose rate to altitude, time, and geographic position became apparent from the following analysis. Before data analysis proceeded, the codes' limitations had to be known. First, EPCARD will only accept altitude inputs greater than 16,400 feet up to 75,000 feet, whereas CARI-6 and EXPACS can accept any altitude input from 0 to 65,000 feet. Since most of the flight data was from commercial altitudes, this was an important consideration and lead to Table VIII.6, comparing the output of all three codes only when the aircraft was above 20,000 or 30,000 feet. Also, the input required for the time of flight varied by predictive code. EXPACS and EPCARD required day, month, and year information whereas CARI-6 only required a month and year.

Section A of this Chapter will discuss all the commercial and military flight data collected in the research while the second section will extend the analysis more specifically to EXPACS. Special attention was placed on determining the appropriate amount of error associated with each code and the TEPC. After considering all the previous research and personal communication with Dr. Lewis and Dr. Tatsuhiko, various ranges of error were used, but for this research project, only the most commonly used error bar discovered in previous research was implemented in the figures presented in the following sections. Considering the same flight was flown through the same atmospheric conditions on the same day, the commercial code outputs may vary as much as 10% for each total dose measured in-flight. The TEPC was found to have a maximum error of 25% for H_T measurements taken during flight [11].

A. Commercial and Military Flight Data

Seventeen flights were conducted in 14 different states during this research across the United States. Table VIII.1 lists the name and location of the airports visited in transit. After each flight, the data were analyzed and organized into Table VI.3, representing each flight flown with the detector. Figure VIII.1 represents a graphical summary of integrated dose equivalent as determined by the HAWK and the predictive codes in all the flights.

Table VIII.1 – List of Airports

Locator	Airport Title	State
BBA	Bay Bridge Airport	Maryland
ANN	Annapolis	Maryland
PAX	Patuxent River Naval Air Station	Maryland
BWI	Baltimore Washington-International Airport	Maryland
ATL	William B Hartsfield International Airport	Georgia
ABQ	Albuquerque International Sunport Airport	New Mexico
SLC	Salt Lake City International Airport	Utah
OKC	Will Rogers World Airport	Oklahoma
DFW	Dallas Fort-Worth International Airport	Texas
DTW	Detroit-Metro Airport	Michigan
CLT	Charlotte Douglas International Airport	North Carolina
GNV	Gainesville Regional Airport	Florida
BOS	Logan International Airport	Massachusetts
ORD	Chicago O'Hare International Airport	Illinois
IND	Indianapolis International Airport	Indiana
SFO	San Francisco International Airport	California
PHX	Phoenix Sky Harbor International Airport	Arizona

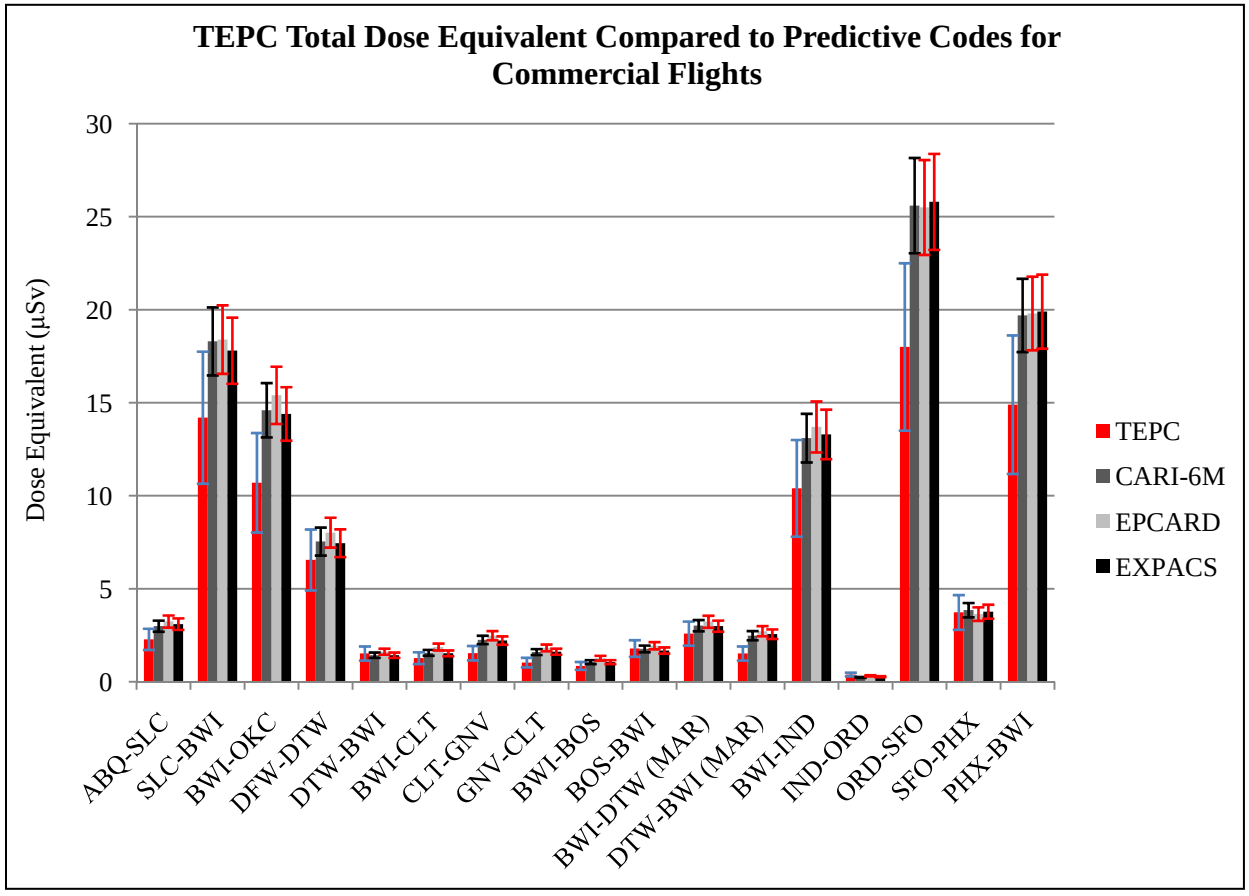

Figure VIII.1 – Summary of All Commercial Flights. Error bars based on 25% uncertainty in TEPC [11] and 10% uncertainty in commercial codes [11].

From Figure VIII.1, the flights were further classified as a high ($H_T > 8\mu Sv$), medium ($8\mu Sv > H_T > 1.5\mu Sv$), or low ($1.5\mu Sv > H_T$) exposure risk. These flights were then grouped together and depicted in corresponding figures below. The high exposure group is represented in Figure VIII.2, medium exposure in Figure VIII.3, and the low exposure flights in VIII.4. Presenting the flights in this way not only creates an easier graph to read and understand, but also provides the reader with a quick glimpse at the type of flight that leads to a high, medium, or low dose. For instance, a flight from Chicago to San Francisco leads to a much higher level of exposure than does a low exposure flight from Baltimore to Boston.

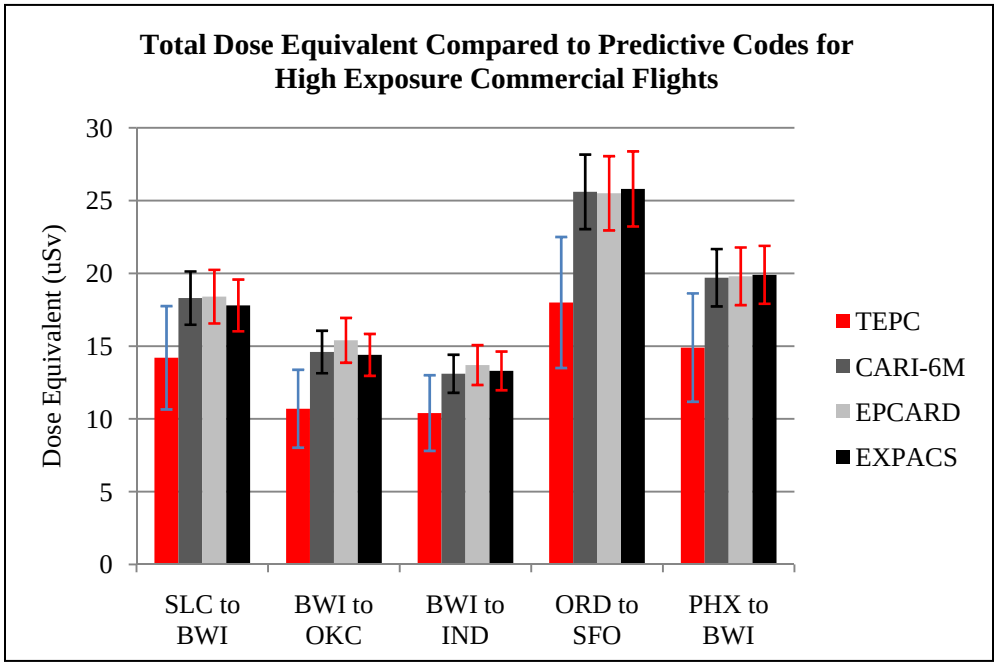

Figure VIII.2 – Summary of All High Exposure Risk Flights

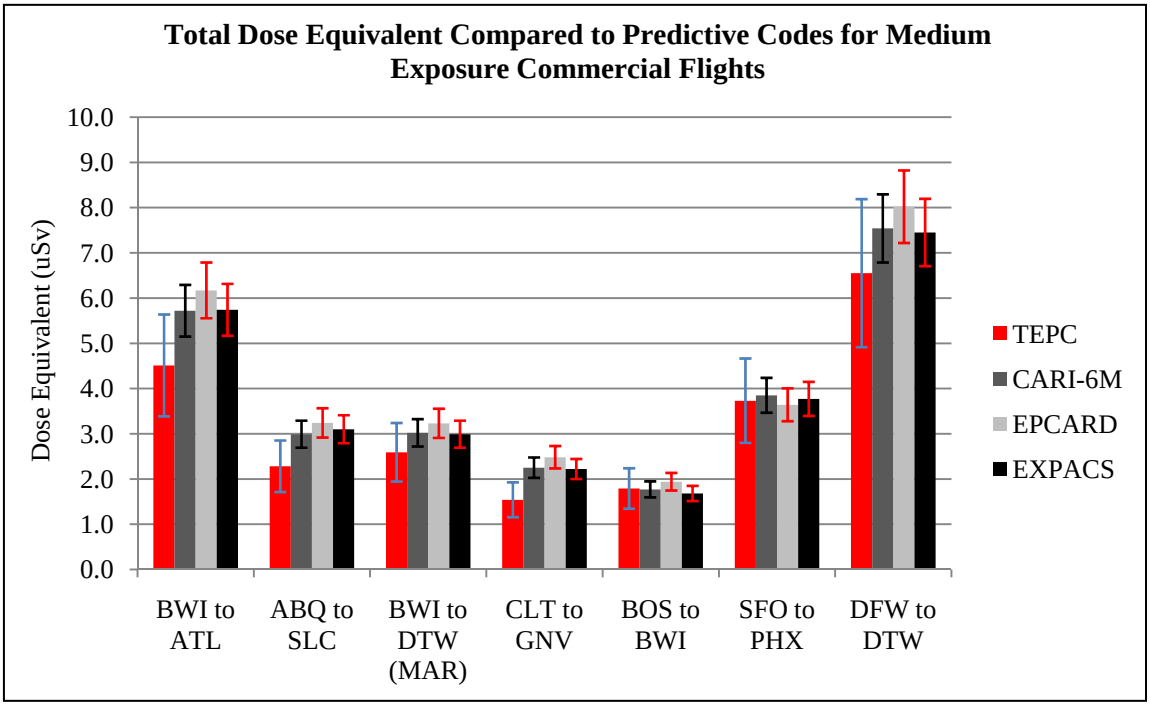

Figure VIII.3 – Summary of All Medium Exposure Risk Flights

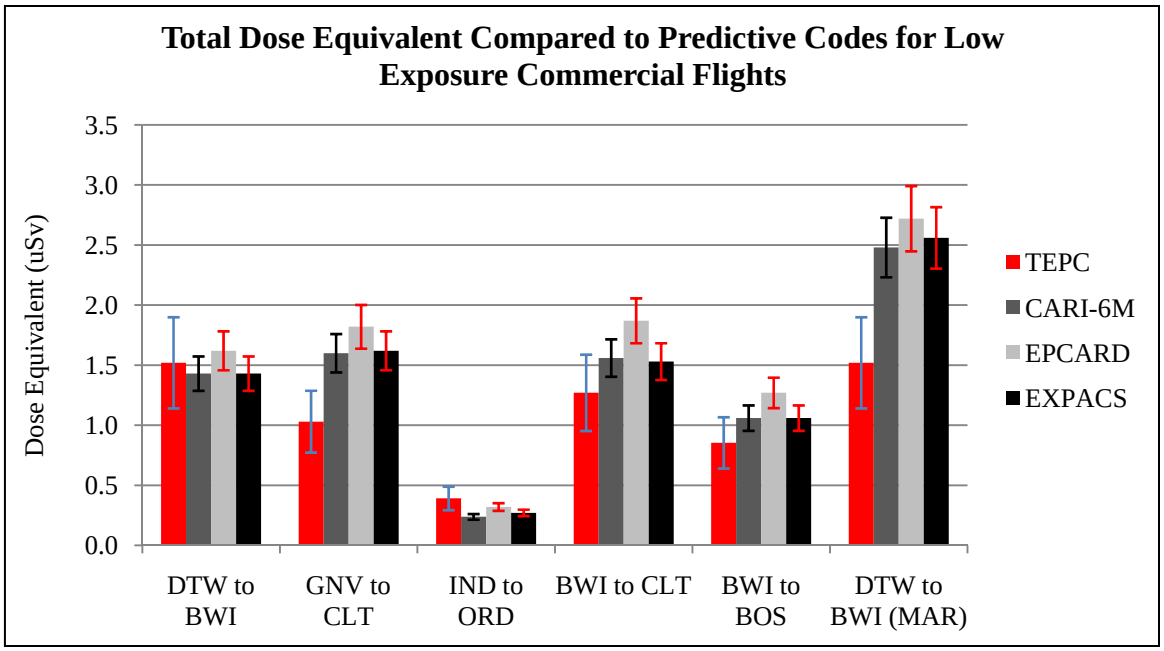

Figure VIII.4 – Summary of All Low Exposure Risk Flights

In addition to the commercial flights, two flights were also flown on a private aircraft and the EA-6B Prowler, shown in Figure VIII.5. While this is a limited data set, the TEPC H_T clearly exceeds the total dose predicted by the codes. Like the IND to ORD commercial flight, the commercial codes begin to underestimate as the altitude decreases. The breakdown becomes apparent in the data collected from flights of low duration and where the majority of dose is from altitudes <15,000 feet.

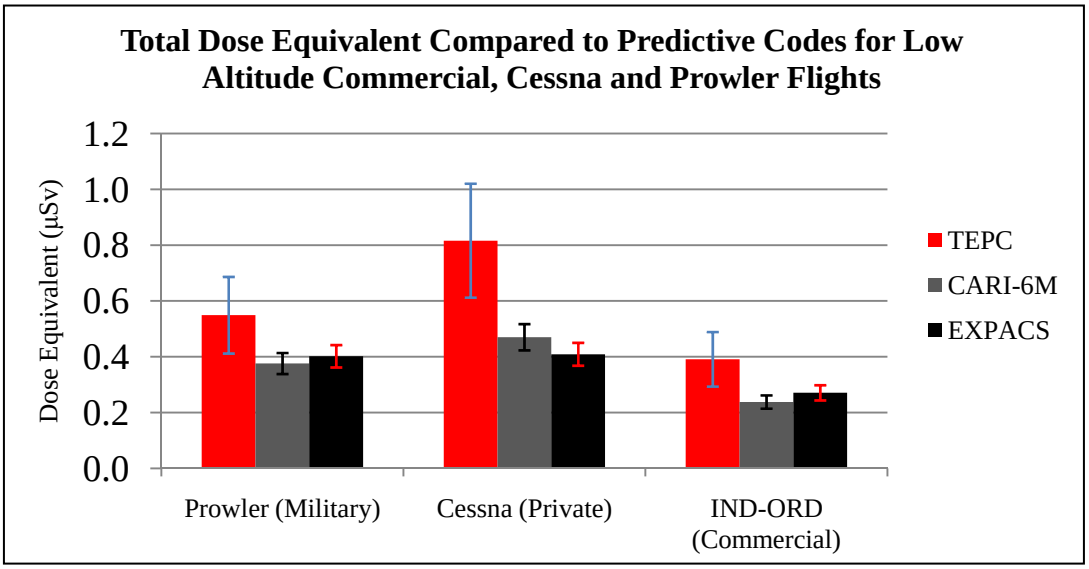

Figure VIII.5 – Commercial, Military, and Private Aircraft Flights

B. Dose Profile

As mentioned in earlier chapters, the risk associated with dose is closely related to the type of radiation received. An identical amount of low LET particles present less of a threat than exposure to the same amount of high LET particles. Below, the increased occurrence of q-factors greater than one is explored. Since high LET is considered to be above 10 keV/micron, it is not possible to classify both parts of the pie as high or low LET [12]. However, according to the ICRP-40 recommendation described in Section c of Chapter II, it is possible to assume greater biological harm may occur when the quality factor rises above one. As a result, for this section, all references to high LET will refer to the particles with a quality factor greater than one. In Figures VIII.6-VIII.8, comparisons of the percentage of high and low LET radiation contributing to the total dose are made between flights of high, medium, and low dose. In Figures VIII.6-VIII.8, the "Q" factor refers to the quality factor mentioned previously in Chapter II. Each pie chart shows the percentage of high LET to low LET detected by the TEPC during the flight's entire duration.

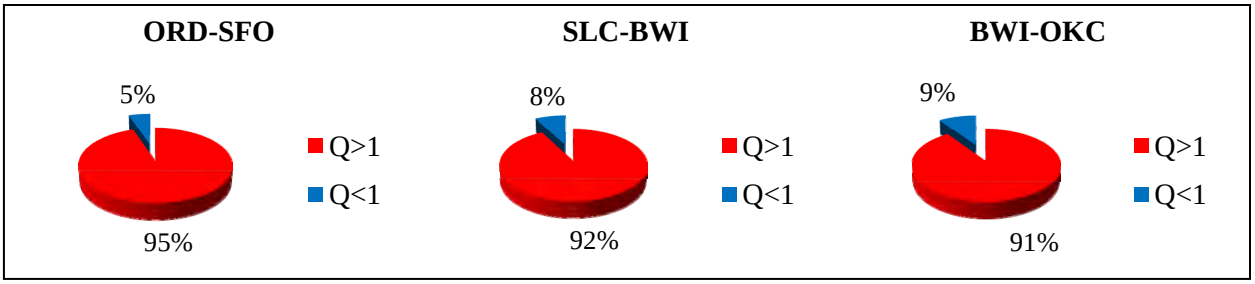

Figure VIII.6 – Dose Distribution of High and Low LET for High Dose Flights

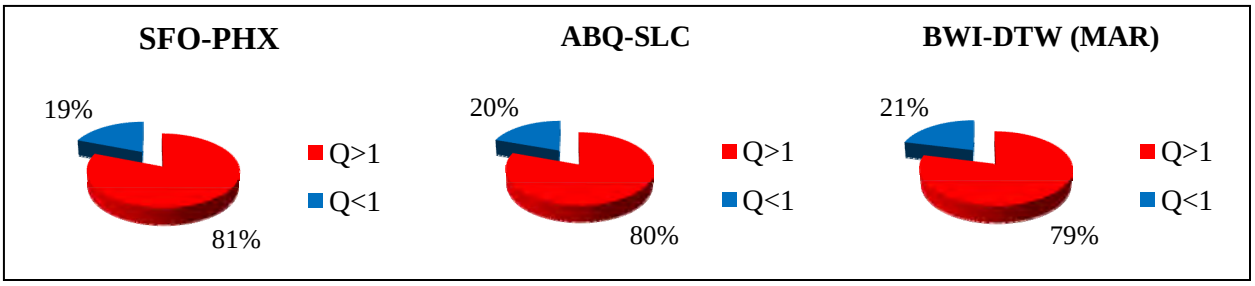

Figure VIII.7 – Dose Distribution of High and Low LET for Medium Dose Flights

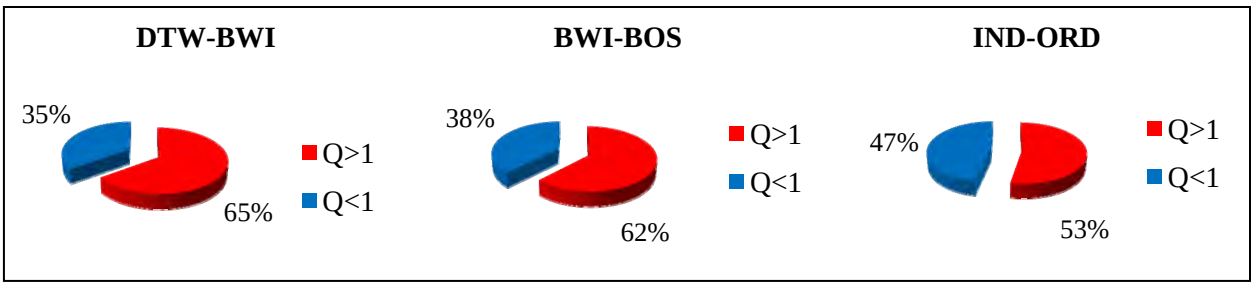

Figure VIII.8 – Dose Distribution of High and Low LET for Low Dose Flights

As can be seen in Figures VIII.6-VIII.8, the percentage of high LET particles recorded by the TEPC substantially increases from 53%-65% with flights of shorter duration and lower altitudes to 91%-95% with flights of longer duration and higher altitudes. When the percentage of high LET particles increases, the dose equivalent value rises accordingly as discussed in Chapter III.

The commercial codes may also be utilized to verify the percentages of high and low LET. Instead of evaluating the Q-factor per minute, both EPCARD and EXPACS output the percentage of total dose expected to be received by various particles, including neutrons, protons, alphas, pions, muons, electrons, positrons and photons. There are slight differences between the outputs of the two codes. EXPACS defines a dose for positrons, alpha particles, and positive and negative muons while EPCARD lumps pions into the proton dose and only has one muon group, including both charges. Pions are also not specifically addressed in EXPACS, just as alpha particles are not addressed in EPCARD. When evaluating EXPACS for percent composition calculations, the dose contribution of positrons was combined with electrons and labeled as "electrons." In EPCARD, the positive and negative muon contributions were combined in order to compare with EXPACS. All the commercial flights were analyzed with the predictive codes and Figure VIII.9 shows the particle contributions to the total dose for all the flights as calculated by EXPACS. Figures VIII.10-VIII.13 show the particle contributions as calculated by EPCARD.

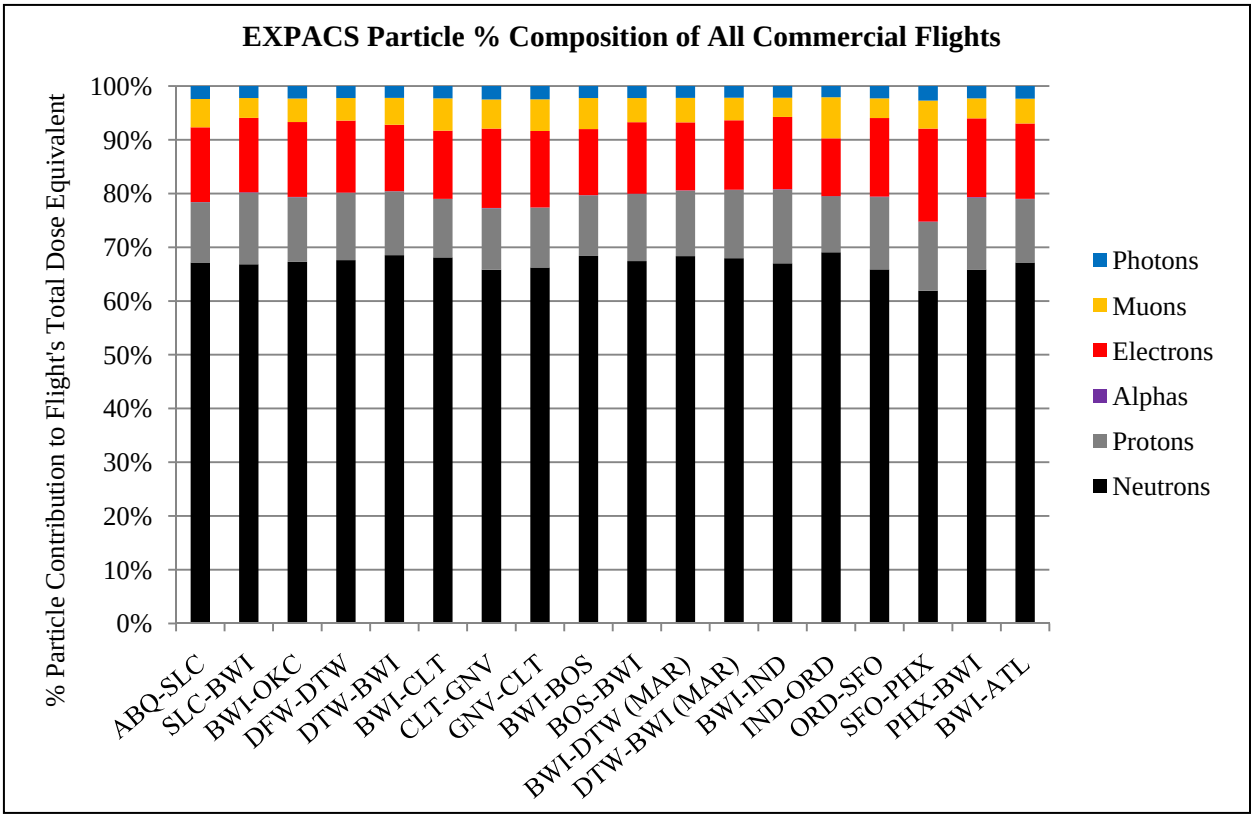

Figure VIII.9 – Particle Dose Contributions for All Commercial flights, Calculated by EXPACS

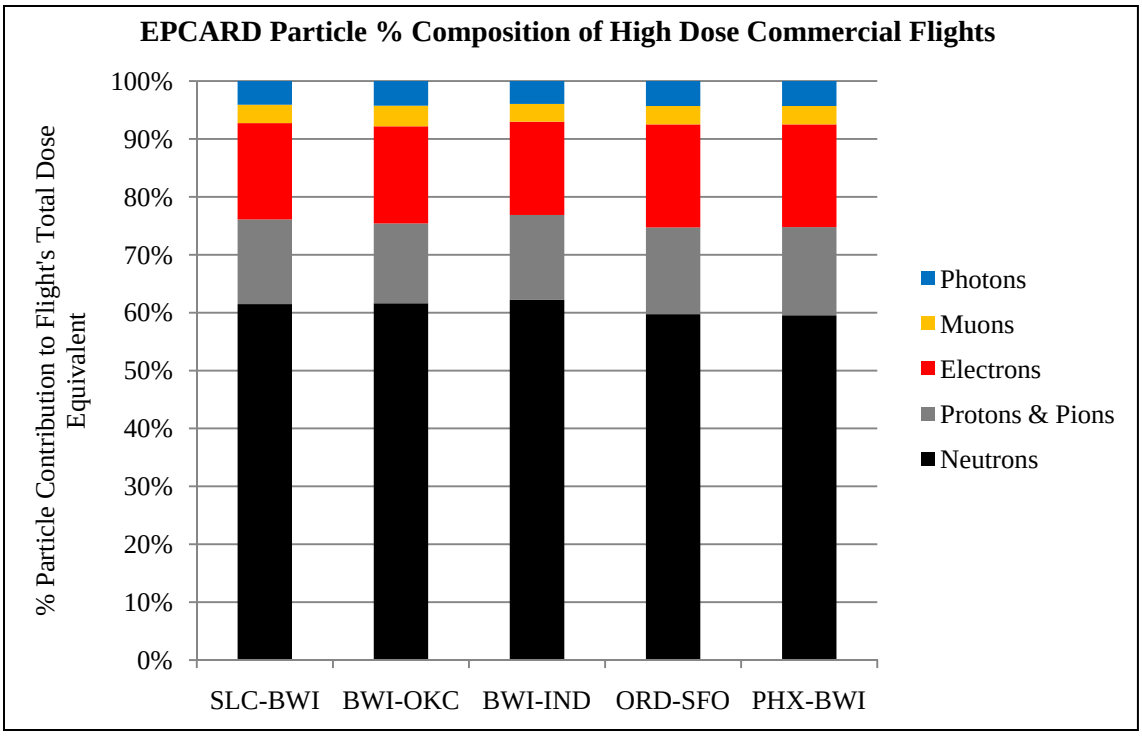

Figure VIII.10 – Particle Dose Contributions for High Dose Flights, Calculated by EPCARD

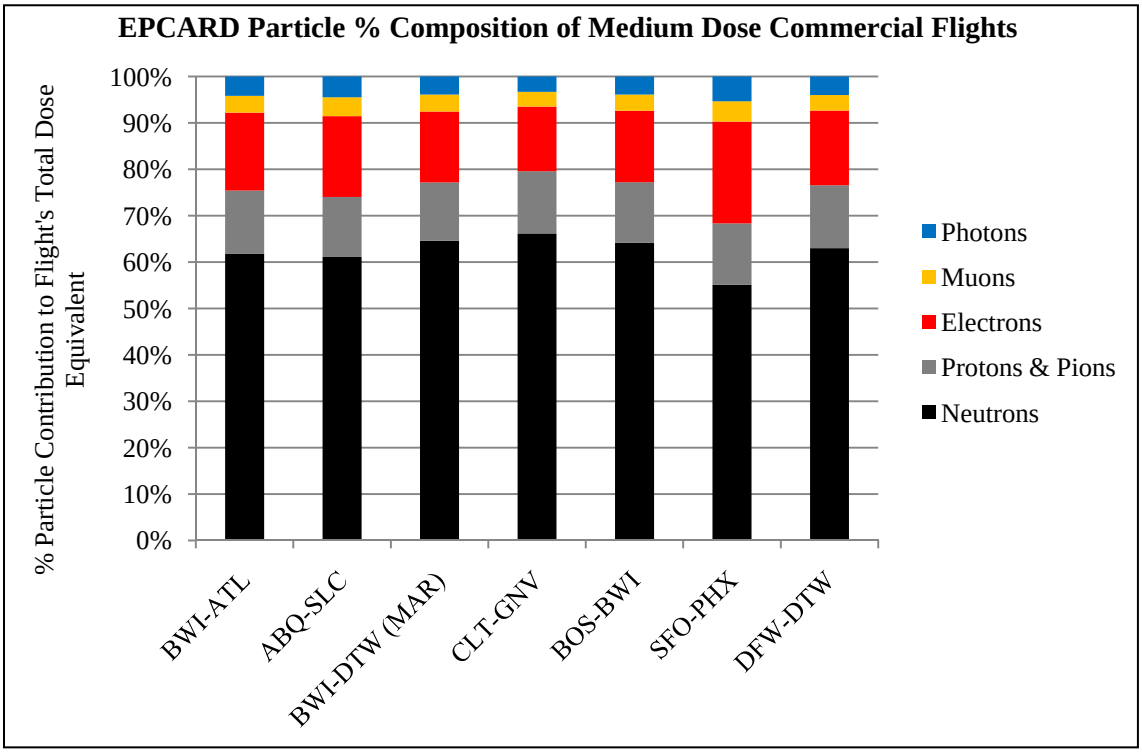

Figure VIII.11 – Particle Dose Contributions for Medium Dose Flights, Calculated by EPCARD

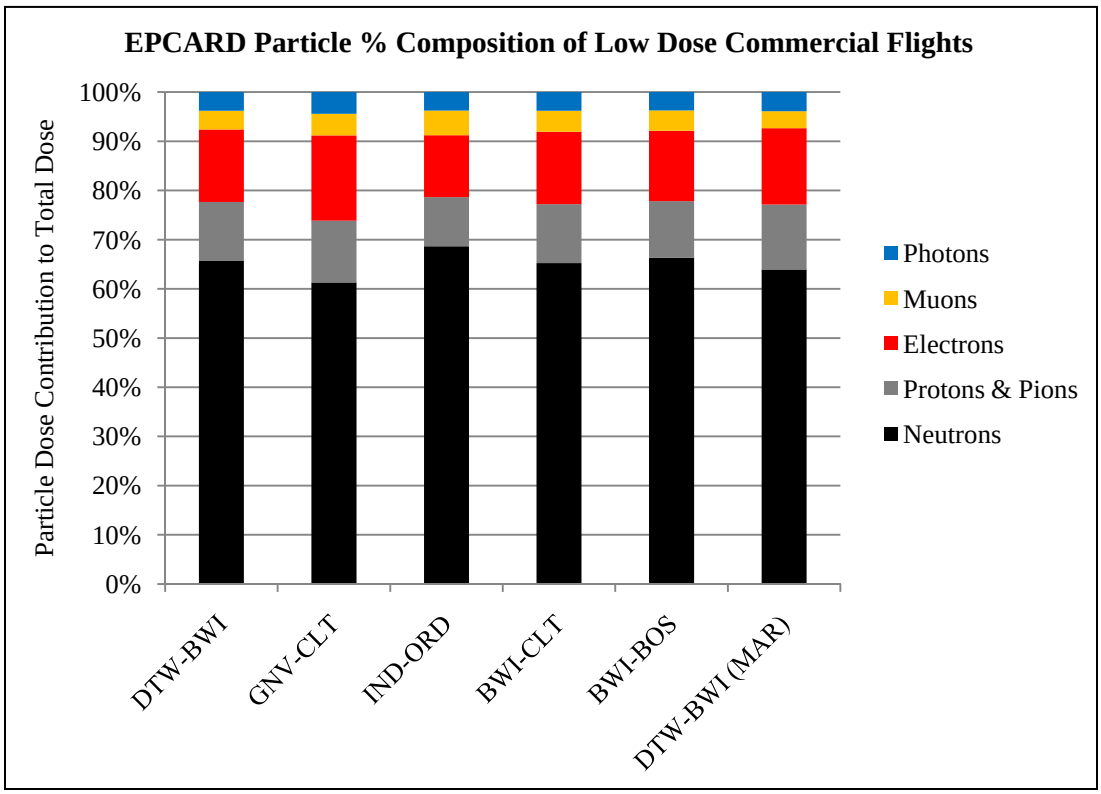

Figure VIII.12 – Particle Dose Contributions for Low Dose Flights, Calculated by EPCARD

As can be seen in Figures VIII.10 – VIII.12, the percentages of different particles significantly change given the duration and altitude of the flight. For instance, flights of high dose have a greater percentage of protons and pions, whereas the percentage of dose from neutrons hovers around 60%. In addition, the higher dose flights also have a greater percentage from photons and electrons. As the altitude and duration increases, the abundance of protons begins to increase, possibly from the solar activity of the sun and the higher energy neutrons colliding with nuclei, especially the helium-3 nucleus which leads to a proton being produced in the reaction with a Q-value of 0.764 MeV [21] described below:

$$ {}^{3}_{2}He + {}^{1}_{0}n \rightarrow {}^{3}_{1}H + {}^{1}_{1}p \qquad \text{(VIII.1)} $$

In Figure VIII.13, the Cessna and Prowler Flights both had reduced amounts of protons and electrons because of their lower altitude and duration. There was also an increased percentage of muons contributing to the total dose.

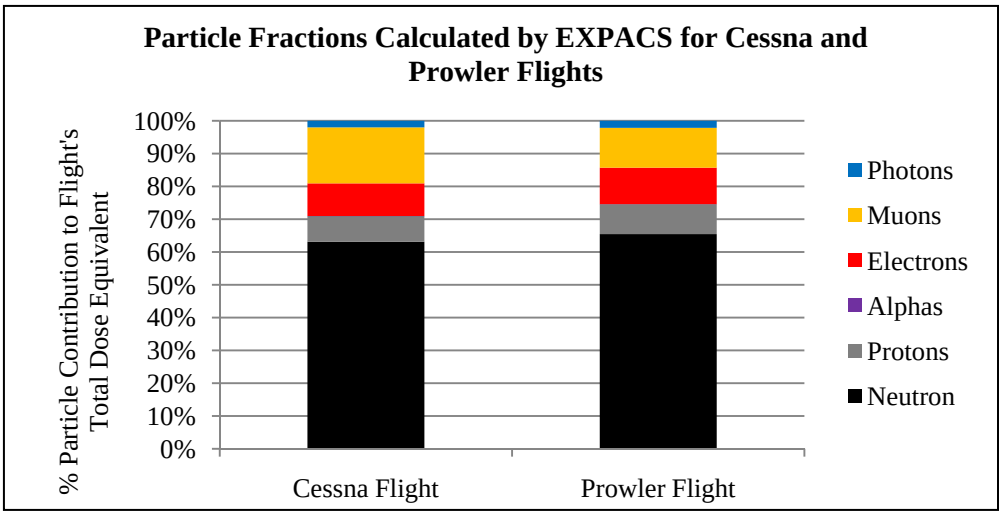

Figure VIII.13 – Particle Dose Contributions for Private and Military Flights, Calculated by EXPACS

By analyzing these graphs, it becomes apparent that neutrons represent a large percentage of the total dose. Also, the percentages of high and low LET recorded by the TEPC in Figures VIII.6–VIII.8 relate loosely to the dose percentages of specific particles predicted by the codes. While electrons, photons, and positrons are typically considered low LET particles, at lower altitudes like those experienced in the low and medium dose flights, the initial energy of a particle colliding with the aviator has already been significantly reduced after traveling through the majority of the atmosphere. Therefore, typically high LET particles like protons, neutrons, pions, and muons might actually deposit lower amounts of energy across a chord length, resulting in a quality factor of one and distorting the percentages encountered in Figures VIII.6-VIII.8 and Figures VIII.9-VIII.13. Regardless, the contribution of particles with a Q-factor greater than one, for almost all the commercial flights, falls between a range of approximately 60 to 95%, based primarily on how many high energy neutrons and protons are present.

C. Microdosimetric Spectra

Microdosimetric spectra are commonly utilized in the field of radiation health as a means to discriminate between particles with varying lineal energy. Plotted on a log-log scale, the spectrum represents the lineal energy, y, as $y \cdot D(y)$ versus y, where $D(y)$ is the absorbed dose defined in Appendix E [38]. In this manner, equal areas under different regions of the curve equal identical dose. In order to generate these plots, a spectrum was first created from the original TEPC data using the program called SPECT2 [19]. Then a series of mathematical procedures were followed as described in Appendix E to create the discrete values which were later graphed as a scatter plot connected with a line between data points. Microdosimetric spectrums were generated for the flights from ORD to SFO, BWI to OKC, BOS to BWI, and BWI to CLT. Figure VIII.14 shows all four flights on the same plot, initially revealing the disparity in total dose experienced on the flights. In addition, the ends of the spectrums also slightly decrease as the duration and altitude of the flight decreases. This demonstrates an interesting correlation for data taken up to 38,000 feet, as altitude increases, more particles with higher LET are more likely to be measured and cause biological harm to the somatic cell.

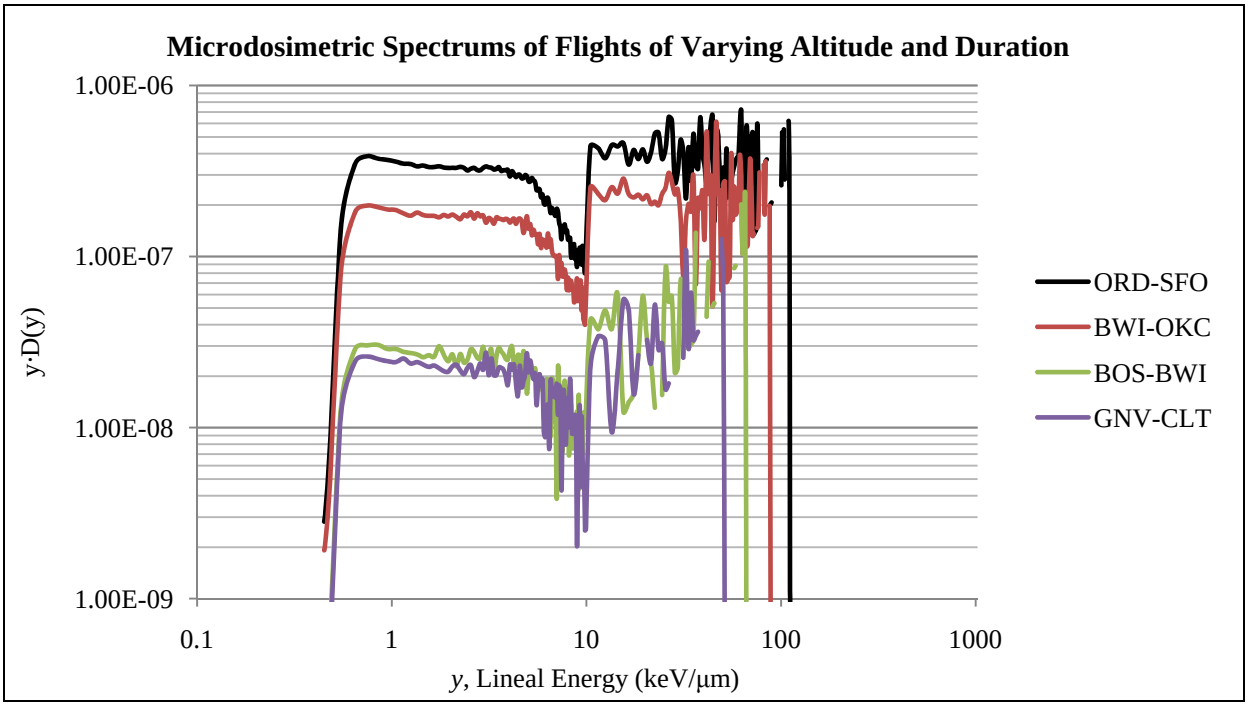

Figure VIII.14 – Selected Microdosimetric Spectrums of Decreasing Altitude and Duration Flights

Figures VIII.15-VIII.18 depict the individual flights, revealing spectra which consist of primarily two regions of interest. The first region represents the amount of dose from low energy electrons and photons, depositing less than 10 keV/micron. From 10 keV/micron to about 100 keV/micron represents the dose from high LET neutrons, protons, pions, and heavy ions that may increase in occurrence as altitude increases. Counts occasionally appear above 100 keV/micron from high energy recoils and heavy ions, but they are usually very rare events, and are not necessary in depicting the more important trends that occur around 100 keV/micron and below. As the flight increases in duration and altitude, notice that the span and integrated value of the resonance region protons and neutrons increases considerably.

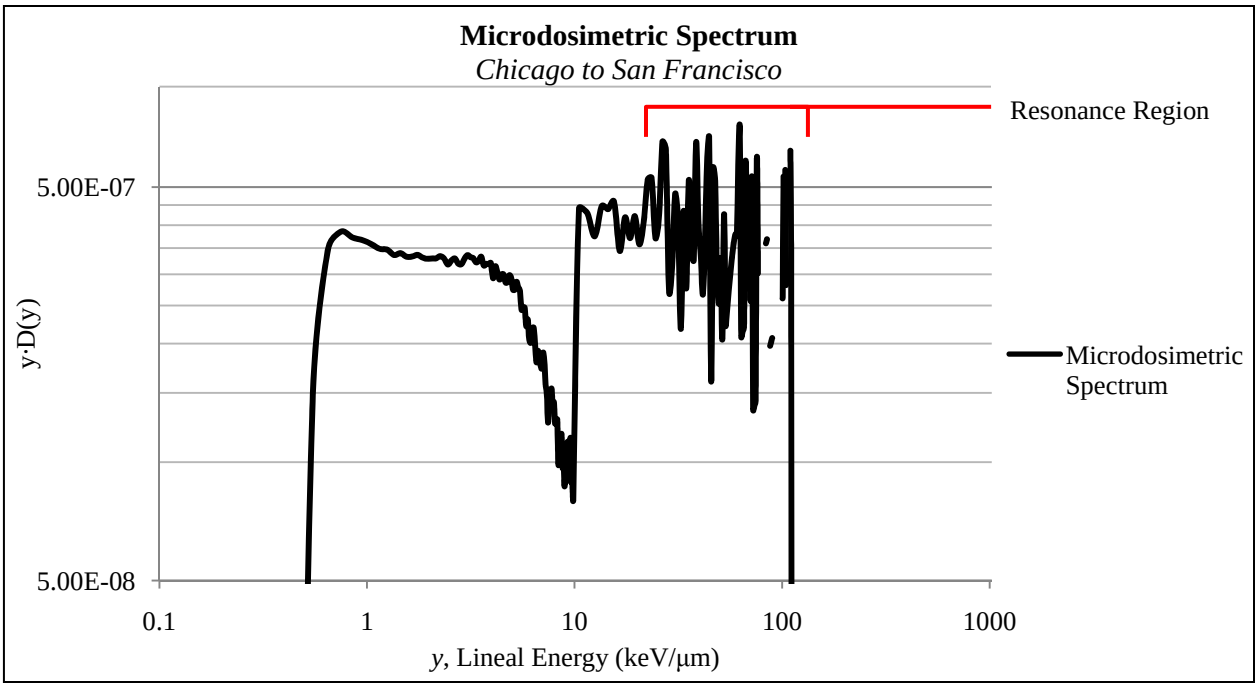

Figure VIII.15 – Microdosimetric Spectrum for Flight from ORD to SFO

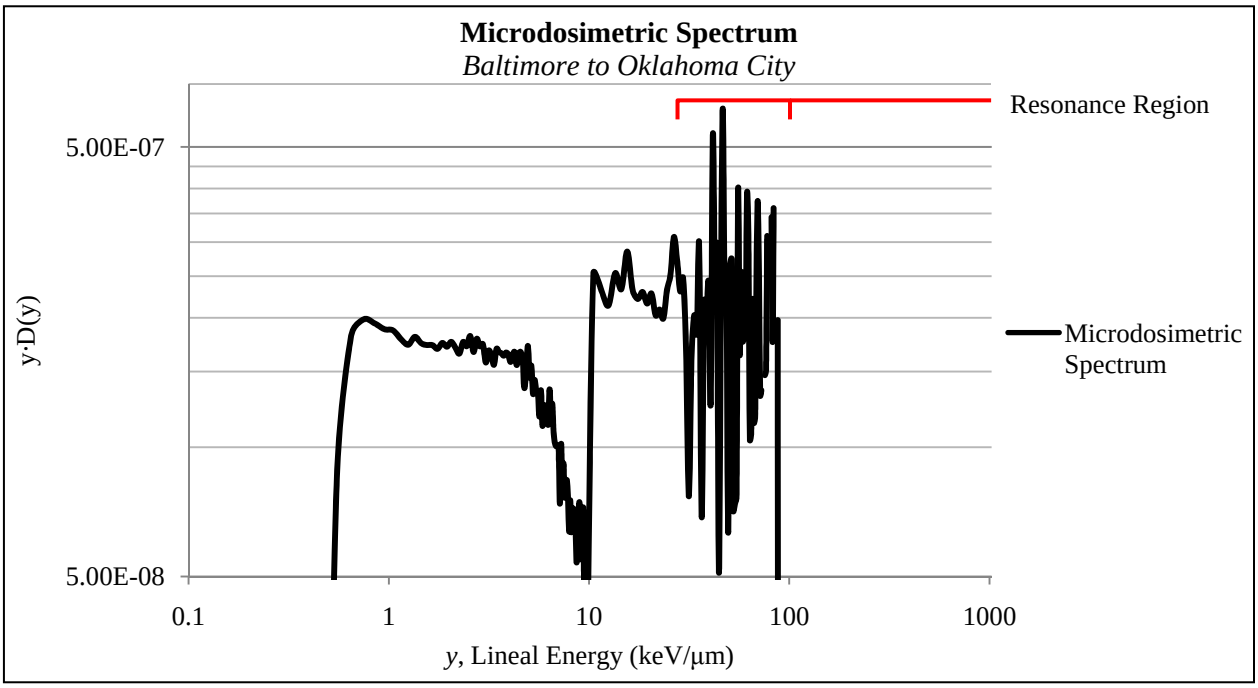

Figure VIII.16 – Microdosimetric Spectrum for Flight from BWI to OKC

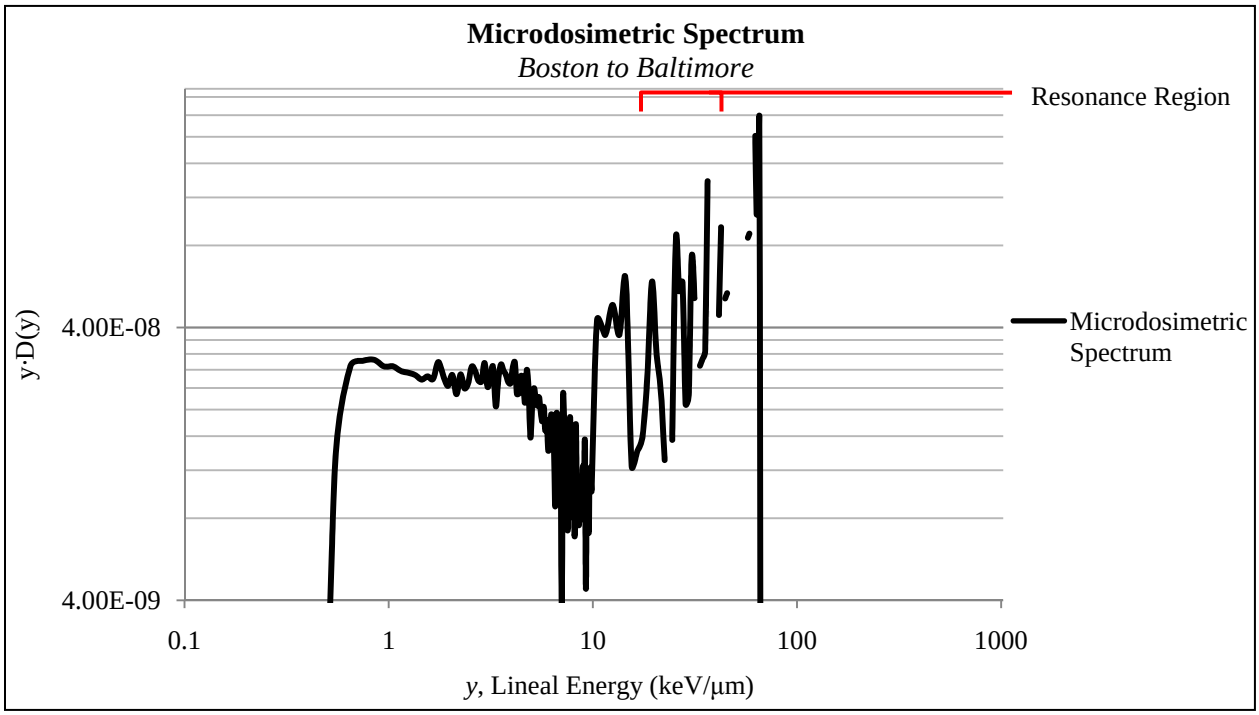

Figure VIII.17 – Microdosimetric Spectrum for Flight from BOS to BWI

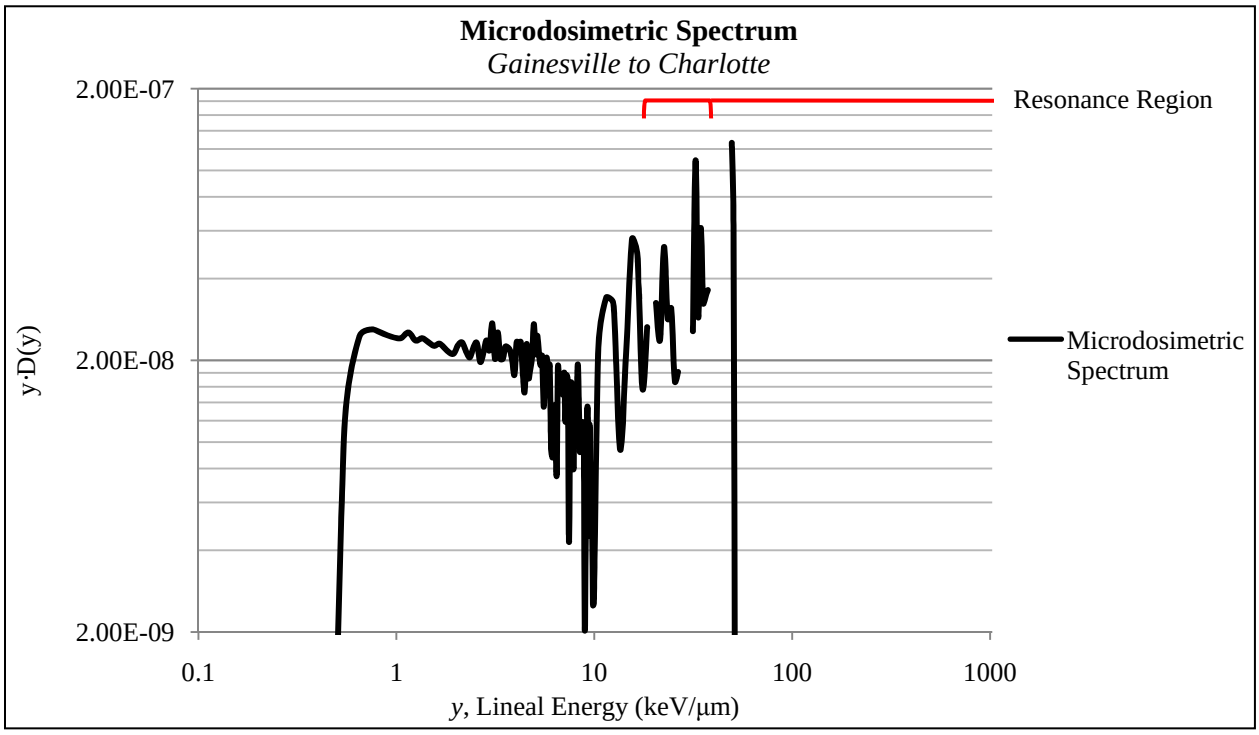

Figure VIII.18 – Microdosimetric Spectrum for Flight from GNV to CLT

D. Further Analysis of EXPACS with Simulated Prowler Data

In addition to H_T measurements on the Prowler, a series of old navigation data was processed by the codes, referred to as "simulations." The data collected from the VX-23 squadron were unclassified and simply consisted of the latitude, longitude, altitude, and date of typical flights flown in the past. Table VIII.2 summarizes the database of old Prowler flights. The column labeled "Average Cruising Altitude (ft)" has two values separated with a backspace. The first number represents the average cruising altitude and the second number represents the duration of time the aircraft spent at that cruising altitude.

Table VIII.2 – Prowler Simulated Data Flights

Flights	Date	Start Time (Zulu)	End Time	Duration (mins)	Average Cruising Altitude (ft)	H_{tot}*(EXPACS) (uSv)	H_{tot}*(CARI-6) (uSv)
Pax River NAS	07AUG06	1450	1626	96	16888 / 23 min	0.49	0.58
Pax River NAS	04AUG08	1640	1828	108	25375 / 78 min	3.16	3.04
Pax River NAS	27MAR08	1758	1911	73	23635 / 54 min	1.93	1.85
Pax River NAS	08APR08	1403	1609	126	23711 / 99 min	3.16	3.06
Pax River NAS	03APR08	1752	1946	114	23445 / 60 min	1.96	1.86
			Total:	517 min (8 hrs 37 min)			

The altitude profiles of these Prowler Flights were useful for further analysis with EXPACS because they were short in duration and reached altitudes commonly flown by naval aviators. As a result, more simulations could be run with EXPACS in a reduced amount of time, demonstrating interesting aspects of EXPACS while also allowing the radiological environment experienced by naval aviators to be evaluated. The first analysis conducted strictly with EXPACS investigated the neutron energy dependent flux. The energy dependent flux is the scalar neutron flux divided by the neutron energy and has units of $\frac{neutrons}{cm^2 sec \cdot MeV}$.

When analyzing the changing radiation field in the atmosphere, an important observation is the subtle increase of proton dose as the flights increase in altitude and duration. At the same time, the contribution of neutrons to total dose decreases as the altitude begins to increase. This was modeled with EXPACS by choosing a specific position in the atmosphere and only modifying the altitude. then plotting the differences in flux. According to the theory of neutron energy dependent flux, as the energy, E, decreases, the logarithmic plots of the flux should reveal a slope greater than the inverse of the energy, 1/E, if there is neutron production [14]. In other words, if the flux is less than $\frac{1}{E}x$ and x represents the slope of the particle line, then absorption dominates production when x is greater than one and production dominates absorption when x is less than one. As can be seen in Figure VIII.19, EXPACS clearly agrees with the theory, as neutron flux patterns show a higher probability of neutron production as altitude decreases. Table VIII.3 also describes the regression fits for the various altitudes, directly showing the increasing slope with altitude.

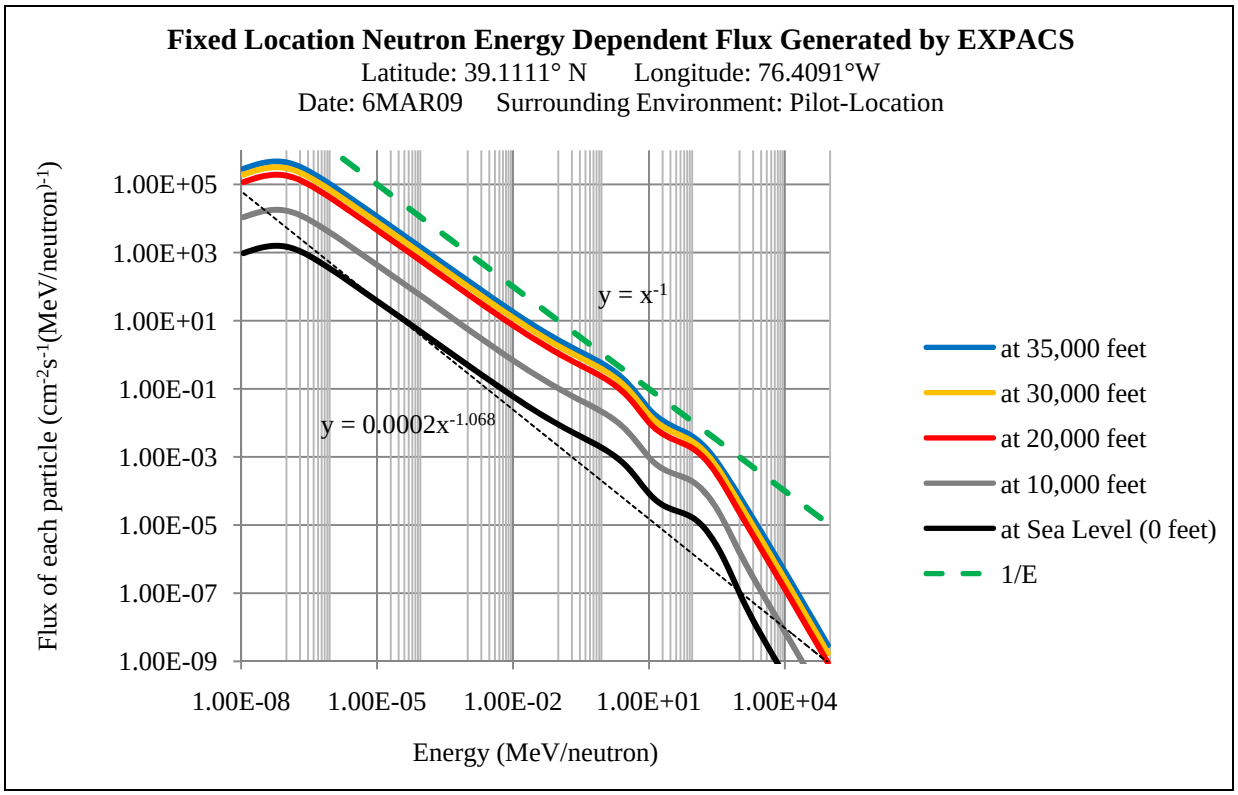

Figure VIII.19 – Neutron Energy Dependent Flux, Calculated by EXPACS

Table VIII.3 – Regression Analysis for Neutron Production of Decreasing Altitude

Altitude (feet)	Neutron Generation Equation
1/E	$Y = x^{-1}$
35,000	$Y = 0.0742 \cdot x^{-1.034}$
30,000	$Y = 0.0488 \cdot x^{-1.037}$
20,000	$Y = 0.0285 \cdot x^{-1.04}$
10,000	$Y = 0.0024 \cdot x^{-1.053}$
0 (Sea Level)	$Y = 0.0002 \cdot x^{-1.068}$

EXPACS typically plots all the particle fluxes on the same plot, however, Appendix G contains graphs where the individual particle flux graphs have been plotted while also varying the altitude to show how the energy dependent flux of individual particles varies with altitude. The purpose is to identify the flux expected from different particles at the low and high energy extremes. This would impact the type of radiation detector needed to measure the dose at certain altitudes in the atmosphere.

The next analysis with EXPACS demonstrates the variations of total dose achievable from input variables unique to EXPACS. These included the day of the month, weight of the aircraft, and detector location. By manipulating individual variables one at a time, a range of possible dose rates was calculated. First, the GPS Data from the Prowler flight on 08 April 2008 was utilized as a model flight profile. The same flight profile was then run through EXPACS 34 times, calculating how the total dose would change on a daily basis from February 1st, 2009 to March 6th, 2009. Below, Figure VIII.20 reveals the small effect date has had on the total dose during this time period.

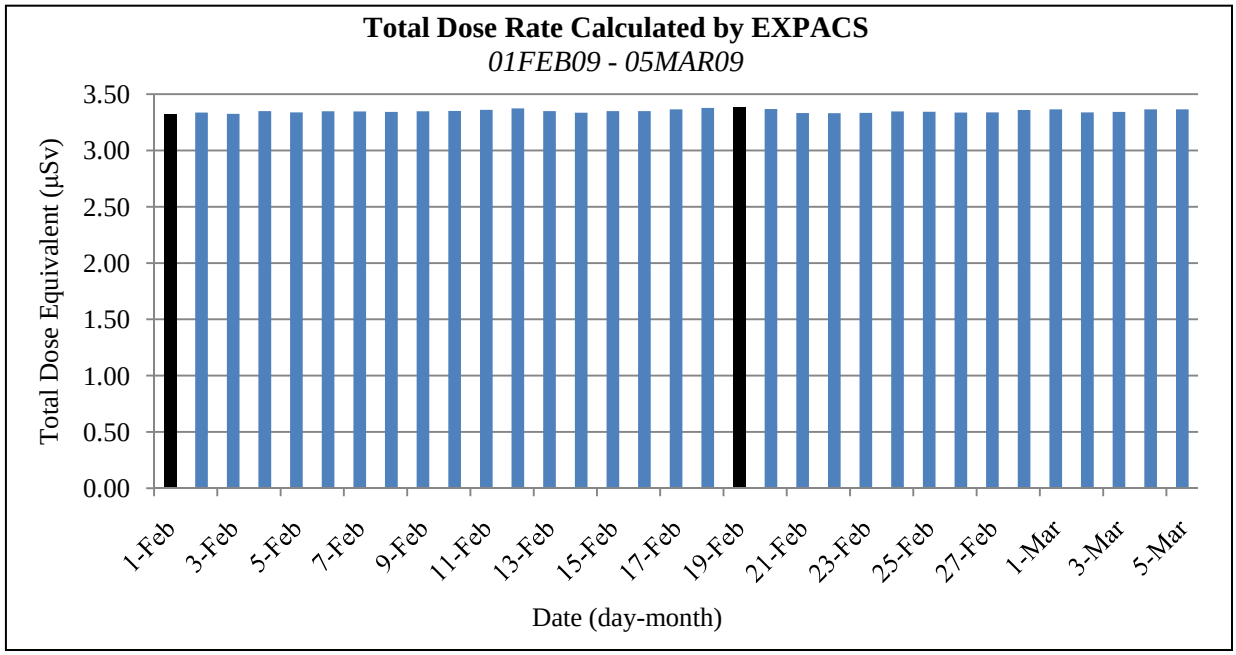

Figure VIII.20 – Daily Variations for Prowler Flight Calculated by EXPACS

Once this was done, February 1st and 19th were identified as the days with the highest and lowest total dose. Taking into account the maximum and minimum values recorded, the percent variation of dose over the time period of experiment was found to be less than three percent. Next, the input of weight was adjusted to the minimum and maximum values for the dates. These were set to 0.16 (16 tons), labeled as "light" and 5 (500 tons), labeled as "heavy." Additionally, the "surrounding environment" or simulated detector location variable was evaluated. These included "pilot-location, cabin, and none." The effects of these variables are shown in Figure VIII.21.

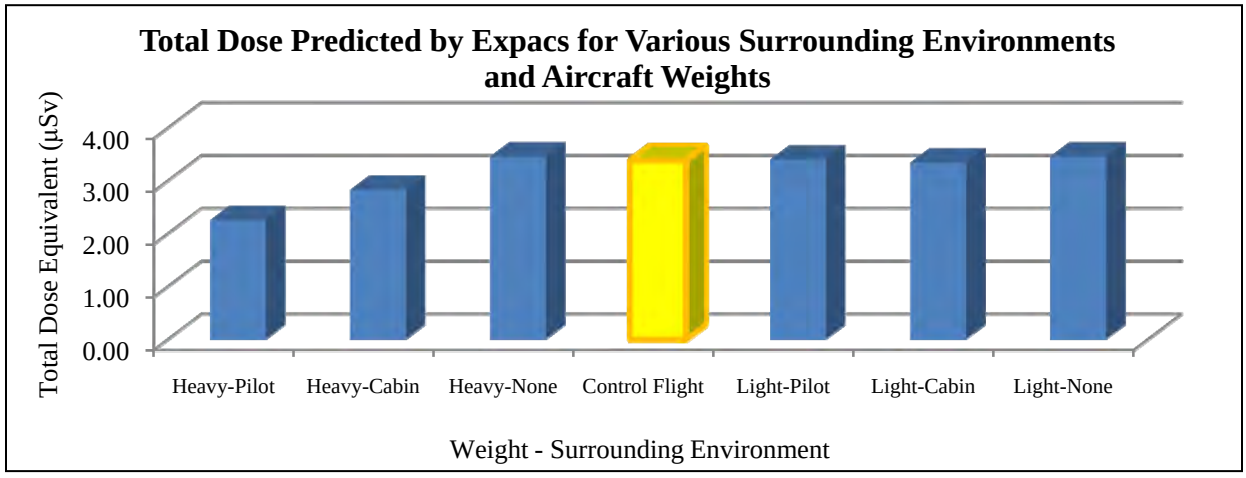

Figure VIII.21 – Variations of Calculated EXPACS Dose with Maximum and Minimum Weight Inputs and Various Surrounding Environments

After all these different runs, EXPACS showed a surprising adjustment to the dose rate calculated through its surrounding environment variable. As expected, the "none" variable, which took into account no shielding/location effect, predicted a greater total dose equivalent compared to the control flight. Meanwhile, the total dose equivalent was slightly lower for the cabin shielding in a light aircraft compared to the pilot shielding. When compared to the heavy or highly shielded aircraft, EXPACS predicted a lower dose for the pilot location. This discrepancy would have to be evaluated further in future research. Regardless, the Prowler weighed approximately 18 tons and EXPACS showed a variation less than 3% for the total dose when taking into account the positioning of the detector. The low variation in total dose makes EXPACS an appropriate tool for evaluating light aircraft, like most military platforms, especially the EA-6B Prowler. Regardless, the shielding effect variable should be evaluated in its entirety since research conducted earlier in this project showed a negligible canopy effect.

In Figure VIII.22, the latitude, longitude, altitude, and date were used from previous VX-23 Prowler flights to determine the effect of increasing altitude from 10 to 40 percent. By increasing the altitude profile for each minute of the flight by 40 percent, the dose equivalent rate was increased by approximately 145% when compared to the control flight, clearly demonstrating the importance of the vertical cut-off rigidity factor in determining radiation dose from the commercial codes. After the control flight's latitude was increased from 10 to 40 percent, only an approximately 22% increase in dose was predicted. Unlike altitude, Figure VIII.23 shows the much smaller, less linear effect of increasing latitude by 10 to 40 percent.

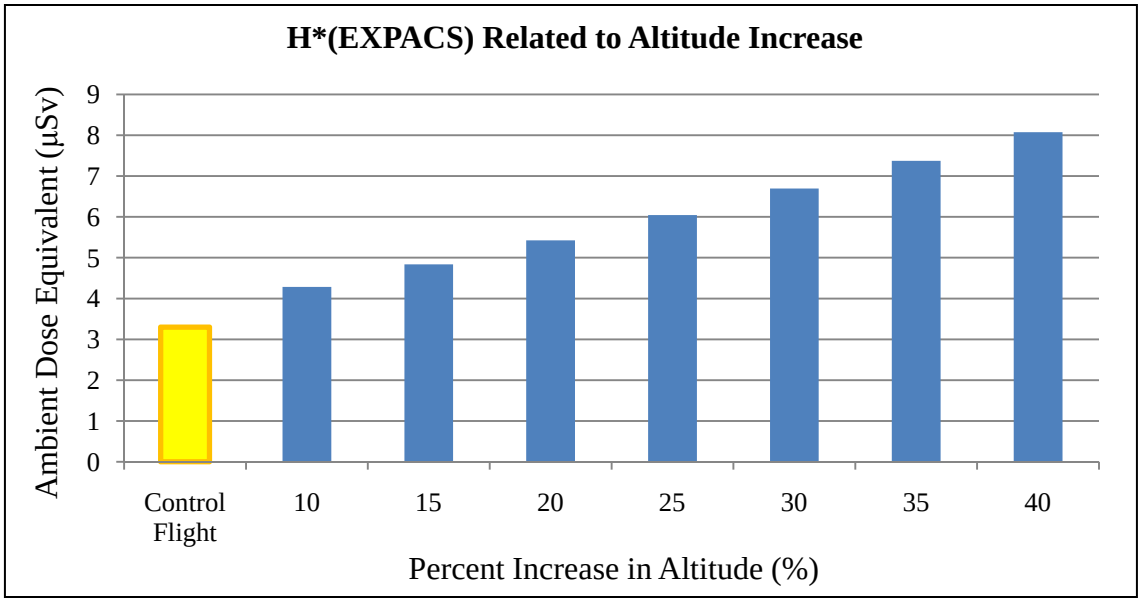

Figure VIII.22 – Effects of Altitude on Calculated EXPACS Dose

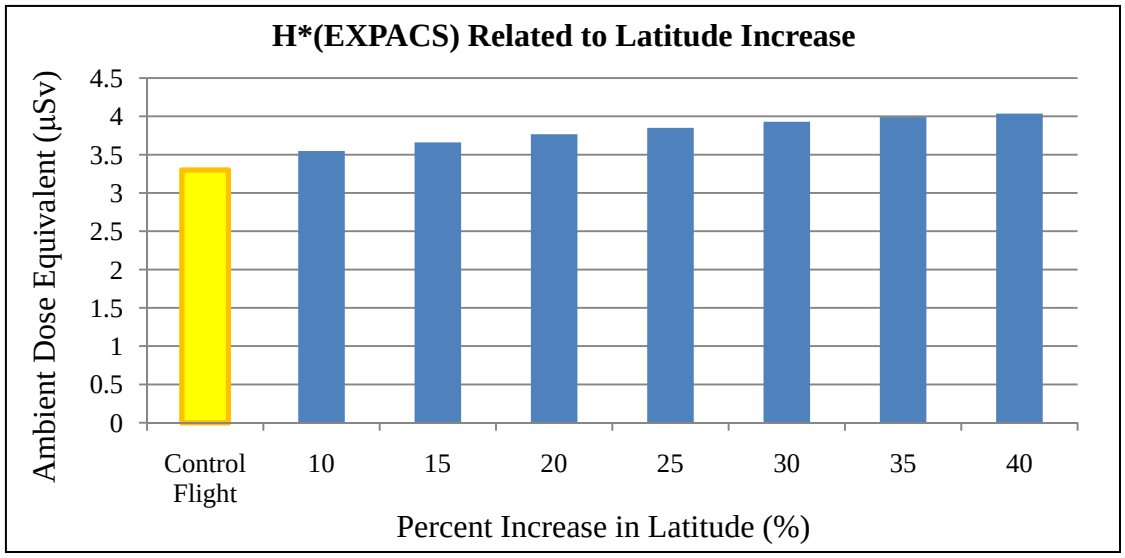

Figure VIII.23 – Effects of Latitude on Calculated EXPACS Dose

E. Code Comparison

After evaluating the unique inputs of EXPACS, the dose equivalent of each flight was compared to actual TEPC dose equivalent measurements in-flight and the ambient dose equivalents of EPCARD, CARI-6, and EXPACS. In order to do this, only the dose data above 20,000 feet, shown in Table VIII.3, was considered. Note, the four columns from the right have two numbers separated by a forward slash. The first number refers to the dose during the duration of the flight above 20,000 feet. The second number refers to the dose during the duration of the flight above 30,000 feet.

Table VIII.4 – TEPC Total Dose Equivalent Measured and Predicted by Codes for Altitude Greater than 20,000 and 30,000 Feet

Flights	Altitude >20,000 ft (min)	Average Cruising Alt. (ft)	Altitude >30,000 ft (min)	Average Cruising Alt. (ft)	$H_{T,tot}$ (uSv)	H_{tot}*(EXPACS) (uSv)	H_{tot}*(EPCARD) (uSv)	H_{tot}*(CARI-6) (uSv)
ABQ-SLC	56	28907	16	30583	2.28/0.726	3.10/0.987	3.24/1.01	2.99/0.961
SLC-BWI	170	35114	157	35969	14.2/13.8	17.8/17.3	18.4/17.5	18.3/17.8
BWI-ATL	84	30346	56	33701	4.51/3.79	5.74/4.81	6.17/5.10	5.72/4.86
BWI-OKC	182	32318	166	33057	10.7/10.2	14.4/13.8	15.4/14.7	14.6/14.0
DFW-DTW	90	32045	81	33217	6.55/6.29	7.45/7.20	8.02/7.73	7.54/7.31
DTW-BWI	26	27369	12	30213	1.52/0.713	1.43/0.838	1.62/0.940	1.43/0.849
BWI-CLT	39	25373	0	n/a	1.27	1.53	1.87	1.56
CLT-GNV	42	29157	23	32104	1.54/1.02	2.22/1.51	2.48/1.64	2.25/1.55
GNV-CLT	36	27668	0	n/a	1.03	1.62	1.82	1.60
BWI-BOS	26	25020	0	n/a	0.854	1.06	1.27	1.06
BOS-BWI	25	29626	14	33660	1.79/1.46	1.68/1.25	1.94/1.43	1.77/1.34
BWI-DTW	44	29372	29	31298	2.59/1.84	2.99/2.29	3.23/2.45	3.02/2.87
DTW-BWI2	32	31017	23	33267	1.52/1.34	2.56/2.17	2.72/2.28	2.48/2.11
BWI-IND	121	34979	108	36291	10.4/9.87	13.3/12.8	13.7/13.1	13.1/12.7
IND-ORD	12	20138	0	n/a	0.391	0.271	0.320	0.238
ORD-SFO	227	37045	218	37544	18/17.6	25.8/25.4	25.5/25.1	25.6/25.3
SFO-PHX	62	31984	44	35026	3.73/3.22	3.77/3.2	3.64/3.05	3.85/3.21
PHX-BWI	186	36132	175	36829	14.9/14.6	19.9/19.5	19.8/19.4	19.7/19.3
Total:	**1376**	**Total:**	**1066**					

For ease of presentation, the flights have been reorganized in order of decreasing duration and altitude. The data in Table VIII.5 has been plotted on Figure VIII.25 for the flights with altitude greater than 20,000 feet and on Figure VIII.26 for flights with altitudes greater than 30,000 feet. The relationship with altitude and the measured and predicted dose equivalents are shown in Figure VIII.24. By averaging only the altitudes above 20,000 feet and then dividing by the duration of time the plane was above 20,000 feet, an average dose equivalent rate was determined for each flight described in Table VIII.4. Figure VIII.24 shows the commercial codes over-estimation of the dose as a function of altitude.

Table VIII.6 shows the ratios of the three commercial codes to the measured value from the HAWK. As the ratios deviate from one, they are in less agreement and when they are closer to one, the ratios indicate a stronger agreement. The data shows fairly accurate agreement, around 25% from the predictive codes for doses of 0.4 to 14.9 μSv as measured by the HAWK.

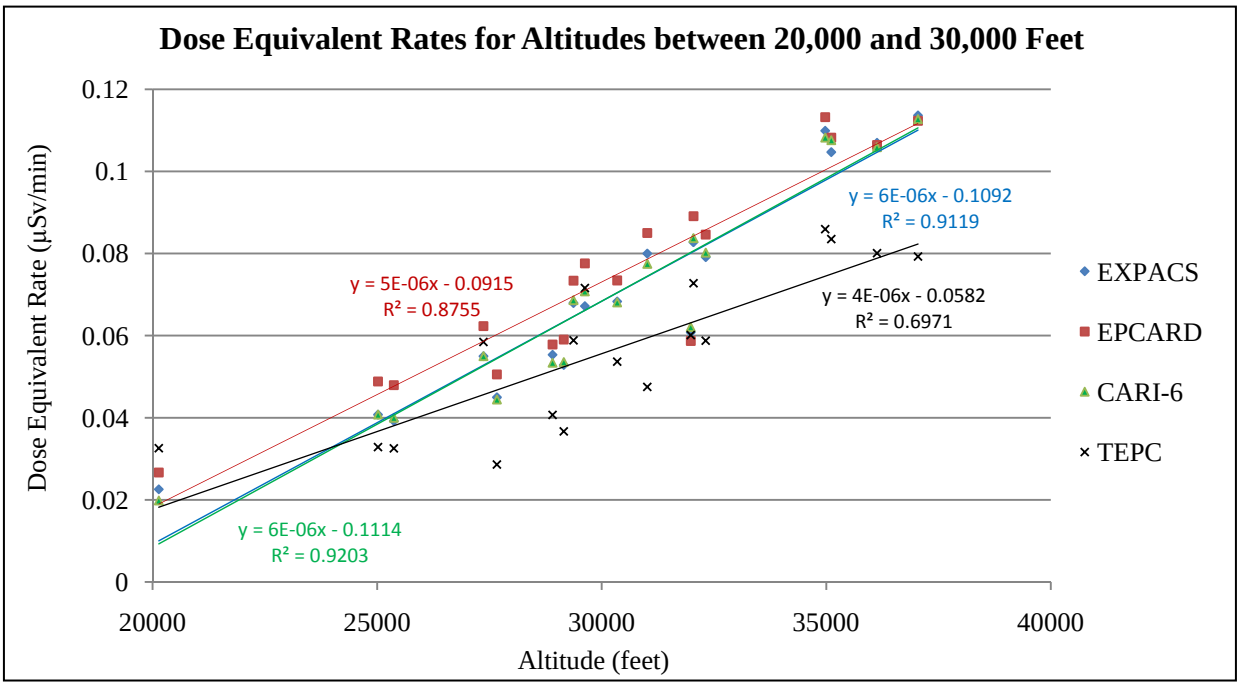

Figure VIII.24 – Average Dose Equivalent Rate vs. Altitude

Table VIII.5 – Flight Departure and Destination Information

Flight #	Flight Departure	Flight Destination
1	ORD	SFO
2	PHX	BWI
3	SLC	BWI
4	BWI	OKC
5	BWI	IND
6	DFW	DTW
7	BWI	ATL
8	SFO	PHX
9	BWI	DTW
10	ABQ	SLC
11	BOS	BWI
12	CLT	GNV
13	DTW(MAR)	BWI(MAR)
14	DTW	BWI
15	BWI	CLT
16	GNV	CLT
17	BWI	BOS
18	IND	ORD

Table VIII.6 – Ratio of H*(TEPC) to Commercial Code H*(10) values

Flights	Average (μSv)	H_T/H_{tot}*(EXPACS)	H_T/H_{tot}*(EPCARD)	H_T/H_{tot}*(CARI-6)
ABQ-SLC	2.28	.735	.704	.763
SLC-BWI	14.2	.798	.772	.776
BWI-ATL	4.51	.786	.730	.788
BWI-OKC	10.7	.743	.695	.733
DFW-DTW	6.55	.879	.817	.869
DTW-BWI	1.52	1.063	.938	1.063
BWI-CLT	1.27	.83	.679	.814
CLT-GNV	1.54	.694	.621	.684
GNV-CLT	1.03	.636	.566	.644
BWI-BOS	.854	.806	.672	.806
BOS-BWI	1.79	1.065	.923	1.011
BWI-DTW	2.59	.866	.802	.858
DTW-BWI2	1.52	.594	.559	.613
BWI-IND	10.4	.782	.759	.794
IND-ORD	0.39	1.443	1.222	1.643
ORD-SFO	18	.698	.706	.703
SFO-PHX	3.73	.989	1.025	.969
PHX-BWI	14.9	.749	.753	.756

The additional column showing the H_T value in Figure VIII.6 is graphed in Figure VIII.25 as a continuous line. Figure VIII.25 utilizes the line to draw attention to the fact that as the total dose equivalent, altitude, and duration of the flights decreases, the unpredictability and ability of the commercial codes to accurately estimate a radiation risk is greatly reduced.

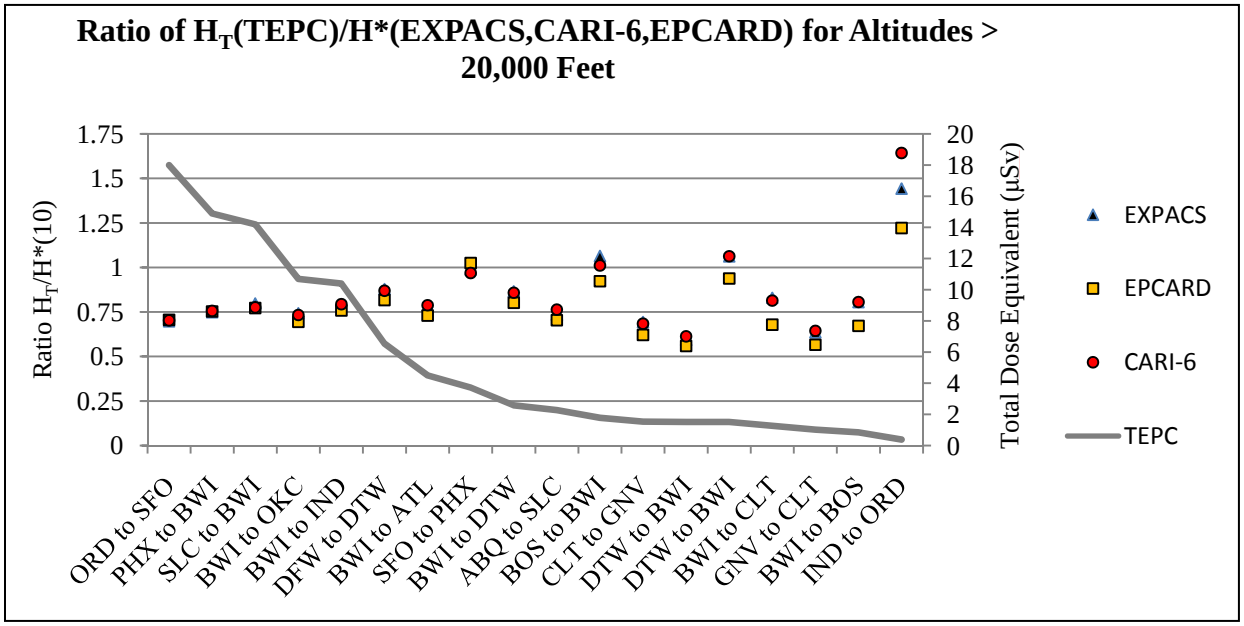

Figure VIII.25 – Graphical Comparison of Ratio of H_T to Commercial Codes

As can be seen in Figure VIII.25, when the total dose equivalent of each flight decreases, the accuracy and deviation increases between the codes. Table VIII.7 shows the ratios of the dose equivalent predicted by EXPACS to those predicted by EPCARD and CARI-6.

Table VIII.7 – Ratio of H*(EXPACS) to H*(EPCARD) and H*(CARI-6)

Flights	H*(EXPACS)/H_{tot}*(EPCARD)	H*(EXPACS)/H_{tot}*(CARI-6)
ABQ-SLC	.957	1.04
SLC-BWI	.967	0.973
BWI-ATL	.930	1.00
BWI-OKC	.935	.986
DFW-DTW	.929	.988
DTW-BWI	.883	1.00
BWI-CLT	.818	.981
CLT-GNV	.895	.987
GNV-CLT	.890	1.01
BWI-BOS	.835	1.00
BOS-BWI	.866	.949
BWI-DTW	.926	.990
DTW-BWI2	.941	1.03
BWI-IND	.971	1.02
IND-ORD	.847	1.14
ORD-SFO	1.01	1.01
SFO-PHX	1.04	.979
PHX-BWI	1.01	1.01
Average	**.925**	**1.01**

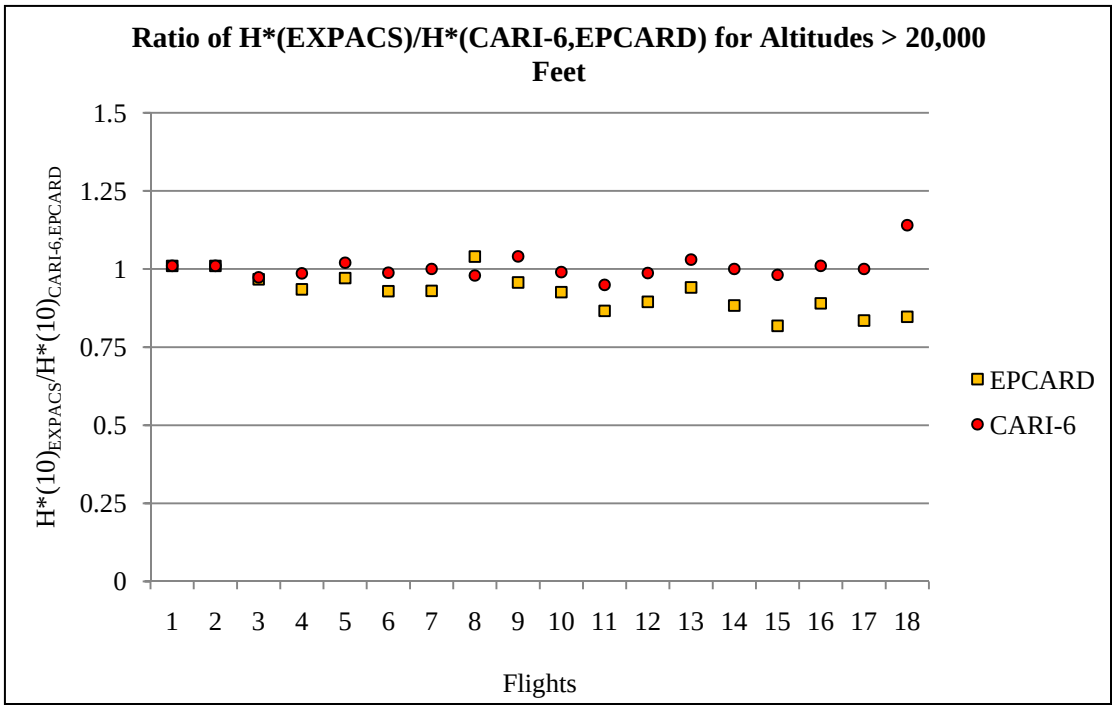

Figure VIII.26 – Graphical Representation of EXPACS Statistical Agreement with EPCARD and CARI-6

Despite having fewer inputs, the CARI-6 code still predicts total doses very similar to EXPACS. This is apparent in Figure VIII.26, where the correlation with CARI-6 is less than 3% until the flight with the lowest total dose, #18. In regards to #18, this flight was the shortest, from Indianapolis, Indiana to Chicago, Illinois, limiting the data and the cruising altitude was also lower than the other flights. The variation between EPCARD and CARI-6 arose primarily from differences in quality factors which are slightly higher for protons greater than 2 MeV in EPCARD. Both EXPACS and CARI-6 utilize the same dose equivalent coefficient regulations from the ICRP-60 regulations. As a result, the transport codes utilized by EXPACS (PHITS) and CARI-6 (PARMA) provide the greatest contribution to error. When evaluating all three codes simultaneously, the differences become most apparent when the aircraft has reached its cruising altitude.

F. Addressing the 1 mSv Regulation for the General Public

As mentioned in earlier chapters, commercial and naval aircrews and pilots are not classified as radiation workers. Therefore, they fall under the regulations for the general public and as a result, may only be exposed to an additional 1 mSv of radiation from flying. The results of these codes may be applied to determine dose rates over a year time period. In Table VIII.8, the hours needed to exceed the 1 mSv regulation for the general public was calculated to show which types of flights are of the most concern for frequent fliers, aircrew, and pilots. Most previous research has dealt with intercontinental travel, which led to much higher dose rates, but even with only flights within the United States, the 1 mSv regulation will certainly be surpassed for any aircrew personnel not classified as a radiation worker since most workers typically fly 700 block hours annually [4].

Table VIII.8 – Hours Needed of Specific Flight Profiles to Exceed 1 mSv/year Regulation

Flight #	Flight Departure	Hours for Dose to Exceed 1 mSv
1	ORD-SFO	231
2	PHX-BWI	311
3	SLC-BWI	223
4	BWI-OKC	315
5	BWI-IND	240
6	DFW-DTW	282
7	BWI-ATL	376
8	SFO-PHX	371
9	ABQ-SLC	597
10	BWI-DTW	434
11	BOS-BWI	445
12	CLT-GNV	634
13	DTW-BWI2	610
14	DTW-BWI	534
15	BWI-CLT	641
16	GNV-CLT	917
17	BWI-BOS	783
18	IND-ORD	1069

The differences in hours needed to exceed the 1 mSv per year regulation arise from the duration and cruising altitudes of the flights. Figures VIII.27-VIII.31 show typical flight profiles for four flights (Boston to Baltimore, Chicago to San Francisco, Baltimore to Oklahoma City, and a Prowler flight in St. Mary's, Maryland) with a corresponding plot of the H_T measured by the TEPC and the red lines being predicted by the codes. The TEPC records the dose rate every minute, so a high fluctuation is expected as a result of discrete events which may bring greater or lesser amounts of lineal energy than the previous minute of flight. As expected, the codes are much more conservative and have almost always predicted more radiation than actually measured. The exception occurs with the low altitude and low duration flights which most likely are a result of the inability of the codes to calculate dose rates under 15,000 feet. When considering that these codes may calculate the amount of radiation exposure an individual receives, it is definitely a matter of safety to over-estimate rather than under-estimate. While these codes could be improved slightly, they are within the deviation allowable to be utilized as a regulatory tool. In Figure VIII.27, only the flight altitude, recorded by a handheld GPS unit, versus the duration of the flight is being plotted.

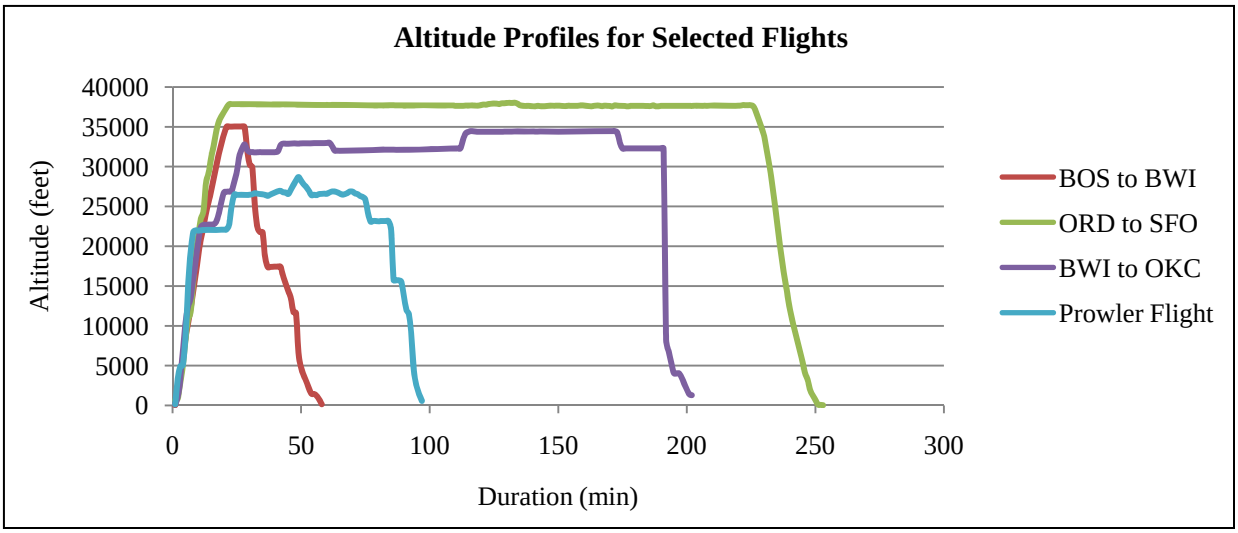

Figure VIII.27 – Flight Profiles of Selected Flights

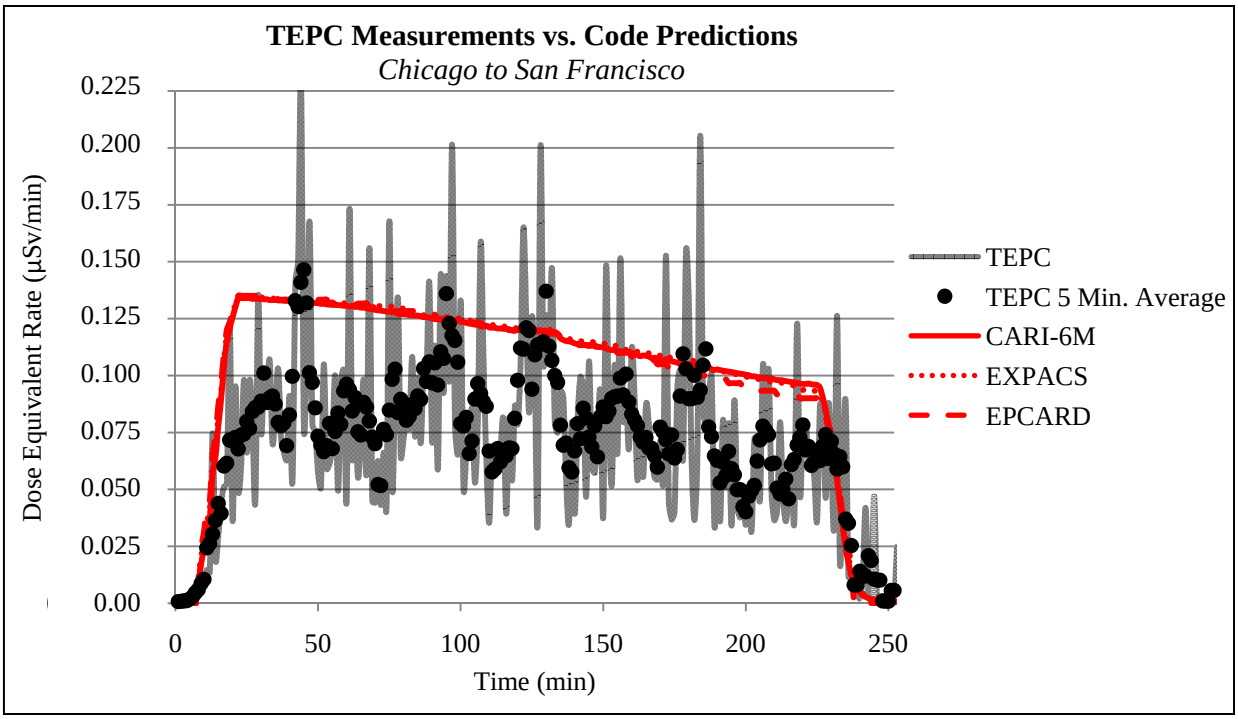

Figure VIII.28 – Dose Equivalent Rate Profile for ORD to SFO

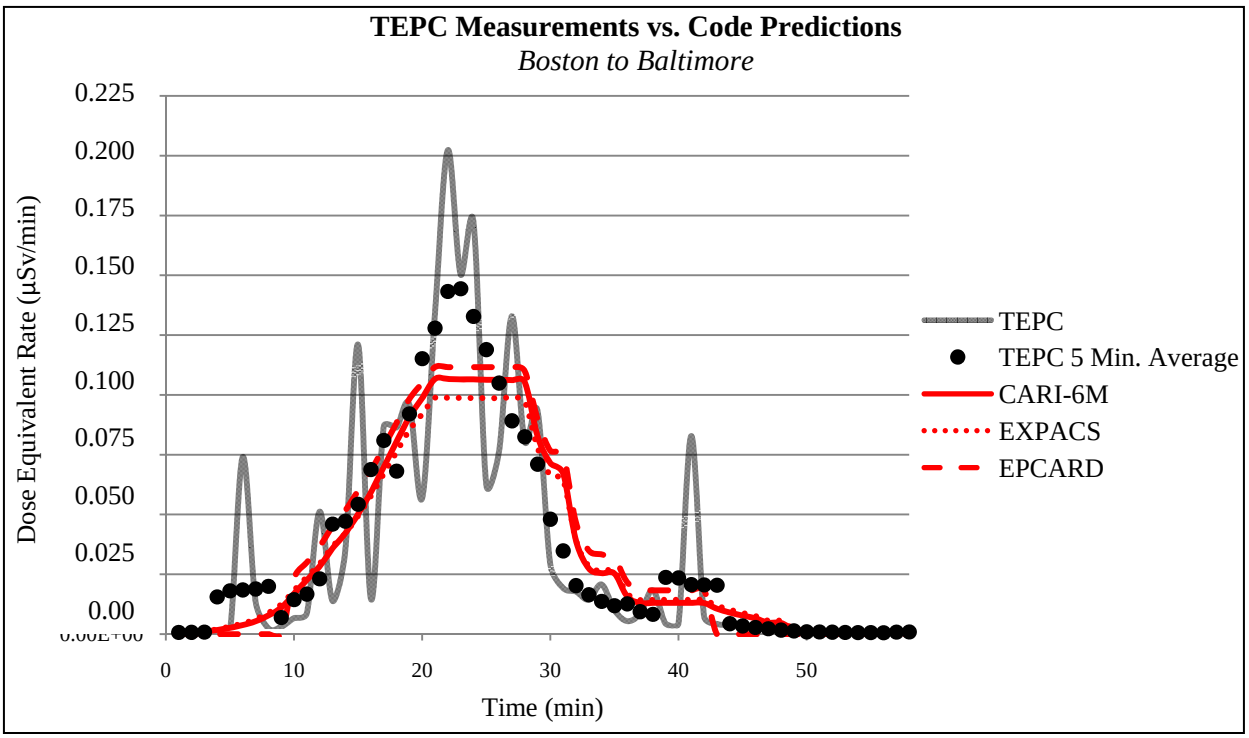

Figure VIII.29 – Dose Equivalent Rate Profile for BOS to BWI

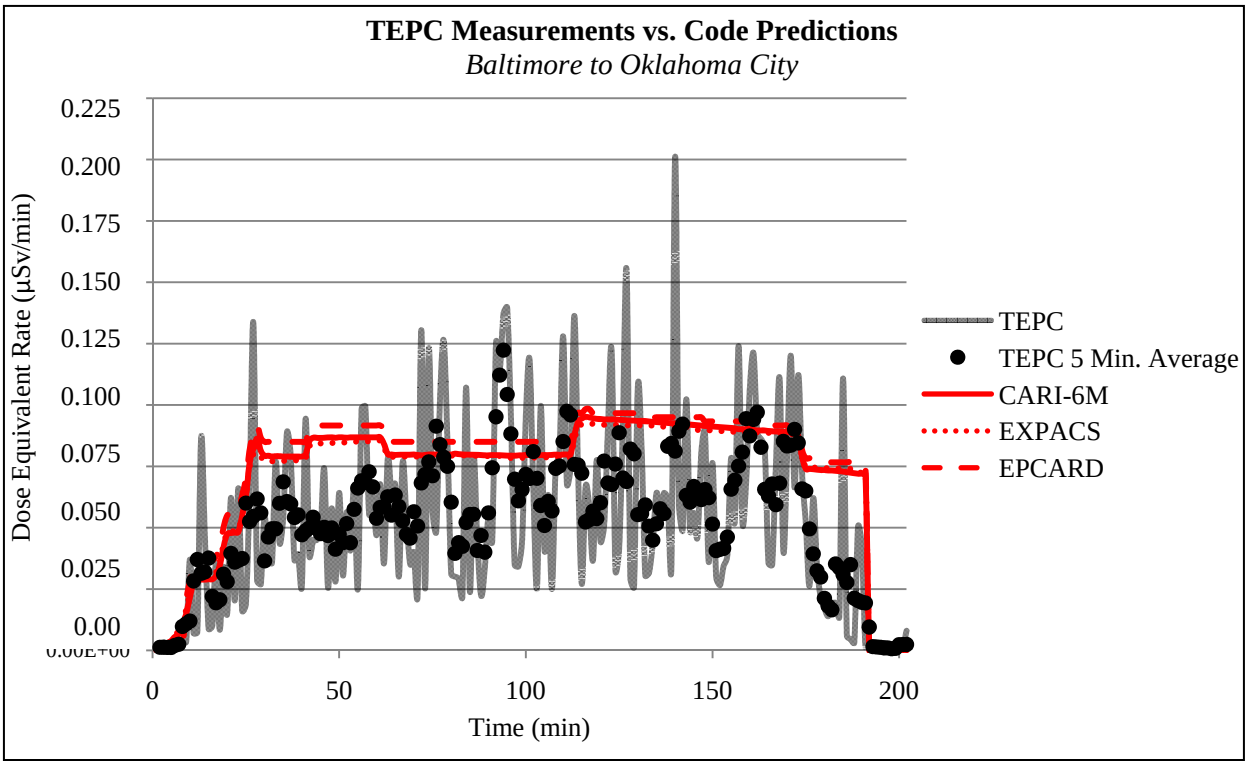

Figure VIII.30 – Dose Equivalent Rate Profile for BWI to OKC

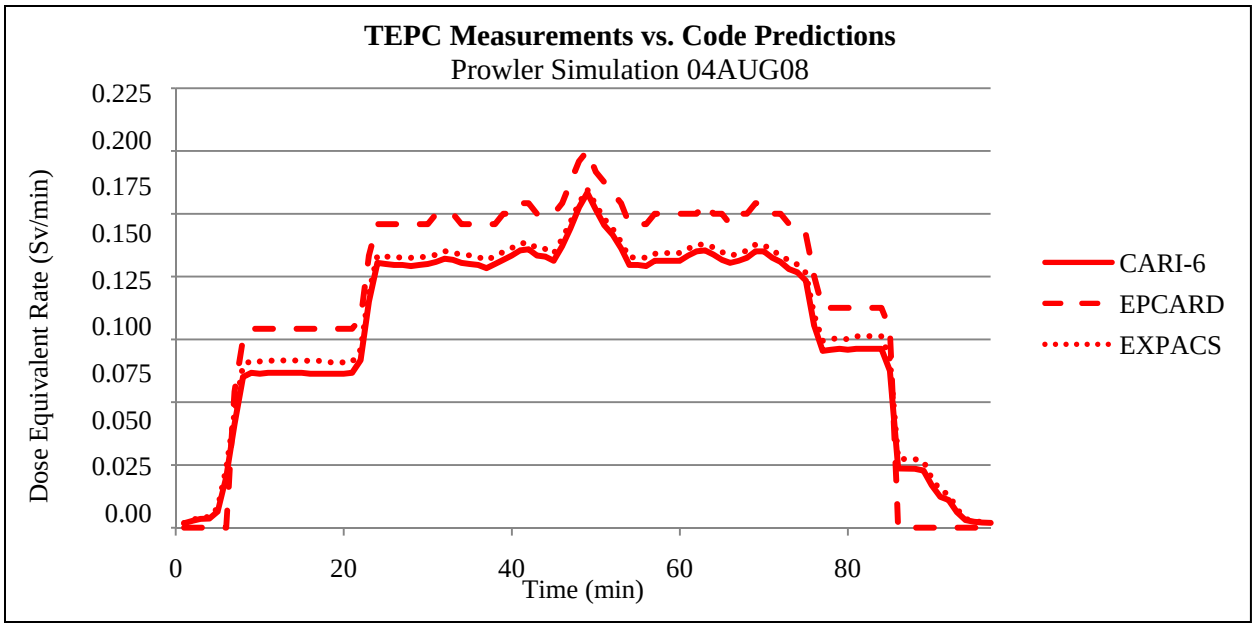

Figure VIII.31 – Dose Equivalent Rate Profile for Prowler Simulation

Figure VIII.31 represents a very typical test flight conducted at Pax River on a weekly basis. Assuming the average test flight results in an exposure of 3 μSv, a pilot would be able to fly about 333 missions of similar altitude and duration in a year before exceeding the 1 mSv/year guideline for the general public. If the duration and altitude of these flights remained constant, at the average cruising altitude of these flights, a pilot could remain in the air for 483 hours. Figure VIII.32 and Figure VIII.33 graphically depict the maximum number of flight hours or flights needed to exceed the 1 mSv/year regulation for the general public for several different flights, based on actual data recorded by the HAWK. The 25 percent uncertainty with HAWK measurements are shown on the graph as error bars.

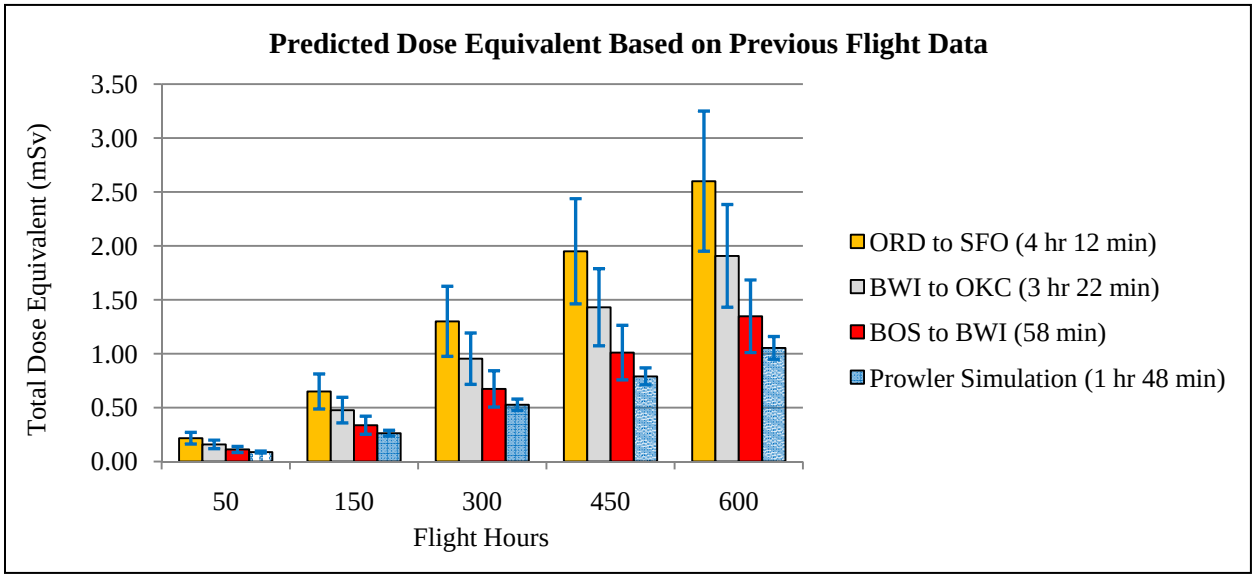

Figure VIII.32 – Maximum Number of Flight Hours Before Exceeding 1 mSv Threshold

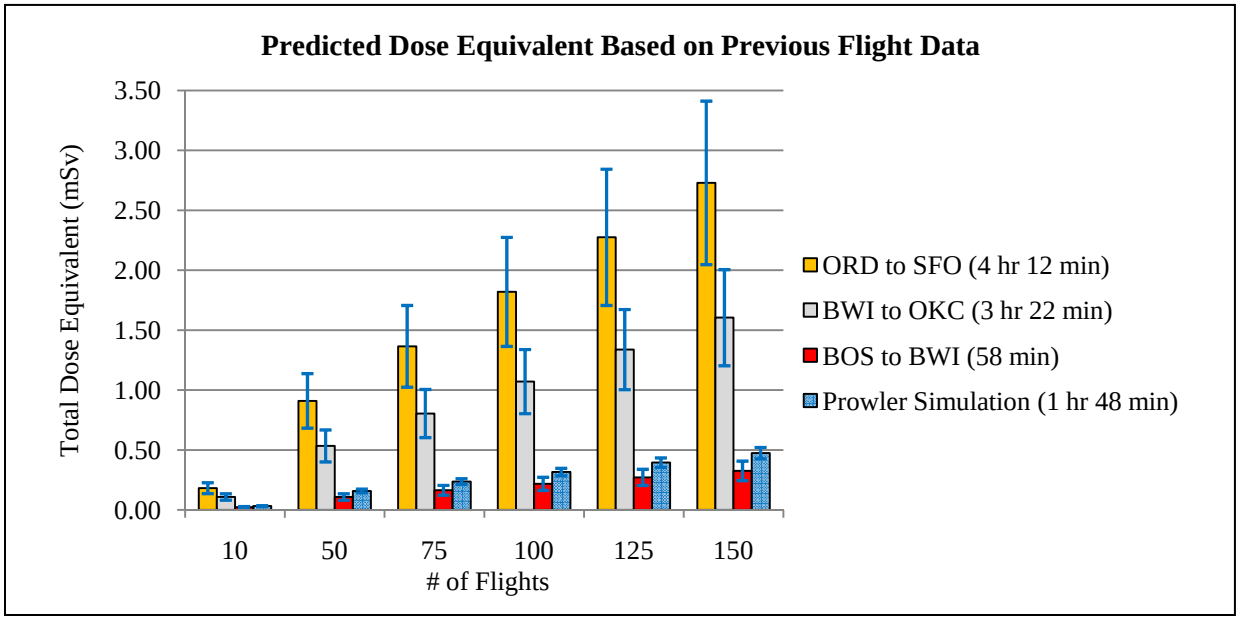

Flight VIII.33 – Maximum Number of Flights Required to Exceed Threshold

When considering the likelihood of exceeding current regulations, the time at cruising altitude is the most significant factor to impact the total dose equivalent experienced during the flight. By separating the flights into low, medium, and high dose rate groups, general predictions could be made for each group. Assuming the dose rates stay fairly constant throughout the year, it was calculated that a person flying flights in the high dose rate group will exceed the regulation in 73 flights or approximately 251 hours. For the medium group, the regulation will be surpassed after 308 flights or approximately 447 hours. Finally, the low group has very little chance of exceeding the regulation with 946 flights being needed or 875 hours. After determining all the hours needed to exceed the 1 mSv regulation, it was determined that approximately 500 hours was found to be the average time period needed to exceed the current limit set forth for the general public.

Chapter IX: Conclusions and Recommended Future Research

Throughout the research project, acquiring high altitude and/or military flight data was very challenging. In December, a decision was made to begin experimentation on commercial aircraft and it led to over 40 hours of new flight data recorded with the Naval Academy's TEPC. Utilizing this unique database of information collected over 14 states in the United States, a systematic comparison between H*(10) values from commercial codes and the H_T recorded by the HAWK revealed a very close correlation. The deviation between TEPC measurements and the predictive codes may be attributed to the initial assumption discussed in Chapter II, where the H_T dose equivalent of the TEPC was assumed to be approximately equal to the ambient dose equivalent which takes into account backscatter and attenuation in 10 mm of tissue.

Overall, the three commercial codes proved to be a fairly accurate and certainly conservative method to calculating the dose experienced by pilots and aircrew. EPCARD varied with the TEPC measured dose by around 23% where EXPACS and CARI-6 did noticeable better, only varying on average by about 15%. In addition, EXPACS proved to have the most user-friendly interface and most transparent calculation scheme. Even though the unique inputs in EXPACS took away from its usability, all the inputs allowed for a more complicated and detailed atmospheric radiation environment to be simulated. Given its close correlation to CARI-6 and the H_T TEPC measurements, EXPACS should be explored further by the United States and the Navy as an efficient method to calculate radiation exposure onboard aircraft. Given the total dose rates calculated throughout the project, frequent fliers and commercial pilots and aircrew who fly more than 500 hours will most likely exceed 1 mSv and should monitor their accumulated radiation exposure. Through the predictive codes, it became apparent that altitude was the largest factor involved in calculating a total dose equivalent. Unfortunately, the data collected on the EA-6B Prowler was too limited to draw legitimate conclusions. However, research at Los Alamos National Laboratory conducted with actual samples of the EA-6B Prowler revealed a negligible attenuation effect from the gold-lined canopy. Through all the traveling involved with this project, the TEPC definitely proved to be a very durable instrument, absorbing bumps and drops while also functioning properly after being passed through airport security x-ray machines.

Recommendations for future research involve further analysis of TEPC simulation with GEANT and MCNP. These programs revealed very interesting characteristics of the project in the beginning of the research, but unfortunately, there was not enough time to fully investigate this aspect of the project. More research could also be conducted into the sensitivity of the TEPC to vibration and temperature. Obviously, more flights on military platforms would also help conclusions to be drawn on the importance of monitoring the radiation exposure of naval pilots and aircrew. Regardless, EXPACS proved to be a highly versatile and accurate code. Further development of this code should be pursued if the United States Navy determines that its pilots and aircrew have an occupational radiation risk.

Documents and Internet References

[1] "Health Risks From Exposure to Low Levels of Ionizing Radiation: BEIR VII Phase 2." National Academy of Sciences: 2005.

[2] "Radiation Protection Standards: 4-1." *Radiation Health Protection Manual: NAVMED P-5055*. Bureau of Medicine and Surgery: 2001.

[3] NAVSEA S0420-AA-RAD-010.

[4] Bailey, S. "Air crew radiation exposure - An overview." *Nuclear News* : January 2000, p. 32.

[5] "Radiation Protection and the NRC." *US Nuclear Regulatory Commission*: 2006.

[6] "Aircrew Exposure from Cosmic Radiation on Commercial Airline Routes." *Radiation Protection Dosimetry: 2001*, p. 293.

[7] B.J. Lewis, M. D. (2004). "Assessment of Aircrew Radiation Exposure by Further Measurements and Model Development." *Radiation Protection Dosimetry: 2004*, p. 152.

[8] Tatsuhiko, S. "EXPACS: Excel-based Program for Calculating Atmospheric Cosmic Ray Spectrum." Online Available 5 September 2008 <https://www.jaea.go.jp/04/nsed/ers/radiation/rpro/EXPACS/expacs-eng.html>.

[9] Pisacane, V. *The Space Environment and its Effects on Systems: 2007.*

[10] Getley, I.A. "The applicability of model based aircraft radiation dose estimates." *Advances in Space Research*: 2005, p.1638.

[11] "Radiation Protection 140: Cosmic Ray Exposure of Aircraft Crew." *European Radiation Dosimetry Group*: 2004.

[12] Lewis, B.J. "Assessment of Aircrew Radiation Exposure by Further Measurements and Model Development." *Radiation Protection Dosimetry*: 2004, p. 155.

[13] "ICRP Publication 40: Protection of the Public in the Event of Major Radiation Accidents: Principles for Planning." *Annals of ICRP*. Pergamon Press: Oxford. Vol. 14: No. 2, 1990.

[14] Lamarsh, J. R., & Baratta, A. J. *Introduction to Nuclear Engineering.* Prentice Hall: New Jersey, 2001.

[15] Schlickeiser, R. *Cosmic Ray Astrophysics*. Berlin: Springer, 2002.

[16] Holmes-Siedle, A., & Adams, L. “Handbook of Radiation Effects.” Oxford University Press: New York, 2002.

[17] “The Stopping and Range of Ions in Matter.” Online Available <http://www.srim.org>.

[18] Close, F. “Particle Physics: A Very Short Introduction.” Oxford University Press: New York, 2004.

[19] “Operations and Repair Manual: Model FWAD-2 HAWK Version 2.” Far West Technology, Inc. 2004.

[20] Oberg, E.; et al. *Machinery’s Handbook (25th Edition ed.)*: Industrial Press Inc., 1996.

[21] Knoll, G. F. *Radiation Detection and Measurement.* John Wiley & Sons: New York, 1989.

[22] “ICRP Publication 21: Protection of the Public in the Event of Major Radiation Accidents: Principles for Planning.” *Annals of ICRP*. Pergamon Press: Oxford. Vol. 14: No. 2, 1990.

[23] “MCNP – A General Monte Carlo N-Particle Transport Code – Version 5.” Online Available 4 April 2009. <http://mcnp-green.lanl.gov>.

[24] Kliauga, P. “Design of Tissue Equivalent Proportional Counters.” *Radiation Protection Dosimetry*: Vol. 61, No. 4. 1995, p. 312.

[25] “SPENVIS.” Online Available <http://www.spenvis.oma.be>.

[26] “GEANT4.” Online Available <http://geant4.web.cern.ch/geant4/>.

[27] “Pilot’s Operating Handbook: 152.” *Cessna*: 1978.

[28] “767: Technical Specifications.” Online Available 4 April 2009. <http://www.boeing.com/commercial/767family/technical>.

[29] NAVAIR 01-85ADC-3-2.1

[30] “Boeing 767-400.” Online Available <https://www.aerospaceweb.org>.

[31] “EA-6B Prowler.” Online Available 4 April 2009. <http://aerospaceweb.org>.

[32] “CARI-6.” Federal Aviation Administration. Online Available 4 April 2009. <http://www.faa.gov/data_research/research/med_humanfacs/aeromedical/radiobiology/cari6m>.

[33] O’Brien, Keran. “Application of the heliocentric potential to aircraft dosimetry.”

[34] "Aircrew Dosimetry Using the Predictive Code for Aircrew Radiation Exposure (PCAIRE)." Radiation Protection Dosimetry: Vol. 116, No. 1-4. 2005, p. 320.

[35] Schraube, H. et. al. "EPCARD: User's Manual for Version 3.2." Institut für Strahlenschutz: 2002.

[36] "EXPACS: Excel-based Program for calculating Atmospheric Cosmic-Ray Spectrum User's Manual." Japan Atomic Energy Agency: 2008.

[37] "ICRP Publication 74: Conversion Coefficients for Use in Radiological Protection Against External Radiation." *Annals of ICRP*. Pergamon Press: Oxford. Vol. 26: No. 3, 1995.

[38] "A New Silicon Detector for Microdosimetry Applications in Proton Therapy." IEEE Transactions on Nuclear Science: Vol. 47, No. 4, 2000.

[39] Orton, Colin G. "Radiation Dosimetry: Physical and Biological Aspects." Springer: 1986, 175.

APPENDIX A: SEE2 Output Example

```
Program SEE2 Version 2.0 02Jul03
 Showing File Data From Far West Hawk2 instrument

=> Open Data File for read mode
=> attempting to open Data File =E0809181.237
--- Display All Data in File
[BOD  ] 12:37:36 18SEP08,  RunId $57
[TEXT ] --Opening File "E0809181.237" For Data Storage
[TEXT ] --Make Sure IORDY is on value should be $409 0409
[TEXT ] --Setup Temperature Device
[TEXT ] --Temp Device: Setup went OK
[TEXT ] --Turn on screen dump of spectrum
[TEXT ] --Open Initialization File To Read Variable Settings
[TEXT ] --Data File: hawk020.ini
[TEXT ] --Finished with Initialization File
[TEXT ] --Software Identification
[TEXT ] --       Hawk2 3.00 22Aug07
[TEXT ] --Open Initialization File to read Table of Q values
[TEXT ] --Data File: hawk2.tab
[TEXT ] --Finished with Table File
[TEXT ] ---------------- McaState Dump-------
[TEXT ] --**TestPulser**
[TEXT ] --  Tp1Enable     False  Tp1Amp       $0300
[TEXT ] --  Tp2Enable     False  Tp2Amp       $0300  Tp2Delay      255uS
[TEXT ] --**High Voltage**  HvSetPoint     -708
[TEXT ] --  HvAmp        $0548
[TEXT ] --**Gamma Cutoff Kev**  6
[TEXT ] --**Adjustment Constant   0.7860
[TEXT ] --**Alpha Source**  Alpha SetChn  100  Alpha Cal Chn  20
[TEXT ] --  AlphaMin         10  AlphaMax       1250
[TEXT ] --**Thresholds**  ThrCal       $0880  ThrHigh      $0828
[TEXT ] --**Offsets**  OffLow       $02FA  OffHigh      $0833
[TEXT ] --**Symbols**        DoseEqu Symbol S  Dose Symbol    G
[TEXT ] --**Screen Contrast** 0B00
[TEXT ] --
[TEXT ] --**Data Version**  2
[TEXT ] --Version 2 Data File
[TEXT ] --Q Table conversion
[TEXT ] --Table 1, for hi gain 0 to 25kev/um 0.1 keV/um steps
[TEXT ] --Begin table
[TEXT ] --  1.000  1.000  1.000  1.000  1.000  1.000  1.000  1.000  1.000  1.000
[TEXT ] --  1.000  1.000  1.000  1.000  1.000  1.000  1.000  1.000  1.000  1.000
[TEXT ] --  1.000  1.000  1.000  1.000  1.000  1.000  1.000  1.000  1.000  1.000
[TEXT ] --  1.000  1.000  1.000  1.000  1.000  1.000  1.000  1.000  1.000  1.000
[TEXT ] --  1.000  1.000  1.000  1.000  1.000  1.000  1.000  1.000  1.000  1.000
[TEXT ] --  1.000  1.000  1.000  1.000  1.000  1.000  1.000  1.000  1.000  1.000
[TEXT ] --  1.000  1.000  1.000  1.000  1.000  1.000  1.000  1.000  1.000  1.000
[TEXT ] --  1.000  1.000  1.000  1.000  1.000  1.000  1.000  1.000  1.000  1.000
[TEXT ] --  1.000  1.000  1.000  1.000  1.000  1.000  1.000  1.000  1.000  1.000
[TEXT ] --  1.000  1.000  1.000  1.000  1.000  1.000  1.000  1.000  1.000  1.000
[TEXT ] --  1.016  1.048  1.080  1.112  1.144  1.176  1.208  1.240  1.272  1.304
[TEXT ] --  1.336  1.368  1.400  1.432  1.464  1.496  1.528  1.560  1.592  1.624
[TEXT ] --  1.656  1.688  1.720  1.752  1.784  1.816  1.848  1.880  1.912  1.944
[TEXT ] --  1.976  2.008  2.040  2.072  2.104  2.136  2.168  2.200  2.232  2.264
[TEXT ] --  2.296  2.328  2.360  2.392  2.424  2.456  2.488  2.520  2.552  2.584
[TEXT ] --  2.616  2.648  2.680  2.712  2.744  2.776  2.808  2.840  2.872  2.904
[TEXT ] --  2.936  2.968  3.000  3.032  3.064  3.096  3.128  3.160  3.192  3.224
[TEXT ] --  3.256  3.288  3.320  3.352  3.384  3.416  3.448  3.480  3.512  3.544
[TEXT ] --  3.576  3.608  3.640  3.672  3.704  3.736  3.768  3.800  3.832  3.864
[TEXT ] --  3.896  3.928  3.960  3.992  4.024  4.056  4.088  4.120  4.152  4.184
[TEXT ] --  4.216  4.248  4.280  4.312  4.344  4.376  4.408  4.440  4.472  4.504
[TEXT ] --  4.536  4.568  4.600  4.632  4.664  4.696  4.728  4.760  4.792  4.824
[TEXT ] --  4.856  4.888  4.920  4.952  4.984  5.016  5.048  5.080  5.112  5.144
[TEXT ] --  5.176  5.208  5.240  5.272  5.304  5.336  5.368  5.400  5.432  5.464
[TEXT ] --  5.496  5.528  5.560  5.592  5.624  5.656  5.688  5.720  5.752  5.784
[TEXT ] --  5.816  5.848  5.880  5.912  5.944  5.976
```

[TEXT] --Q Table conversion
[TEXT] --Table 2, for low gain 0 to 1536 kev/um 1.5 keV/um steps
[TEXT] --
[TEXT] -- 1.000 1.000 1.000 1.000 1.000 1.000 1.000 1.400 1.880 2.360
[TEXT] -- 2.840 3.320 3.800 4.280 4.760 5.240 5.720 6.200 6.680 7.160
[TEXT] -- 7.640 8.120 8.600 9.080 9.560 10.040 10.520 11.000 11.480 11.960
[TEXT] -- 12.440 12.920 13.400 13.880 14.360 14.840 15.320 15.800 16.280 16.760
[TEXT] -- 17.240 17.720 18.200 18.680 19.160 19.640 20.120 20.600 21.080 21.560
[TEXT] -- 22.040 22.520 23.000 23.480 23.960 24.440 24.920 25.400 25.880 26.360
[TEXT] -- 26.840 27.320 27.800 28.280 28.760 29.240 29.720 29.810 29.600 29.380
[TEXT] -- 29.170 28.970 28.770 28.570 28.380 28.190 28.010 27.820 27.650 27.470
[TEXT] -- 27.300 27.130 26.970 26.810 26.650 26.490 26.340 26.190 26.040 25.890
[TEXT] -- 25.750 25.610 25.470 25.330 25.200 25.070 24.940 24.810 24.680 24.560
[TEXT] -- 24.430 24.310 24.190 24.080 23.960 23.850 23.740 23.620 23.520 23.410
[TEXT] -- 23.300 23.200 23.090 22.990 22.890 22.790 22.690 22.600 22.500 22.410
[TEXT] -- 22.310 22.220 22.130 22.040 21.950 21.870 21.780 21.690 21.610 21.520
[TEXT] -- 21.440 21.360 21.280 21.200 21.120 21.040 20.970 20.890 20.810 20.740
[TEXT] -- 20.670 20.590 20.520 20.450 20.380 20.310 20.240 20.170 20.100 20.030
[TEXT] -- 19.970 19.900 19.840 19.770 19.710 19.640 19.580 19.520 19.460 19.400
[TEXT] -- 19.330 19.270 19.220 19.160 19.100 19.040 18.980 18.930 18.870 18.810
[TEXT] -- 18.760 18.700 18.650 18.600 18.540 18.490 18.440 18.390 18.330 18.280
[TEXT] -- 18.230 18.180 18.130 18.080 18.030 17.980 17.940 17.890 17.840 17.790
[TEXT] -- 17.750 17.700 17.650 17.610 17.560 17.520 17.470 17.430 17.390 17.340
[TEXT] -- 17.300 17.260 17.210 17.170 17.130 17.090 17.050 17.000 16.960 16.920
[TEXT] -- 16.880 16.840 16.800 16.760 16.720 16.690 16.650 16.610 16.570 16.530
[TEXT] -- 16.500 16.460 16.420 16.380 16.350 16.310 16.280 16.240 16.200 16.170
[TEXT] -- 16.130 16.100 16.060 16.030 16.000 15.960 15.930 15.890 15.860 15.830
[TEXT] -- 15.790 15.760 15.730 15.700 15.670 15.630 15.600 15.570 15.540 15.510
[TEXT] -- 15.480 15.450 15.420 15.380 15.350 15.320 15.290 15.260 15.240 15.210
[TEXT] -- 15.180 15.150 15.120 15.090 15.060 15.030 15.000 14.980 14.950 14.920
[TEXT] -- 14.890 14.870 14.840 14.810 14.780 14.760 14.730 14.700 14.680 14.650
[TEXT] -- 14.630 14.600 14.570 14.550 14.520 14.500 14.470 14.450 14.420 14.400
[TEXT] -- 14.370 14.350 14.320 14.300 14.270 14.250 14.230 14.200 14.180 14.150
[TEXT] -- 14.130 14.110 14.080 14.060 14.040 14.010 13.990 13.970 13.950 13.920
[TEXT] -- 13.900 13.880 13.860 13.830 13.810 13.790 13.770 13.750 13.730 13.700
[TEXT] -- 13.680 13.660 13.640 13.620 13.600 13.580 13.560 13.540 13.510 13.490
[TEXT] -- 13.470 13.450 13.430 13.410 13.390 13.370 13.350 13.330 13.310 13.290
[TEXT] -- 13.270 13.260 13.240 13.220 13.200 13.180 13.160 13.140 13.120 13.100
[TEXT] -- 13.080 13.070 13.050 13.030 13.010 12.990 12.970 12.960 12.940 12.920
[TEXT] -- 12.900 12.880 12.870 12.850 12.830 12.810 12.790 12.780 12.760 12.740
[TEXT] -- 12.730 12.710 12.690 12.670 12.660 12.640 12.620 12.610 12.590 12.570
[TEXT] -- 12.560 12.540 12.520 12.510 12.490 12.480 12.460 12.440 12.430 12.410
[TEXT] -- 12.400 12.380 12.360 12.350 12.330 12.320 12.300 12.290 12.270 12.260
[TEXT] -- 12.240 12.220 12.210 12.190 12.180 12.160 12.150 12.130 12.120 12.100
[TEXT] -- 12.090 12.080 12.060 12.050 12.030 12.020 12.000 11.990 11.970 11.960
[TEXT] -- 11.950 11.930 11.920 11.900 11.890 11.870 11.860 11.850 11.830 11.820
[TEXT] -- 11.810 11.790 11.780 11.760 11.750 11.740 11.720 11.710 11.700 11.680
[TEXT] -- 11.670 11.660 11.640 11.630 11.620 11.610 11.590 11.580 11.570 11.550
[TEXT] -- 11.540 11.530 11.520 11.500 11.490 11.480 11.460 11.450 11.440 11.430
[TEXT] -- 11.410 11.400 11.390 11.380 11.370 11.350 11.340 11.330 11.320 11.300
[TEXT] -- 11.290 11.280 11.270 11.260 11.240 11.230 11.220 11.210 11.200 11.190
[TEXT] -- 11.170 11.160 11.150 11.140 11.130 11.120 11.110 11.090 11.080 11.070
[TEXT] -- 11.060 11.050 11.040 11.030 11.020 11.000 10.990 10.980 10.970 10.960
[TEXT] -- 10.950 10.940 10.930 10.920 10.910 10.890 10.880 10.870 10.860 10.850
[TEXT] -- 10.840 10.830 10.820 10.810 10.800 10.790 10.780 10.770 10.760 10.750
[TEXT] -- 10.740 10.730 10.720 10.710 10.700 10.690 10.680 10.670 10.650 10.640
[TEXT] -- 10.630 10.620 10.610 10.600 10.600 10.590 10.580 10.570 10.560 10.550
[TEXT] -- 10.540 10.530 10.520 10.510 10.500 10.490 10.480 10.470 10.460 10.450
[TEXT] -- 10.440 10.430 10.420 10.410 10.400 10.390 10.380 10.370 10.360 10.360
[TEXT] -- 10.350 10.340 10.330 10.320 10.310 10.300 10.290 10.280 10.270 10.260
[TEXT] -- 10.260 10.250 10.240 10.230 10.220 10.210 10.200 10.190 10.180 10.180
[TEXT] -- 10.170 10.160 10.150 10.140 10.130 10.120 10.110 10.110 10.100 10.090
[TEXT] -- 10.080 10.070 10.060 10.050 10.050 10.040 10.030 10.020 10.010 10.000
[TEXT] -- 10.000 9.990 9.980 9.970 9.960 9.950 9.950 9.940 9.930 9.920
[TEXT] -- 9.910 9.910 9.900 9.890 9.880 9.870 9.870 9.860 9.850 9.840
[TEXT] -- 9.830 9.830 9.820 9.810 9.800 9.790 9.790 9.780 9.770 9.760
[TEXT] -- 9.760 9.750 9.740 9.730 9.720 9.720 9.710 9.700 9.690 9.690
[TEXT] -- 9.680 9.670 9.660 9.660 9.650 9.640 9.630 9.630 9.620 9.610
[TEXT] -- 9.600 9.600 9.590 9.580 9.570 9.570 9.560 9.550 9.550 9.540

[TEXT] -- 9.530 9.520 9.520 9.510 9.500 9.500 9.490 9.480 9.470 9.470
[TEXT] -- 9.460 9.450 9.450 9.440 9.430 9.420 9.420 9.410 9.400 9.400
[TEXT] -- 9.390 9.380 9.380 9.370 9.360 9.360 9.350 9.340 9.340 9.330
[TEXT] -- 9.320 9.310 9.310 9.300 9.290 9.290 9.280 9.270 9.270 9.260
[TEXT] -- 9.250 9.250 9.240 9.240 9.230 9.220 9.220 9.210 9.200 9.200
[TEXT] -- 9.190 9.180 9.180 9.170 9.160 9.160 9.150 9.140 9.140 9.130
[TEXT] -- 9.130 9.120 9.110 9.110 9.100 9.090 9.090 9.080 9.080 9.070
[TEXT] -- 9.060 9.060 9.050 9.040 9.040 9.030 9.030 9.020 9.010 9.010
[TEXT] -- 9.000 9.000 8.990 8.980 8.980 8.970 8.970 8.960 8.950 8.950
[TEXT] -- 8.940 8.940 8.930 8.920 8.920 8.910 8.910 8.900 8.890 8.890
[TEXT] -- 8.880 8.880 8.870 8.860 8.860 8.850 8.850 8.840 8.840 8.830
[TEXT] -- 8.820 8.820 8.810 8.810 8.800 8.800 8.790 8.780 8.780 8.770
[TEXT] -- 8.770 8.760 8.760 8.750 8.750 8.740 8.730 8.730 8.720 8.720
[TEXT] -- 8.710 8.710 8.700 8.700 8.690 8.680 8.680 8.670 8.670 8.660
[TEXT] -- 8.660 8.650 8.650 8.640 8.640 8.630 8.630 8.620 8.610 8.610
[TEXT] -- 8.600 8.600 8.590 8.590 8.580 8.580 8.570 8.570 8.560 8.560
[TEXT] -- 8.550 8.550 8.540 8.540 8.530 8.530 8.520 8.520 8.510 8.500
[TEXT] -- 8.500 8.490 8.490 8.480 8.480 8.470 8.470 8.460 8.460 8.450
[TEXT] -- 8.450 8.440 8.440 8.430 8.430 8.420 8.420 8.410 8.410 8.400
[TEXT] -- 8.400 8.390 8.390 8.380 8.380 8.370 8.370 8.360 8.360 8.360
[TEXT] -- 8.350 8.350 8.340 8.340 8.330 8.330 8.320 8.320 8.310 8.310
[TEXT] -- 8.300 8.300 8.290 8.290 8.280 8.280 8.270 8.270 8.260 8.260
[TEXT] -- 8.250 8.250 8.250 8.240 8.240 8.230 8.230 8.220 8.220 8.210
[TEXT] -- 8.210 8.200 8.200 8.190 8.190 8.190 8.180 8.180 8.170 8.170
[TEXT] -- 8.160 8.160 8.150 8.150 8.140 8.140 8.140 8.130 8.130 8.120
[TEXT] -- 8.120 8.110 8.110 8.100 8.100 8.100 8.090 8.090 8.080 8.080
[TEXT] -- 8.070 8.070 8.060 8.060 8.060 8.050 8.050 8.040 8.040 8.030
[TEXT] -- 8.030 8.030 8.020 8.020 8.010 8.010 8.000 8.000 8.000 7.990
[TEXT] -- 7.990 7.980 7.980 7.970 7.970 7.970 7.960 7.960 7.950 7.950
[TEXT] -- 7.950 7.940 7.940 7.930 7.930 7.920 7.920 7.920 7.910 7.910
[TEXT] -- 7.900 7.900 7.900 7.890 7.890 7.880 7.880 7.870 7.870 7.870
[TEXT] -- 7.860 7.860 7.850 7.850 7.850 7.840 7.840 7.830 7.830 7.830
[TEXT] -- 7.820 7.820 7.810 7.810 7.810 7.800 7.800 7.790 7.790 7.790
[TEXT] -- 7.780 7.780 7.780 7.770 7.770 7.760 7.760 7.760 7.750 7.750
[TEXT] -- 7.740 7.740 7.740 7.730 7.730 7.720 7.720 7.720 7.710 7.710
[TEXT] -- 7.710 7.700 7.700 7.690 7.690 7.690 7.680 7.680 7.680 7.670
[TEXT] -- 7.670 7.660 7.660 7.660
[TEXT] --GPS RX OK
[TEXT] --Flash Disk Size Installed is 966 Mega-Bytes
[TEXT] --Hawk Startup
[TEXT] --Flush Tepc Data File
[TEXT] --Opening File "E0809181.237" For Data Storage
[TEXT] --Temperature Device Serial # 22FD3206000000A3
[TEXT] [UnitId] 22FD3206000000A3
[TOD] 12:38:52 18SEP08 ET=0000:00:00
[TEXT] [VERSION] Hawk23.0022Aug07
[TEXT] The Unit MUST BE SETUP with a 64 channel DC offset
[TEXT] In the low gain channel. This correct for non-linearity
[TEXT] The range is reduced by 1.5 keV/um * 64
[TEXT] These upper channels are set to zero
[DOS2] 0.001 pG
[DOS2] 0.001 pG
[DOS2] 0.001 pG
[DOS2] 0.001 pG
[TEXT] -388 , V , 1.0 , uA , 25 , C ,
[TEXT] --Flush Tepc Data File

APPENDIX B: CONDEQU2 Output Example

```
CONDEQU2 VERSION 2.1 27May04
 File : E0809181.237
-- Open Initialization File To Read Variable Settings
-- Data File: hawk020.ini
-- Finished with Initialization File
-------------------------------------------
 New values to be used in this calculation
-------------------------------------------
Adjustment Constant = 7.8600000000E-01
-- Open Initialization File to read Table of Q values
-- Data File: hawk2.tab
-- Finished with Table File
-- Version 2 Data File
-- Q Table conversion
-- Table 1, for hi gain 0 to 25kev/um 0.1 keV/um steps
-- Begin table
--   1.000  1.000  1.000  1.000  1.000  1.000  1.000  1.000  1.000  1.000
--   1.000  1.000  1.000  1.000  1.000  1.000  1.000  1.000  1.000  1.000
--   1.000  1.000  1.000  1.000  1.000  1.000  1.000  1.000  1.000  1.000
--   1.000  1.000  1.000  1.000  1.000  1.000  1.000  1.000  1.000  1.000
--   1.000  1.000  1.000  1.000  1.000  1.000  1.000  1.000  1.000  1.000
--   1.000  1.000  1.000  1.000  1.000  1.000  1.000  1.000  1.000  1.000
--   1.000  1.000  1.000  1.000  1.000  1.000  1.000  1.000  1.000  1.000
--   1.000  1.000  1.000  1.000  1.000  1.000  1.000  1.000  1.000  1.000
--   1.000  1.000  1.000  1.000  1.000  1.000  1.000  1.000  1.000  1.000
--   1.000  1.000  1.000  1.000  1.000  1.000  1.000  1.000  1.000  1.000
--   1.016  1.048  1.080  1.112  1.144  1.176  1.208  1.240  1.272  1.304
--   1.336  1.368  1.400  1.432  1.464  1.496  1.528  1.560  1.592  1.624
--   1.656  1.688  1.720  1.752  1.784  1.816  1.848  1.880  1.912  1.944
--   1.976  2.008  2.040  2.072  2.104  2.136  2.168  2.200  2.232  2.264
--   2.296  2.328  2.360  2.392  2.424  2.456  2.488  2.520  2.552  2.584
--   2.616  2.648  2.680  2.712  2.744  2.776  2.808  2.840  2.872  2.904
--   2.936  2.968  3.000  3.032  3.064  3.096  3.128  3.160  3.192  3.224
--   3.256  3.288  3.320  3.352  3.384  3.416  3.448  3.480  3.512  3.544
--   3.576  3.608  3.640  3.672  3.704  3.736  3.768  3.800  3.832  3.864
--   3.896  3.928  3.960  3.992  4.024  4.056  4.088  4.120  4.152  4.184
--   4.216  4.248  4.280  4.312  4.344  4.376  4.408  4.440  4.472  4.504
--   4.536  4.568  4.600  4.632  4.664  4.696  4.728  4.760  4.792  4.824
--   4.856  4.888  4.920  4.952  4.984  5.016  5.048  5.080  5.112  5.144
--   5.176  5.208  5.240  5.272  5.304  5.336  5.368  5.400  5.432  5.464
--   5.496  5.528  5.560  5.592  5.624  5.656  5.688  5.720  5.752  5.784
--   5.816  5.848  5.880  5.912  5.944  5.976
-- Q Table conversion
-- Table 2, for low gain 0 to 1536 kev/um 1.5 keV/um steps
--
--   1.000  1.000  1.000  1.000  1.000  1.000  1.000  1.400  1.880  2.360
--   2.840  3.320  3.800  4.280  4.760  5.240  5.720  6.200  6.680  7.160
--   7.640  8.120  8.600  9.080  9.560 10.040 10.520 11.000 11.480 11.960
--  12.440 12.920 13.400 13.880 14.360 14.840 15.320 15.800 16.280 16.760
--  17.240 17.720 18.200 18.680 19.160 19.640 20.120 20.600 21.080 21.560
--  22.040 22.520 23.000 23.480 23.960 24.440 24.920 25.400 25.880 26.360
--  26.840 27.320 27.800 28.280 28.760 29.240 29.720 29.810 29.600 29.380
--  29.170 28.970 28.770 28.570 28.380 28.190 28.010 27.820 27.650 27.470
--  27.300 27.130 26.970 26.810 26.650 26.490 26.340 26.190 26.040 25.890
--  25.750 25.610 25.470 25.330 25.200 25.070 24.940 24.810 24.680 24.560
--  24.430 24.310 24.190 24.080 23.960 23.850 23.740 23.620 23.520 23.410
--  23.300 23.200 23.090 22.990 22.890 22.790 22.690 22.600 22.500 22.410
--  22.310 22.220 22.130 22.040 21.950 21.870 21.780 21.690 21.610 21.520
--  21.440 21.360 21.280 21.200 21.120 21.040 20.970 20.890 20.810 20.740
--  20.670 20.590 20.520 20.450 20.380 20.310 20.240 20.170 20.100 20.030
--  19.970 19.900 19.840 19.770 19.710 19.640 19.580 19.520 19.460 19.400
--  19.330 19.270 19.220 19.160 19.100 19.040 18.980 18.930 18.870 18.810
--  18.760 18.700 18.650 18.600 18.540 18.490 18.440 18.390 18.330 18.280
--  18.230 18.180 18.130 18.080 18.030 17.980 17.940 17.890 17.840 17.790
--  17.750 17.700 17.650 17.610 17.560 17.520 17.470 17.430 17.390 17.340
--  17.300 17.260 17.210 17.170 17.130 17.090 17.050 17.000 16.960 16.920
```

```
-- 16.880 16.840 16.800 16.760 16.720 16.690 16.650 16.610 16.570 16.530
-- 16.500 16.460 16.420 16.380 16.350 16.310 16.280 16.240 16.200 16.170
-- 16.130 16.100 16.060 16.030 16.000 15.960 15.930 15.890 15.860 15.830
-- 15.790 15.760 15.730 15.700 15.670 15.630 15.600 15.570 15.540 15.510
-- 15.480 15.450 15.420 15.380 15.350 15.320 15.290 15.260 15.240 15.210
-- 15.180 15.150 15.120 15.090 15.060 15.030 15.000 14.980 14.950 14.920
-- 14.890 14.870 14.840 14.810 14.780 14.760 14.730 14.700 14.680 14.650
-- 14.630 14.600 14.570 14.550 14.520 14.500 14.470 14.450 14.420 14.400
-- 14.370 14.350 14.320 14.300 14.270 14.250 14.230 14.200 14.180 14.150
-- 14.130 14.110 14.080 14.060 14.040 14.010 13.990 13.970 13.950 13.920
-- 13.900 13.880 13.860 13.830 13.810 13.790 13.770 13.750 13.730 13.700
-- 13.680 13.660 13.640 13.620 13.600 13.580 13.560 13.540 13.510 13.490
-- 13.470 13.450 13.430 13.410 13.390 13.370 13.350 13.330 13.310 13.290
-- 13.270 13.260 13.240 13.220 13.200 13.180 13.160 13.140 13.120 13.100
-- 13.080 13.070 13.050 13.030 13.010 12.990 12.970 12.960 12.940 12.920
-- 12.900 12.880 12.870 12.850 12.830 12.810 12.790 12.780 12.760 12.740
-- 12.730 12.710 12.690 12.670 12.660 12.640 12.620 12.610 12.590 12.570
-- 12.560 12.540 12.520 12.510 12.490 12.480 12.460 12.440 12.430 12.410
-- 12.400 12.380 12.360 12.350 12.330 12.320 12.300 12.290 12.270 12.260
-- 12.240 12.220 12.210 12.190 12.180 12.160 12.150 12.130 12.120 12.100
-- 12.090 12.080 12.060 12.050 12.030 12.020 12.000 11.990 11.970 11.960
-- 11.950 11.930 11.920 11.900 11.890 11.870 11.860 11.850 11.830 11.820
-- 11.810 11.790 11.780 11.760 11.750 11.740 11.720 11.710 11.700 11.680
-- 11.670 11.660 11.640 11.630 11.620 11.610 11.590 11.580 11.570 11.550
-- 11.540 11.530 11.520 11.500 11.490 11.480 11.460 11.450 11.440 11.430
-- 11.410 11.400 11.390 11.380 11.370 11.350 11.340 11.330 11.320 11.300
-- 11.290 11.280 11.270 11.260 11.240 11.230 11.220 11.210 11.200 11.190
-- 11.170 11.160 11.150 11.140 11.130 11.120 11.110 11.090 11.080 11.070
-- 11.060 11.050 11.040 11.030 11.020 11.000 10.990 10.980 10.970 10.960
-- 10.950 10.940 10.930 10.920 10.910 10.890 10.880 10.870 10.860 10.850
-- 10.840 10.830 10.820 10.810 10.800 10.790 10.780 10.770 10.760 10.750
-- 10.740 10.730 10.720 10.710 10.700 10.690 10.680 10.670 10.650 10.640
-- 10.630 10.620 10.610 10.600 10.600 10.590 10.580 10.570 10.560 10.550
-- 10.540 10.530 10.520 10.510 10.500 10.490 10.480 10.470 10.460 10.450
-- 10.440 10.430 10.420 10.410 10.400 10.390 10.380 10.370 10.360 10.360
-- 10.350 10.340 10.330 10.320 10.310 10.300 10.290 10.280 10.270 10.260
-- 10.260 10.250 10.240 10.230 10.220 10.210 10.200 10.190 10.180 10.180
-- 10.170 10.160 10.150 10.140 10.130 10.120 10.110 10.110 10.100 10.090
-- 10.080 10.070 10.060 10.050 10.050 10.040 10.030 10.020 10.010 10.000
-- 10.000  9.990  9.980  9.970  9.960  9.950  9.950  9.940  9.930  9.920
--  9.910  9.910  9.900  9.890  9.880  9.870  9.870  9.860  9.850  9.840
--  9.830  9.830  9.820  9.810  9.800  9.790  9.790  9.780  9.770  9.760
--  9.760  9.750  9.740  9.730  9.720  9.720  9.710  9.700  9.690  9.690
--  9.680  9.670  9.660  9.660  9.650  9.640  9.630  9.630  9.620  9.610
--  9.600  9.600  9.590  9.580  9.570  9.570  9.560  9.550  9.550  9.540
--  9.530  9.520  9.520  9.510  9.500  9.500  9.490  9.480  9.470  9.470
--  9.460  9.450  9.450  9.440  9.430  9.420  9.420  9.410  9.400  9.400
--  9.390  9.380  9.380  9.370  9.360  9.360  9.350  9.340  9.340  9.330
--  9.320  9.310  9.310  9.300  9.290  9.290  9.280  9.270  9.270  9.260
--  9.250  9.250  9.240  9.240  9.230  9.220  9.220  9.210  9.200  9.200
--  9.190  9.180  9.180  9.170  9.160  9.160  9.150  9.140  9.140  9.130
--  9.130  9.120  9.110  9.110  9.100  9.090  9.090  9.080  9.080  9.070
--  9.060  9.060  9.050  9.040  9.040  9.030  9.030  9.020  9.010  9.010
--  9.000  9.000  8.990  8.980  8.980  8.970  8.970  8.960  8.950  8.950
--  8.940  8.940  8.930  8.920  8.920  8.910  8.910  8.900  8.890  8.890
--  8.880  8.880  8.870  8.860  8.860  8.850  8.850  8.840  8.840  8.830
--  8.820  8.820  8.810  8.810  8.800  8.800  8.790  8.780  8.780  8.770
--  8.770  8.760  8.760  8.750  8.750  8.740  8.730  8.730  8.720  8.720
--  8.710  8.710  8.700  8.700  8.690  8.680  8.680  8.670  8.670  8.660
--  8.660  8.650  8.650  8.640  8.640  8.630  8.630  8.620  8.610  8.610
--  8.600  8.600  8.590  8.590  8.580  8.580  8.570  8.570  8.560  8.560
--  8.550  8.550  8.540  8.540  8.530  8.530  8.520  8.520  8.510  8.500
--  8.500  8.490  8.490  8.480  8.480  8.470  8.470  8.460  8.460  8.450
--  8.450  8.440  8.440  8.430  8.430  8.420  8.420  8.410  8.410  8.400
--  8.400  8.390  8.390  8.380  8.380  8.370  8.370  8.360  8.360  8.360
--  8.350  8.350  8.340  8.340  8.330  8.330  8.320  8.320  8.310  8.310
--  8.300  8.300  8.290  8.290  8.280  8.280  8.270  8.270  8.260  8.260
--  8.250  8.250  8.250  8.240  8.240  8.230  8.230  8.220  8.220  8.210
--  8.210  8.200  8.200  8.190  8.190  8.190  8.180  8.180  8.170  8.170
```

```
--   8.160  8.160  8.150  8.150  8.140  8.140  8.140  8.130  8.130  8.120
--   8.120  8.110  8.110  8.100  8.100  8.100  8.090  8.090  8.080  8.080
--   8.070  8.070  8.060  8.060  8.060  8.050  8.050  8.040  8.040  8.030
--   8.030  8.030  8.020  8.020  8.010  8.010  8.000  8.000  8.000  7.990
--   7.990  7.980  7.980  7.970  7.970  7.970  7.960  7.960  7.950  7.950
--   7.950  7.940  7.940  7.930  7.930  7.920  7.920  7.920  7.910  7.910
--   7.900  7.900  7.900  7.890  7.890  7.880  7.880  7.870  7.870  7.870
--   7.860  7.860  7.850  7.850  7.850  7.840  7.840  7.830  7.830  7.830
--   7.820  7.820  7.810  7.810  7.810  7.800  7.800  7.790  7.790  7.790
--   7.780  7.780  7.780  7.770  7.770  7.760  7.760  7.760  7.750  7.750
--   7.740  7.740  7.740  7.730  7.730  7.720  7.720  7.720  7.710  7.710
--   7.710  7.700  7.700  7.690  7.690  7.690  7.680  7.680  7.680  7.670
--   7.670  7.660  7.660  7.660
------------------------------------------------------------
 Old *.ini *.tab Data from Hawk File with recomputed values
------------------------------------------------------------

*Power On*
[TEXT ] --Opening File "E0809181.237" For Data Storage
[TEXT ] --Make Sure IORDY is on value should be $409 0409
[TEXT ] --Setup Temperature Device
[TEXT ] --Temp Device: Setup went OK
[TEXT ] --Turn on screen dump of spectrum
[TEXT ] --Open Initialization File To Read Variable Settings
[TEXT ] --Data File: hawk020.ini
[TEXT ] --Finished with Initialization File
[TEXT ] --Software Identification
[TEXT ] --       Hawk2 3.00 22Aug07
[TEXT ] --Open Initialization File to read Table of Q values
[TEXT ] --Data File: hawk2.tab
[TEXT ] --Finished with Table File
[TEXT ] ---------------- McaState Dump-------
[TEXT ] --**TestPulser**
[TEXT ] --  Tp1Enable     False  Tp1Amp       $0300
[TEXT ] --  Tp2Enable     False  Tp2Amp       $0300  Tp2Delay      255uS
[TEXT ] --**High Voltage**  HvSetPoint     -708
[TEXT ] --  HvAmp        $0548
[TEXT ] --**Gamma Cutoff Kev**  6
[TEXT ] --**Adjustment Constant   0.7860
[TEXT ] --**Alpha Source**  Alpha SetChn  100  Alpha Cal Chn  20
[TEXT ] --  AlphaMin         10  AlphaMax       1250
[TEXT ] --**Thresholds**  ThrCal       $0880  ThrHigh      $0828
[TEXT ] --**Offsets**  OffLow       $02FA  OffHigh      $0833
[TEXT ] --**Symbols**        DoseEqu Symbol S  Dose Symbol    G
[TEXT ] --**Screen Contrast** 0B00
[TEXT ] --
[TEXT ] --**Data Version**  2
[TEXT ] --Version 2 Data File
[TEXT ] --Q Table conversion
[TEXT ] --Table 1, for hi gain 0 to 25kev/um 0.1 keV/um steps
[TEXT ] --Begin table
[TEXT ] --  1.000  1.000  1.000  1.000  1.000  1.000  1.000  1.000  1.000  1.000
[TEXT ] --  1.000  1.000  1.000  1.000  1.000  1.000  1.000  1.000  1.000  1.000
[TEXT ] --  1.000  1.000  1.000  1.000  1.000  1.000  1.000  1.000  1.000  1.000
[TEXT ] --  1.000  1.000  1.000  1.000  1.000  1.000  1.000  1.000  1.000  1.000
[TEXT ] --  1.000  1.000  1.000  1.000  1.000  1.000  1.000  1.000  1.000  1.000
[TEXT ] --  1.000  1.000  1.000  1.000  1.000  1.000  1.000  1.000  1.000  1.000
[TEXT ] --  1.000  1.000  1.000  1.000  1.000  1.000  1.000  1.000  1.000  1.000
[TEXT ] --  1.000  1.000  1.000  1.000  1.000  1.000  1.000  1.000  1.000  1.000
[TEXT ] --  1.000  1.000  1.000  1.000  1.000  1.000  1.000  1.000  1.000  1.000
[TEXT ] --  1.000  1.000  1.000  1.000  1.000  1.000  1.000  1.000  1.000  1.000
[TEXT ] --  1.016  1.048  1.080  1.112  1.144  1.176  1.208  1.240  1.272  1.304
[TEXT ] --  1.336  1.368  1.400  1.432  1.464  1.496  1.528  1.560  1.592  1.624
[TEXT ] --  1.656  1.688  1.720  1.752  1.784  1.816  1.848  1.880  1.912  1.944
[TEXT ] --  1.976  2.008  2.040  2.072  2.104  2.136  2.168  2.200  2.232  2.264
[TEXT ] --  2.296  2.328  2.360  2.392  2.424  2.456  2.488  2.520  2.552  2.584
[TEXT ] --  2.616  2.648  2.680  2.712  2.744  2.776  2.808  2.840  2.872  2.904
[TEXT ] --  2.936  2.968  3.000  3.032  3.064  3.096  3.128  3.160  3.192  3.224
[TEXT ] --  3.256  3.288  3.320  3.352  3.384  3.416  3.448  3.480  3.512  3.544
```

[TEXT] -- 3.576 3.608 3.640 3.672 3.704 3.736 3.768 3.800 3.832 3.864
[TEXT] -- 3.896 3.928 3.960 3.992 4.024 4.056 4.088 4.120 4.152 4.184
[TEXT] -- 4.216 4.248 4.280 4.312 4.344 4.376 4.408 4.440 4.472 4.504
[TEXT] -- 4.536 4.568 4.600 4.632 4.664 4.696 4.728 4.760 4.792 4.824
[TEXT] -- 4.856 4.888 4.920 4.952 4.984 5.016 5.048 5.080 5.112 5.144
[TEXT] -- 5.176 5.208 5.240 5.272 5.304 5.336 5.368 5.400 5.432 5.464
[TEXT] -- 5.496 5.528 5.560 5.592 5.624 5.656 5.688 5.720 5.752 5.784
[TEXT] -- 5.816 5.848 5.880 5.912 5.944 5.976
[TEXT] --Q Table conversion
[TEXT] --Table 2, for low gain 0 to 1536 kev/um 1.5 keV/um steps
[TEXT] --
[TEXT] -- 1.000 1.000 1.000 1.000 1.000 1.000 1.000 1.400 1.880 2.360
[TEXT] -- 2.840 3.320 3.800 4.280 4.760 5.240 5.720 6.200 6.680 7.160
[TEXT] -- 7.640 8.120 8.600 9.080 9.560 10.040 10.520 11.000 11.480 11.960
[TEXT] -- 12.440 12.920 13.400 13.880 14.360 14.840 15.320 15.800 16.280 16.760
[TEXT] -- 17.240 17.720 18.200 18.680 19.160 19.640 20.120 20.600 21.080 21.560
[TEXT] -- 22.040 22.520 23.000 23.480 23.960 24.440 24.920 25.400 25.880 26.360
[TEXT] -- 26.840 27.320 27.800 28.280 28.760 29.240 29.720 29.810 29.600 29.380
[TEXT] -- 29.170 28.970 28.770 28.570 28.380 28.190 28.010 27.820 27.650 27.470
[TEXT] -- 27.300 27.130 26.970 26.810 26.650 26.490 26.340 26.190 26.040 25.890
[TEXT] -- 25.750 25.610 25.470 25.330 25.200 25.070 24.940 24.810 24.680 24.560
[TEXT] -- 24.430 24.310 24.190 24.080 23.960 23.850 23.740 23.620 23.520 23.410
[TEXT] -- 23.300 23.200 23.090 22.990 22.890 22.790 22.690 22.600 22.500 22.410
[TEXT] -- 22.310 22.220 22.130 22.040 21.950 21.870 21.780 21.690 21.610 21.520
[TEXT] -- 21.440 21.360 21.280 21.200 21.120 21.040 20.970 20.890 20.810 20.740
[TEXT] -- 20.670 20.590 20.520 20.450 20.380 20.310 20.240 20.170 20.100 20.030
[TEXT] -- 19.970 19.900 19.840 19.770 19.710 19.640 19.580 19.520 19.460 19.400
[TEXT] -- 19.330 19.270 19.220 19.160 19.100 19.040 18.980 18.930 18.870 18.810
[TEXT] -- 18.760 18.700 18.650 18.600 18.540 18.490 18.440 18.390 18.330 18.280
[TEXT] -- 18.230 18.180 18.130 18.080 18.030 17.980 17.940 17.890 17.840 17.790
[TEXT] -- 17.750 17.700 17.650 17.610 17.560 17.520 17.470 17.430 17.390 17.340
[TEXT] -- 17.300 17.260 17.210 17.170 17.130 17.090 17.050 17.000 16.960 16.920
[TEXT] -- 16.880 16.840 16.800 16.760 16.720 16.690 16.650 16.610 16.570 16.530
[TEXT] -- 16.500 16.460 16.420 16.380 16.350 16.310 16.280 16.240 16.200 16.170
[TEXT] -- 16.130 16.100 16.060 16.030 16.000 15.960 15.930 15.890 15.860 15.830
[TEXT] -- 15.790 15.760 15.730 15.700 15.670 15.630 15.600 15.570 15.540 15.510
[TEXT] -- 15.480 15.450 15.420 15.380 15.350 15.320 15.290 15.260 15.240 15.210
[TEXT] -- 15.180 15.150 15.120 15.090 15.060 15.030 15.000 14.980 14.950 14.920
[TEXT] -- 14.890 14.870 14.840 14.810 14.780 14.760 14.730 14.700 14.680 14.650
[TEXT] -- 14.630 14.600 14.570 14.550 14.520 14.500 14.470 14.450 14.420 14.400
[TEXT] -- 14.370 14.350 14.320 14.300 14.270 14.250 14.230 14.200 14.180 14.150
[TEXT] -- 14.130 14.110 14.080 14.060 14.040 14.010 13.990 13.970 13.950 13.920
[TEXT] -- 13.900 13.880 13.860 13.830 13.810 13.790 13.770 13.750 13.730 13.700
[TEXT] -- 13.680 13.660 13.640 13.620 13.600 13.580 13.560 13.540 13.510 13.490
[TEXT] -- 13.470 13.450 13.430 13.410 13.390 13.370 13.350 13.330 13.310 13.290
[TEXT] -- 13.270 13.260 13.240 13.220 13.200 13.180 13.160 13.140 13.120 13.100
[TEXT] -- 13.080 13.070 13.050 13.030 13.010 12.990 12.970 12.960 12.940 12.920
[TEXT] -- 12.900 12.880 12.870 12.850 12.830 12.810 12.790 12.780 12.760 12.740
[TEXT] -- 12.730 12.710 12.690 12.670 12.660 12.640 12.620 12.610 12.590 12.570
[TEXT] -- 12.560 12.540 12.520 12.510 12.490 12.480 12.460 12.440 12.430 12.410
[TEXT] -- 12.400 12.380 12.360 12.350 12.330 12.320 12.300 12.290 12.270 12.260
[TEXT] -- 12.240 12.220 12.210 12.190 12.180 12.160 12.150 12.130 12.120 12.100
[TEXT] -- 12.090 12.080 12.060 12.050 12.030 12.020 12.000 11.990 11.970 11.960
[TEXT] -- 11.950 11.930 11.920 11.900 11.890 11.870 11.860 11.850 11.830 11.820
[TEXT] -- 11.810 11.790 11.780 11.760 11.750 11.740 11.720 11.710 11.700 11.680
[TEXT] -- 11.670 11.660 11.640 11.630 11.620 11.610 11.590 11.580 11.570 11.550
[TEXT] -- 11.540 11.530 11.520 11.500 11.490 11.480 11.460 11.450 11.440 11.430
[TEXT] -- 11.410 11.400 11.390 11.380 11.370 11.350 11.340 11.330 11.320 11.300
[TEXT] -- 11.290 11.280 11.270 11.260 11.240 11.230 11.220 11.210 11.200 11.190
[TEXT] -- 11.170 11.160 11.150 11.140 11.130 11.120 11.110 11.090 11.080 11.070
[TEXT] -- 11.060 11.050 11.040 11.030 11.020 11.000 10.990 10.980 10.970 10.960
[TEXT] -- 10.950 10.940 10.930 10.920 10.910 10.890 10.880 10.870 10.860 10.850
[TEXT] -- 10.840 10.830 10.820 10.810 10.800 10.790 10.780 10.770 10.760 10.750
[TEXT] -- 10.740 10.730 10.720 10.710 10.700 10.690 10.680 10.670 10.650 10.640
[TEXT] -- 10.630 10.620 10.610 10.600 10.600 10.590 10.580 10.570 10.560 10.550
[TEXT] -- 10.540 10.530 10.520 10.510 10.500 10.490 10.480 10.470 10.460 10.450
[TEXT] -- 10.440 10.430 10.420 10.410 10.400 10.390 10.380 10.370 10.360 10.360
[TEXT] -- 10.350 10.340 10.330 10.320 10.310 10.300 10.290 10.280 10.270 10.260
[TEXT] -- 10.260 10.250 10.240 10.230 10.220 10.210 10.200 10.190 10.180 10.180

[TEXT] -- 10.170 10.160 10.150 10.140 10.130 10.120 10.110 10.110 10.100 10.090
[TEXT] -- 10.080 10.070 10.060 10.050 10.050 10.040 10.030 10.020 10.010 10.000
[TEXT] -- 10.000 9.990 9.980 9.970 9.960 9.950 9.950 9.940 9.930 9.920
[TEXT] -- 9.910 9.910 9.900 9.890 9.880 9.870 9.870 9.860 9.850 9.840
[TEXT] -- 9.830 9.830 9.820 9.810 9.800 9.790 9.790 9.780 9.770 9.760
[TEXT] -- 9.760 9.750 9.740 9.730 9.720 9.720 9.710 9.700 9.690 9.690
[TEXT] -- 9.680 9.670 9.660 9.660 9.650 9.640 9.630 9.630 9.620 9.610
[TEXT] -- 9.600 9.600 9.590 9.580 9.570 9.570 9.560 9.550 9.550 9.540
[TEXT] -- 9.530 9.520 9.520 9.510 9.500 9.500 9.490 9.480 9.470 9.470
[TEXT] -- 9.460 9.450 9.450 9.440 9.430 9.420 9.420 9.410 9.400 9.400
[TEXT] -- 9.390 9.380 9.380 9.370 9.360 9.360 9.350 9.340 9.340 9.330
[TEXT] -- 9.320 9.310 9.310 9.300 9.290 9.290 9.280 9.270 9.270 9.260
[TEXT] -- 9.250 9.250 9.240 9.240 9.230 9.220 9.220 9.210 9.200 9.200
[TEXT] -- 9.190 9.180 9.180 9.170 9.160 9.160 9.150 9.140 9.140 9.130
[TEXT] -- 9.130 9.120 9.110 9.110 9.100 9.090 9.090 9.080 9.080 9.070
[TEXT] -- 9.060 9.060 9.050 9.040 9.040 9.030 9.030 9.020 9.010 9.010
[TEXT] -- 9.000 9.000 8.990 8.980 8.980 8.970 8.970 8.960 8.950 8.950
[TEXT] -- 8.940 8.940 8.930 8.920 8.920 8.910 8.910 8.900 8.890 8.890
[TEXT] -- 8.880 8.880 8.870 8.860 8.860 8.850 8.850 8.840 8.840 8.830
[TEXT] -- 8.820 8.820 8.810 8.810 8.800 8.800 8.790 8.780 8.780 8.770
[TEXT] -- 8.770 8.760 8.760 8.750 8.750 8.740 8.730 8.730 8.720 8.720
[TEXT] -- 8.710 8.710 8.700 8.700 8.690 8.680 8.680 8.670 8.670 8.660
[TEXT] -- 8.660 8.650 8.650 8.640 8.640 8.630 8.630 8.620 8.610 8.610
[TEXT] -- 8.600 8.600 8.590 8.590 8.580 8.580 8.570 8.570 8.560 8.560
[TEXT] -- 8.550 8.550 8.540 8.540 8.530 8.530 8.520 8.520 8.510 8.500
[TEXT] -- 8.500 8.490 8.490 8.480 8.480 8.470 8.470 8.460 8.460 8.450
[TEXT] -- 8.450 8.440 8.440 8.430 8.430 8.420 8.420 8.410 8.410 8.400
[TEXT] -- 8.400 8.390 8.390 8.380 8.380 8.370 8.370 8.360 8.360 8.360
[TEXT] -- 8.350 8.350 8.340 8.340 8.330 8.330 8.320 8.320 8.310 8.310
[TEXT] -- 8.300 8.300 8.290 8.290 8.280 8.280 8.270 8.270 8.260 8.260
[TEXT] -- 8.250 8.250 8.250 8.240 8.240 8.230 8.230 8.220 8.220 8.210
[TEXT] -- 8.210 8.200 8.200 8.190 8.190 8.190 8.180 8.180 8.170 8.170
[TEXT] -- 8.160 8.160 8.150 8.150 8.140 8.140 8.140 8.130 8.130 8.120
[TEXT] -- 8.120 8.110 8.110 8.100 8.100 8.100 8.090 8.090 8.080 8.080
[TEXT] -- 8.070 8.070 8.060 8.060 8.060 8.050 8.050 8.040 8.040 8.030
[TEXT] -- 8.030 8.030 8.020 8.020 8.010 8.010 8.000 8.000 8.000 7.990
[TEXT] -- 7.990 7.980 7.980 7.970 7.970 7.970 7.960 7.960 7.950 7.950
[TEXT] -- 7.950 7.940 7.940 7.930 7.930 7.920 7.920 7.920 7.910 7.910
[TEXT] -- 7.900 7.900 7.900 7.890 7.890 7.880 7.880 7.870 7.870 7.870
[TEXT] -- 7.860 7.860 7.850 7.850 7.850 7.840 7.840 7.830 7.830 7.830
[TEXT] -- 7.820 7.820 7.810 7.810 7.810 7.800 7.800 7.790 7.790 7.790
[TEXT] -- 7.780 7.780 7.780 7.770 7.770 7.760 7.760 7.760 7.750 7.750
[TEXT] -- 7.740 7.740 7.740 7.730 7.730 7.720 7.720 7.720 7.710 7.710
[TEXT] -- 7.710 7.700 7.700 7.690 7.690 7.690 7.680 7.680 7.680 7.670
[TEXT] -- 7.670 7.660 7.660 7.660
[TEXT] --GPS RX OK
[TEXT] --Flash Disk Size Installed is 966 Mega-Bytes
[TEXT] --Hawk Startup
[TEXT] --Flush Tepc Data File
[TEXT] --Opening File "E0809181.237" For Data Storage
[TEXT] --Temperature Device Serial # 22FD3206000000A3
[TEXT] [UnitId] 22FD3206000000A3
Ini File Unit Id is 22FD3206000000A3
Data File Unit Id is 22FD3206000000A3
,Local, Local, Elapsed, High , Units, HV , Units , Temp., Temp., GPS , GPS, GPS , GPS , GPS , North, GPS , East, GPS ,
Units, Error, Total , Gamma Counts, Total, Dose, Gamma Dose, Units , Total , Units , Q , DeadTime , Cal Status, Estimated, Counts,
Cal. Adj. , Cal Status, Estimated, Counts, Cal. Adj.New Gamma, New_Dose , Units , New , Units , New_Total , Units ,
,Time, Date, Time, Voltage, Volts, Current, microAmps, Inside, Units, Status1, Status2, Time, Date, Latitude, South, Longitude, West,
Altitude, meter, Codes, Counts (cpm), < cutoff , Dose , Units, < cutoff, Gamma Dose, Dose Equ., Dose Equ., Factor, Correction, mPeak ,
mPeak, mPeak, mPeak, cPeak, cPeak , cPeak, cPeakCnts < cutoff, Total , Dose , Gamma_Dose, Gamma , Dose_Equ. , Dose_Equ.
, 12:38:52, 18SEP08, 0000:00:00, -388 , V , 1.0 , uA , 25 , C , OkGPS , OkAntRam, 12:39:12, 18Sep08 , 39.0, N, 76.3, W, -31, m
,_____, 2, 2, 48.86, pG, 48.86, pG, 48.86, pS, 1.00, 1.00000, No mPeak, 0, 0, 0.00000, NoCalPk, 1.00000 ,2 ,48.86, pG, 48.86, pG,
48.86, pS,
, 12:39:57, 18SEP08, 0000:01:04, -680 , V , 1.7 , uA , 26 , C , OkGPS , OkAntRam, 12:40:12, 18Sep08 , 39.0, N, 76.3, W, -36, m
,__H+_____, 30, 30, 931.3, pG, 931.3, pG, 931.3, pS, 1.00, 1.00003, No mPeak, 0, 0, 0.00000, NoCalPk, 1.00000 ,30 ,931.3, pG, 931.3,
pG, 931.3, pS,

... ... ••• ••• •••

APPENDIX C: HAWK020 Output Example

175 --Hawk Startup
176 --Flush Tape Data File
177 --Opening File "E0803181.237" For Data Storage
178 --Temperature Device Serial # 22FD3206000000A3
179 [UnitId] 22FD3206000000A3
180

181	Local	Local	Elapsed	High	Units	HV	Units	Temp.	Temp.	GPS	GPS	GPS	GPS	GPS	North	GPS	East	GPS	Units	Error	Total	Gamma	Total	Dose	Gamma	Units	Total	Units	G	DeadTir	Cal Stat	Estimat	Counts	Cal Stat	Estimat	Counts
182	Time	Date	Time	Voltage	Volts	Current	microAr	Inside	Units	Status1	Status2	Time	Date	Latitude	South	Longitu	West	Altitude	meter	Codes	Counts	< cutoff	Dose	Units	< cutoff	Gamma	Dose Ec	Dose Ec	Factor	Correct	mPeak	mPeak	mPeak	cPeak	cPeak	cPeak
183	12:38:58	18SEP0	0000:0(	-388	V	1	uA	25	C	OkGPS	OkAntR	12:33:12	18Sep0:	33	N	76.3	W	-31	m	_____	2	2	48.86	pG	48.86	pG	48.86	pS	1	1	No mPe	0	0	0	NoCalP	1
184	12:39:51	18SEP0	0000:0(	-680	V	1.7	uA	26	C	OkGPS	OkAntR	12:40:12	18Sep0:	33	N	76.3	W	-36	m	__H+__	30	30	931.3	pG	931.3	pG	931.3	pS	1	1	No mPe	0	0	0	NoCalP	1
185	12:40:51	18SEP0	0000:0:	-700	V	1.7	uA	26	C	PdopTc	OkAntR									__H+__	23	22	2.126	nG	808.3	pG	39.96	nS	18.79	1	No mPe	67	1	0.67	NoCalP	1
186	12:41:58	18SEP0	0000:0:	-707	V	1.7	uA	26	C	PdopTc	OkAntR									__H8_G	27	26	1.561	nG	1.155	nG	4.257	nS	2.73	1	No mPe	21	1	0.21	NoCalP	1
187	12:42:58	18SEP0	0000:0-	-707	V	1.7	uA	26	C	OkGPS	OkAntR	12:43:12	18Sep0:	33	N	76.3	W	-23	m	_____G	24	24	730.2	pG	730.2	pG	730.2	pS	1	1	No mPe	0	0	0	NoCalP	1
188	12:43:51	18SEP0	0000:0!	-707	V	1.7	uA	26	C	OkGPS	OkAntR	12:44:12	18Sep0:	33	N	76.3	W	-34	m	_____	15	15	230.4	pG	230.4	pG	230.4	pS	1	1	No mPe	0	0	0	NoCalP	1
189	12:44:51	18SEP0	0000:0!	-706	V	1.7	uA	26	C	Only3Sa	OkAntR									_____	27	26	384	pG	302.8	pG	384	pS	1	1	No mPe	0	0	0	NoCalP	1
190	12:45:58	18SEP0	0000:0"	-707	V	1.7	uA	26	C	OkGPS	OkAntR	12:46:12	18Sep0:	33	N	76.3	W	-54	m	_____G	16	16	575.2	pG	575.2	pG	575.2	pS	1	1	No mPe	0	0	0	NoCalP	1
191	12:46:51	18SEP0	0000:0#	-707	V	1.7	uA	26	C	OkGPS	OkAntR	12:47:12	18Sep0:	33	N	76.3	W	-71	m	_____	26	26	758.7	pG	758.7	pG	758.7	pS	1	1	No mPe	0	0	0	NoCalP	1
192	12:47:57	18SEP0	0000:0:	-706	V	1.7	uA	26	C	Only3Sa	OkAntR									_____	37	37	1.239	nG	1.239	nG	1.239	nS	1	1	No mPe	0	0	0	NoCalP	1
193	12:48:58	18SEP0	0000:10	-707	V	1.7	uA	26	C	Only3Sa	OkAntR									_____G	26	26	892.3	pG	892.3	pG	892.3	pS	1	1	No mPe	0	0	0	NoCalP	1
194	12:49:51	18SEP0	0000:11	-706	V	1.7	uA	26	C	OkGPS	OkAntR	12:50:12	18Sep0:	33	N	76.3	W	-44	m	_____G	23	22	310.3	pG	829.1	pG	310.3	pS	1	1	No mPe	0	0	0	NoCalP	1
195	12:50:58	18SEP0	0000:12	-707	V	1.7	uA	26	C	OkGPS	OkAntR	12:51:12	18Sep0:	33	N	76.3	W	41	m	_____	25	24	1.367	nG	530.1	pG	41.03	nS	20.87	1	No mPe	70	1	0.7	NoCalP	1
196	12:51:58	18SEP0	0000:13	-707	V	1.7	uA	26	C	OkGPS	OkAntR	12:52:12	18Sep0:	33	N	76.3	W	183	m	_____	20	20	574.5	pG	574.5	pG	574.5	pS	1	1	No mPe	0	0	0	NoCalP	1
197	12:52:57	18SEP0	0000:14	-707	V	1.7	uA	26	C	OkGPS	OkAntR	12:53:12	18Sep0:	33	N	76.3	W	343	m	_____	14	13	1.301	nG	386	pG	42.83	nS	22.53	1	No mPe	77	1	0.77	NoCalP	1
198	12:53:58	18SEP0	0000:15	-706	V	1.7	uA	26	C	OkGPS	OkAntR	12:54:12	18Sep0:	33	N	76.2	W	473	m	_____	16	16	563.6	pG	563.6	pG	563.6	pS	1	1	No mPe	0	0	0	NoCalP	1
199	12:54:58	18SEP0	0000:16	-706	V	1.6	uA	26	C	OkGPS	OkAntR	12:55:12	18Sep0:	33	N	76.2	W	604	m	_____	22	22	806.8	pG	806.8	pG	806.8	pS	1	1	No mPe	0	0	0	NoCalP	1
200	12:55:58	18SEP0	0000:17	-706	V	1.6	uA	26	C	OkGPS	OkAntR	12:56:12	18Sep0:	33	N	76.2	W	729	m	_____	17	16	1.018	nG	512.5	pG	5.584	nS	5.49	1	No mPe	26	1	0.26	NoCalP	1
201	12:56:55	18SEP0	0000:18	-707	V	1.6	uA	26	C	OkGPS	OkAntR	12:57:12	18Sep0:	33	N	76.2	W	828	m	_____	17	17	484.7	pG	484.7	pG	484.7	pS	1	1	No mPe	0	0	0	NoCalP	1
202	12:57:57	18SEP0	0000:19	-706	V	1.6	uA	26	C	OkGPS	OkAntR	12:58:12	18Sep0:	33	N	76.1	W	937	m	_____	14	14	543.3	pG	543.3	pG	543.3	pS	1	1	No mPe	0	0	0	NoCalP	1
203	12:58:58	18SEP0	0000:2(	-707	V	1.7	uA	26	C	OkGPS	OkAntR	12:59:12	18Sep0:	38.9	N	76.1	W	1064	m	_____	24	24	1.266	nG	1.266	nG	1.266	nS	1	1	No mPe	0	0	0	NoCalP	1
204	12:59:58	18SEP0	0000:2"	-706	V	1.6	uA	26	C	OkGPS	OkAntR	13:00:12	18Sep0:	38.9	N	76.2	W	1173	m	_____	21	21	705.9	pG	705.9	pG	705.9	pS	1	1	No mPe	0	0	0	NoCalP	1
205	13:00:58	18SEP0	0000:2:	-707	V	1.6	uA	26	C	OkGPS	OkAntR	13:01:12	18Sep0:	38.9	N	76.2	W	1287	m	_____	20	20	680.6	pG	680.6	pG	680.6	pS	1	1	No mPe	0	0	0	NoCalP	1
206	13:01:58	18SEP0	0000:2:	-707	V	1.6	uA	26	C	OkGPS	OkAntR	13:02:12	18Sep0:	38.9	N	76.1	W	1401	m	_____	18	16	833.2	pG	508.3	pG	1.469	nS	1.76	1	No mPe	0	0	0	NoCalP	1
207	13:02:58	18SEP0	0000:2-	-707	V	1.6	uA	26	C	OkGPS	OkAntR	13:03:12	18Sep0:	38.9	N	76.1	W	1505	m	_____	18	18	1.207	nG	1.207	nG	1.207	nS	1	1	No mPe	0	0	0	NoCalP	1
208	13:03:58	18SEP0	0000:2!	-706	V	1.6	uA	26	C	OkGPS	OkAntR	13:04:12	18Sep0:	38.9	N	76.1	W	1686	m	_____	19	19	826.6	pG	826.6	pG	826.6	pS	1	1	No mPe	0	0	0	NoCalP	1
209	13:04:51	18SEP0	0000:2#	-706	V	1.6	uA	26	C	OkGPS	OkAntR	13:05:12	18Sep0:	38.9	N	76.2	W	1709	m	_____	30	23	1.064	nG	357.5	pG	1.064	nS	1	1	No mPe	0	0	0	NoCalP	1
210	13:05:58	18SEP0	0000:2$	-707	V	1.6	uA	26	C	OkGPS	OkAntR	13:06:12	18Sep0:	38.9	N	76.1	W	1793	m	_____	21	21	594.1	pG	594.1	pG	594.1	pS	1	1	No mPe	0	0	0	NoCalP	1
211	13:06:58	18SEP0	0000:2%	-706	V	1.6	uA	26	C	OkGPS	OkAntR	13:07:12	18Sep0:	38.9	N	76.1	W	1896	m	_____	26	25	1.007	nG	303	pG	1.007	nS	1	1	No mPe	0	0	0	NoCalP	1
212	13:07:58	18SEP0	0000:2^	-707	V	1.6	uA	26	C	OkGPS	OkAntR	13:08:12	18Sep0:	38.9	N	76.1	W	1977	m	_____	27	27	683.2	pG	683.2	pG	683.2	pS	1	1	No mPe	0	0	0	NoCalP	1
213	13:08:58	18SEP0	0000:3(	-706	V	1.6	uA	26	C	OkGPS	OkAntR	13:09:12	18Sep0:	38.9	N	76.2	W	2047	m	_____	26	24	2.386	nG	751.1	pG	43.82	nS	18.37	1	No mPe	79	1	0.79	NoCalP	1
214	13:09:58	18SEP0	0000:3)	-707	V	1.6	uA	26	C	OkGPS	OkAntR	13:10:12	18Sep0:	38.9	N	76.2	W	2147	m	_____	23	22	792.6	pG	710.1	pG	792.6	pS	1	1	No mPe	0	0	0	NoCalP	1
215	13:10:58	18SEP0	0000:3_	-706	V	1.6	uA	26	C	OkGPS	OkAntR	13:11:12	18Sep0:	38.9	N	76.2	W	2248	m	_____	31	31	943.2	pG	943.2	pG	943.2	pS	1	1	No mPe	0	0	0	NoCalP	1
216	13:11:58	18SEP0	0000:3+	-706	V	1.6	uA	26	C	OkGPS	OkAntR	13:12:12	18Sep0:	38.9	N	76.1	W	2315	m	_____	31	29	1.535	nG	1.008	nG	4.922	nS	3.21	1	No mPe	23	1	0.23	NoCalP	1
217	13:12:59	18SEP0	0000:3-	-706	V	1.6	uA	26	C	OkGPS	OkAntR	13:13:12	18Sep0:	38.9	N	76.1	W	2383	m	_____	27	27	1.1	nG	1.1	nG	1.1	nS	1	1	No mPe	0	0	0	NoCalP	1
218	13:13:58	18SEP0	0000:3=	-706	V	1.6	uA	26	C	OkGPS	OkAntR	13:14:12	18Sep0:	39	N	76.1	W	2420	m	_____	34	34	1.1	nG	1.1	nG	1.1	nS	1	1	No mPe	0	0	0	NoCalP	1
219	13:14:58	18SEP0	0000:3{	-706	V	1.6	uA	26	C	OkGPS	OkAntR	13:15:12	18Sep0:	39	N	76.1	W	2464	m	_____	38	37	1.843	nG	1.265	nG	8.254	nS	4.46	1	No mPe	30	1	0.3	NoCalP	1
220	13:15:59	18SEP0	0000:3'	-707	V	1.6	uA	26	C	OkGPS	OkAntR	13:16:12	18Sep0:	39	N	76.2	W	2528	m	_____	32	32	990.2	pG	990.2	pS	1	1	No mPe	0	0	0	NoCalP	1
221	13:16:58	18SEP0	0000:3}	-707	V	1.6	uA	26	C	OkGPS	OkAntR	13:17:12	18Sep0:	38.9	N	76.2	W	2593	m	_____	33	33	1.14	nG	1.14	nG	1.14	nS	1	1	No mPe	0	0	0	NoCalP	1
222	13:17:58	18SEP0	0000:3:	-706	V	1.6	uA	26	C	OkGPS	OkAntR	13:18:12	18Sep0:	38.9	N	76.2	W	2657	m	_____	35	33	1.364	nG	1.138	nG	1.364	nS	1	1	No mPe	0	0	0	NoCalP	1
223	13:18:58	18SEP0	0000:4(	-706	V	1.6	uA	25	C	OkGPS	OkAntR	13:19:12	18Sep0:	38.9	N	75.2	W	2718	m	_____	40	40	1.126	nG	1.126	nG	1.126	nS	1	1	No mPe	0	0	0	NoCalP	1
224	13:19:58	18SEP0	0000:4'	-706	V	1.6	uA	25	C	OkGPS	OkAntR	13:20:12	18Sep0:	38.9	N	3.2	W	2794	m	_____	31	30	866.6	pG	733.9	pG	868.8	pS	1	1	No mPe	0	0	0	NoCalP	1

APPENDIX D: SPECT2 Output File

Program SPECT2 10Dec04 Version 2.01
File : E0805140.652
spect2 14MAY08 06:50 14MAY08 10:30 e0805140.652
Accumulating Spectrum .... please wait...

Power On
14MAY08 06:53
14MAY08 06:54
14MAY08 06:55
… …
14MAY08 08:53
14MAY08 08:54
14MAY08 08:55
14MAY08 08:56

Ready to Close Data File
Accumulated 123 minutes of data

Table of Accumulated Spectrum

Lo-Gain Data			Hi-Gain Data		
Chn#	keV/um	Counts	Chn#	keV/um	Counts
0	0 to 1	445	0	0.000 to 0.100	0
1	1 to 2	3263	1	0.100 to 0.200	0
2	2 to 3	430	2	0.200 to 0.300	0
3	3 to 4	113	3	0.300 to 0.400	0
…	…	…	…	…	…
255	255 to 256	0	255	25.500 to 25.600	20
256	256 to 257	0			
257	257 to 258	0			
258	258 to 259	0			
259	259 to 260	0			
260	260 to 261	0			
261	261 to 262	0			
262	262 to 263	0			
263	263 to 264	0			
264	264 to 265	0			
265	265 to 266	0			
266	266 to 267	0			
267	267 to 268	0			
268	268 to 269	0			
269	269 to 270	0			
270	270 to 271	0			
271	271 to 272	0			
272	272 to 273	0			
273	273 to 274	0			
274	274 to 275	0			
275	275 to 276	0			
…	…	…			
1023	1023 to 1024	0			

APPENDIX E: Deriving Dose from Spectrum Data (completed by Dr. Lewis at the Royal Military College)

Detecting particles in the atmosphere requires a device capable of measuring a wide range of energies and careful consideration in the theory behind operation. As particles enter and deposit energy within the TEPC's propane sphere, the electric charge produced migrates toward a very thin (0.006 cm) anode. These pulses are recorded by a multichannel analyzer (MCA) which analyzes the pulse height and assigns a lineal energy bin. The spectrum recorded and outputted to the user is an event frequency distribution which reads total counts per energy bin. It is important to remember that the energy imparted on the spherical detector is a stochastic quantity.

$$\varepsilon = \sum_i \varepsilon_i \tag{E.1}$$

Each interaction follows this general rule for energy deposition:

$$\varepsilon_i = T_{in} - T_{out} + Q_{\Delta m} \tag{E.2}$$

T_{in} = incident energy of ionizing particle

T_{out} = total energy of all ionizing particles leaving the interaction

$Q_{\Delta m}$ = changes of the rest mass energy of the atom and all particles involved in the interaction, a positive value for when the rest mass decreases and a negative value for when rest mass increases.

There must also be a relation between the energy loss of charged particles passing through a tissue sphere and a gas sphere with "tissue-equivalent" properties.

$$\Delta E_t = \left(\frac{S}{\rho}\right)_t \rho_t d_t = \Delta E_g = \left(\frac{S}{\rho}\right)_g \rho_g d_g \tag{E.3}$$

ΔE_t, ΔE_g = mean energy losses from particles in tissue (t) and gas (g)

ρ = density

$\left(\frac{S}{\rho}\right)_t$ = mass stopping powers

$d_{t,g}$ = diameter of tissue and gas, respectively

Assuming the atomic composition of tissue and gas are identical and the mass stopping powers are independent of density, the absorbed dose D in the detector and tissue site should be equal:

$$D_d = \frac{\varepsilon_d}{\rho_d V_d} = D_t = \frac{\varepsilon_t}{\rho_t V_t} \tag{E.4}$$

$D_{d,t}$ = absorbed dose in detector and tissue

$\rho_t V_t, \rho_d V_d$ = mass of tissue and detector, respectively

The volume of both detector and tissue sphere is given by:

$$V_d = \frac{\pi}{6} d_d^3 \tag{E.5}$$

$$V_t = \frac{\pi}{6} d_t^3 \tag{E.6}$$

Another important characteristic of this device is to understand that even though the diameter of the detecting sphere is much greater than a single cell, the energy deposited per event is the same in the detector and tissue site because of the equivalence in their respective chemical compositions. Thus, the detector is known as a tissue equivalent counter. The term that describes this equivalence is the specific energy, z, in units of Joules per kilogram. For each event, the below relation will serve as the correction factor for energy deposited in a 5 inch detecting sphere rather than a one micron-sized tissue cell.

$$z_t = z_d = \frac{\varepsilon_t}{m_t} = \frac{\varepsilon_d}{m_d} \rightarrow \varepsilon_t = \varepsilon_d \left(\frac{\rho_t}{\rho_d}\right)\left(\frac{V_t}{V_d}\right) = \varepsilon_d \left(\frac{\rho_t}{\rho_d}\right)\left(\frac{d_t^3}{d_d^3}\right) = \varepsilon_d \left(\frac{d_t^2}{d_d^2}\right) \tag{E.7}$$

For a dose calculation, there must also be a relation of the *lineal* energy, *y*, to the specific energy (J/kg) deposited along the mean chord length:

$$y = \frac{\varepsilon}{\bar{l}} = \frac{z \cdot m}{\bar{l}} \tag{E.8}$$

The mean chord length is determined from Cauchy's theorem [39] for a convex site with a volume V and surface area S and takes into account the probability of a particle entering the sphere at different locations and having varying chord lengths:

$$\bar{l} = \frac{4V}{S} \tag{E.9}$$

Relating the lineal energy to the mean chord length and specific energy in a sphere leads to:

$$y = \frac{z \cdot m \cdot S}{4V} = \frac{z \cdot p \cdot S}{4} \quad \rightarrow \quad z = \frac{4y}{\rho \cdot S} = \frac{y}{\rho \pi r^2} \tag{E.10}$$

After assumptions are made, like a spherical tissue site of radius r and a tissue density of 1 g/cm^3, equation E.10 can be simplified:

$$z\left(\frac{J}{kg}\right) = \frac{y\left(\frac{keV}{\mu m}\right)}{\pi \cdot \frac{d_t^2}{2}\,(\mu m^2) \cdot 1\left(\frac{g}{cm^3}\right)} \text{x} \frac{1000\ g}{1\ kg} \text{x} \frac{1.602E{-}16\ J}{keV} \text{x} \frac{1\ \mu m^3}{(1E^{-4})^3 cm^3} \rightarrow \quad z = \frac{0.204y}{d_t^2} \tag{E.11}$$

The total absorbed dose in the ideal spherical gas cavity is equal to the average (frequency-mean) specific energy per event (z_f) times the total number of events in the cavity. The specific energy

may be due to one or more energy deposition events. The probability density of the specific energy deposited in a single event is $f_1(z)$, and it is assumed that the probability density is equivalent for both specific energy and lineal energy, $f_1(z)dz = f(y)dy$. Multiplying both sides by z and integrating from zero to infinity leads to the frequency mean:

$$\bar{z}_f = \int_0^\infty z f_1(z) dz = \int_0^\infty z f(y) dy = \frac{0.204}{d_t^2} \int_0^\infty y f(y) dy = \frac{0.204}{d_t^2} \bar{y}_f \quad \text{(E.12)}$$

To arrive at the frequency-mean lineal energy, the probability of detecting particles of different energies needs to be addressed. First, the probability that the lineal energy is equal to or less than a certain value of y is given by the cumulative distribution function F(y):

$$F(y_i) = \frac{\sum_{i=0}^{i} n(y_i)}{\sum_{i=0}^{\infty} n(y_i)} \quad \text{(E.13)}$$

The probability density, or lineal energy distribution, is further defined from probability theory as:

$$f(y) = \frac{dF(y)}{dy} \approx \frac{\Delta F(y_i)}{\Delta y_i} = f(y_i) \quad \text{(E.14)}$$

and normalized:

$$\int_0^\infty f(y) dy = 1 \quad \text{(E.15)}$$

For the numerical implementation of the above equation, the standard difference approximation is:

$$\Delta F(y_i) = F(y_i) - F(y_{i-1}) = \frac{\sum_{i=0}^{i} n(y_i) - \sum_{i=0}^{i-1} n(y_i)}{\sum_{i=0}^{\infty} n(y_i)} = \frac{n(y_i)}{\sum_{i=0}^{\infty} n(y_i)} \quad \text{(E.16)}$$

Now, the probability density function becomes:

$$f(y_i) = \frac{n(y_i)}{\Delta y_i \sum_0^\infty n(y_i)} \quad \text{(E.17)}$$

The frequency-mean lineal energy $\bar{y}_F$ is the expectation value of lineal energy, *y*, as weighted by the frequency probability density:

$$\bar{y}_f = \frac{\int_0^\infty y f(y) dy}{\int_0^\infty f(y) dy} = \int_0^\infty y f(y) dy \approx \sum_{i=0}^{\infty} y_i f(y_i) \Delta y_i \quad \text{(E.18)}$$

The final step involves relating the specific energy that takes into account the geometry of the detector, to the surface area correction factor applied to the entire spectrum, and the frequency mean lineal energy.

$$D = z * \text{EnerDepCorrectFactor} * \bar{y}_F = \frac{0.204}{d_t^2}\sum_{i=0}^{\infty} n(y_i)\left(\frac{d_t^2}{d_d^2}\right)\bar{y}_F$$

$$= \frac{0.204}{d_d^2}\left(\sum_{i=0}^{\infty} n(y_i)\right)\left(\sum_{i=0}^{\infty} y_i f(y_i)\Delta y_i\right)$$

$$D = \frac{0.204}{d_d^2}\left(\sum_{i=0}^{\infty} y_i\right)\left(\sum_{i=0}^{\infty} y_i \frac{n(y_i)}{\Delta y_i \sum_{i=0\infty}^{\infty} n(y_i)}\Delta y_i\right) = \frac{0.204}{d_d^2}\sum_{i=0}^{\infty} y_i n(y_i) \quad \text{(E.19)}$$

To determine the dose equivalent, a quality factor is simply applied to each event, based upon the amount of energy deposited, and multiplied by the dose from the corresponding event.

$$H = \frac{0.204}{d_d^2}\sum_{i=0}^{\infty} q(y_i) y_i n(y_i) \quad \text{(E.20)}$$

Where q(y) = quality factor

Appendix F – MCNP Cobalt-60 Source Code

```
JpdCo-60 no steel container
c   Photon interactions in Tissue Equivalent Proportional Counter
c   Rossi-Type spherical detector
c   Trident Research:  “Analyzing the Mixed Radiation Field of Navy Pilots and
c   Aircrew”
c   Created on: Saturday, September 06, 2008
c   Modified: Wednesday, October 22, 2008
c   Created by: MIDN 1/c Dobisesky
c
c   Cells
c
    1     2 -1.000000 -1            $soft tissue
    8     1 -0.001205 1 -6 7        $source air cell
c
    20    0          6              $outer space
c
c   Surfaces
c
    1        so 0.000001
    4        py 0
    5        px 0
    6        so 300
    7        py 9
c
c   Data
c
mode  p e
imp:p   1 10r 0
imp:e   1 10r 0
SDEF PAR=P POS=0 10 0 ERG=D1      $ for Cobalt-60 Source
SI1 L  1.173 1.332                $ the 2 discrete energies (MeV)
SP1   0.5 0.5                     $ frequency of each energy
*f8:P,E 1
f1:P 1                          $surface current
f6:P 1                          $energy deposited in the detector gas (MeV/g)
e8: 0 1E-006 1024I 1.4
m1    6000.04p      -0.000124  &  $ Dry Air (Near Sea Level)
      7000.04p      -0.755268  &
      8000.04p      -0.231781  &
      18000.04p     -0.012827
m2    1000.04p      -0.104472  &  $ Soft Tissue (ICRP)
      6000.04p      -0.232190  &
      7000.04p      -0.024880  &
      8000.04p      -0.630238  &
      11000.04p     -0.001130  &
      12000.04p     -0.000130  &
      15000.04p     -0.001330  &
      16000.04p     -0.001990  &
      17000.04p     -0.001340  &
      19000.04p     -0.001990  &
      20000.04p     -0.000230  &
      26000.04p     -0.000050  &
      30000.04p     -0.000030
CTME 1440          $ one day run
print
```

Appendix G – Energy Dependent Particle Flux Plots Calculated with EXPACS

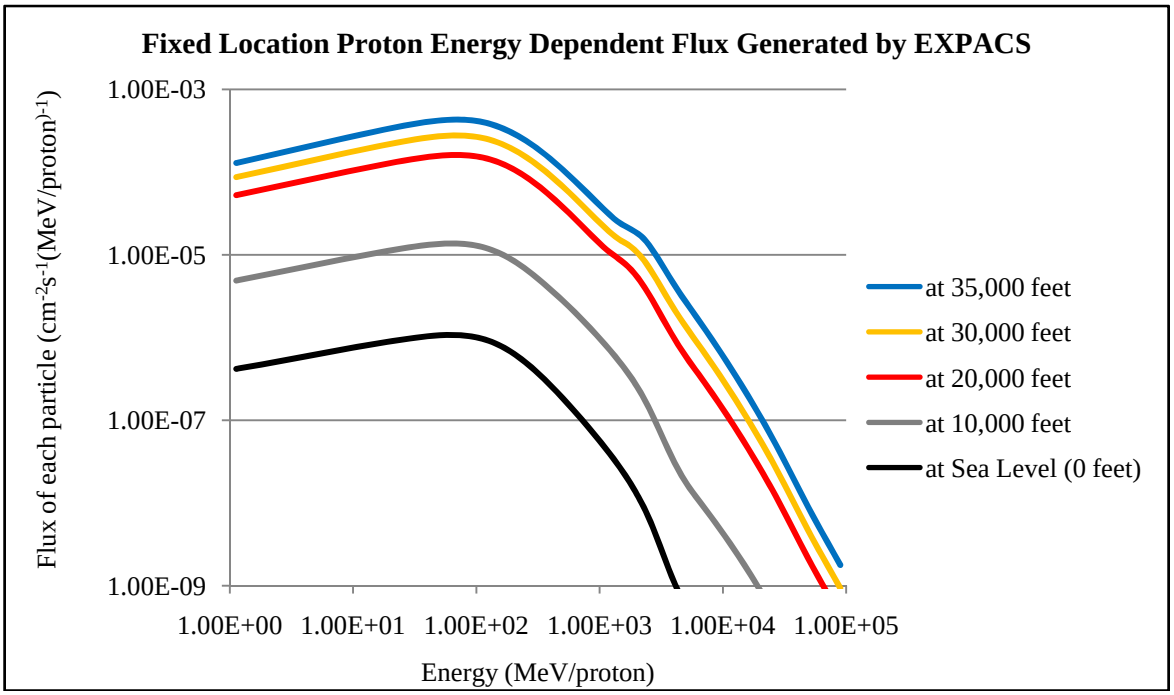

Figure G.1 – Proton Energy Dependent Flux from 35,000 feet to Sea Level, Calculated by EXPACS

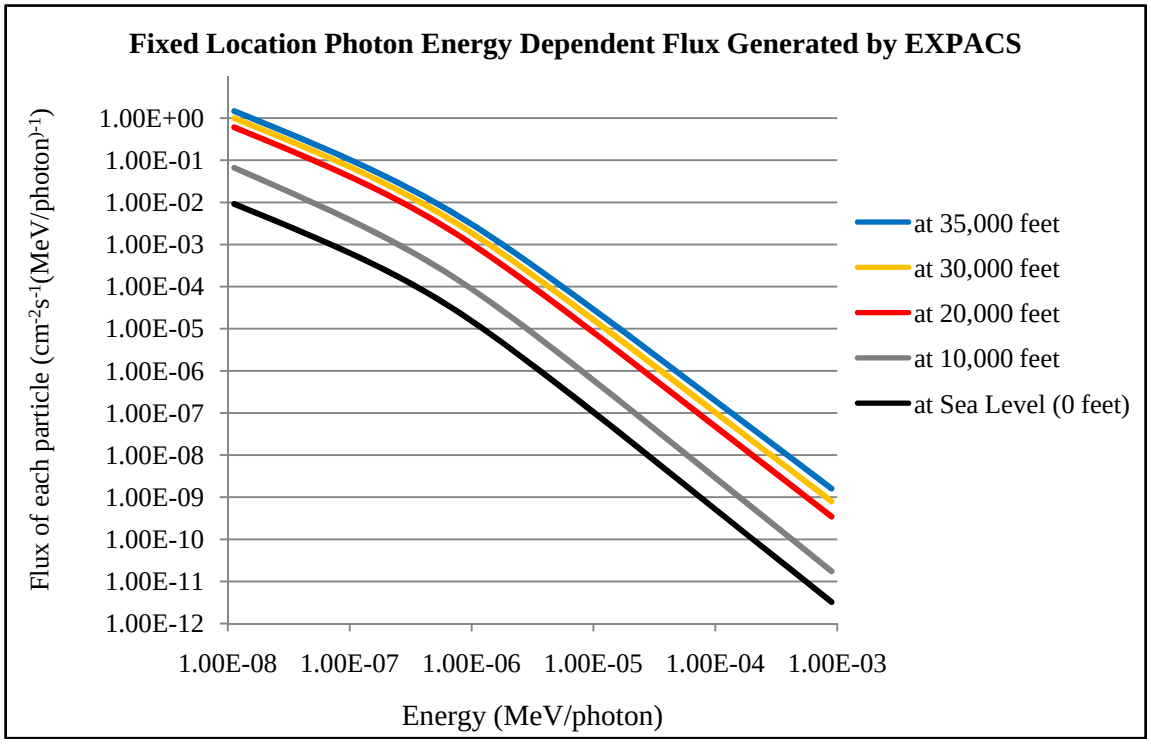

Figure G.2 – Photon Energy Dependent Flux at Various Altitudes

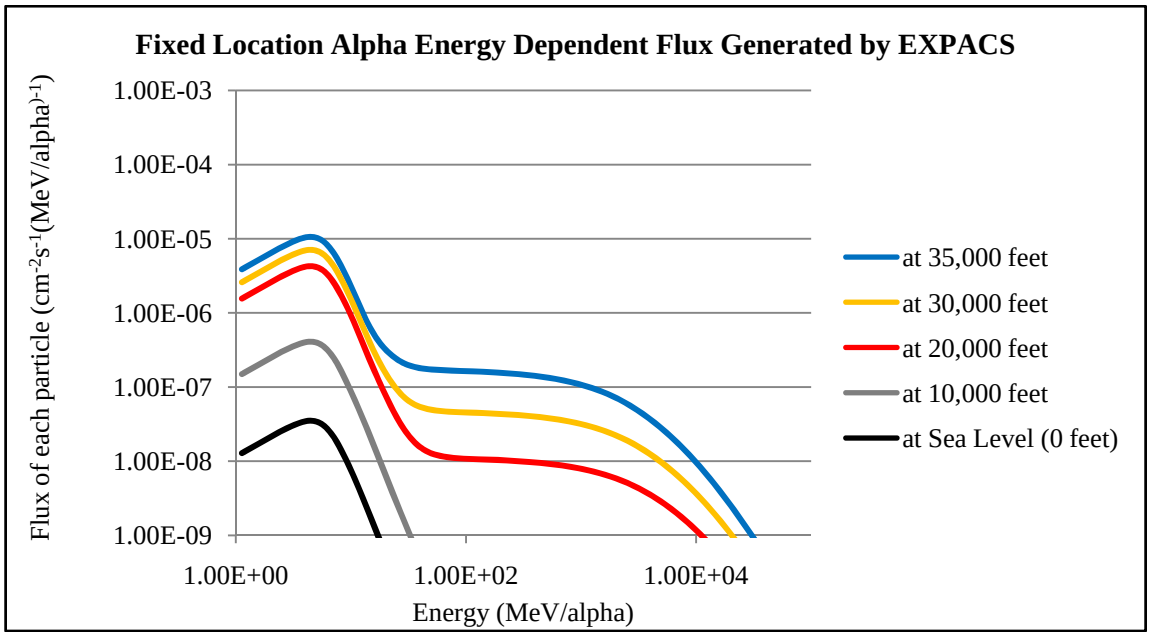

Figure G.3 – Alpha Energy Dependent Flux at Various Altitudes

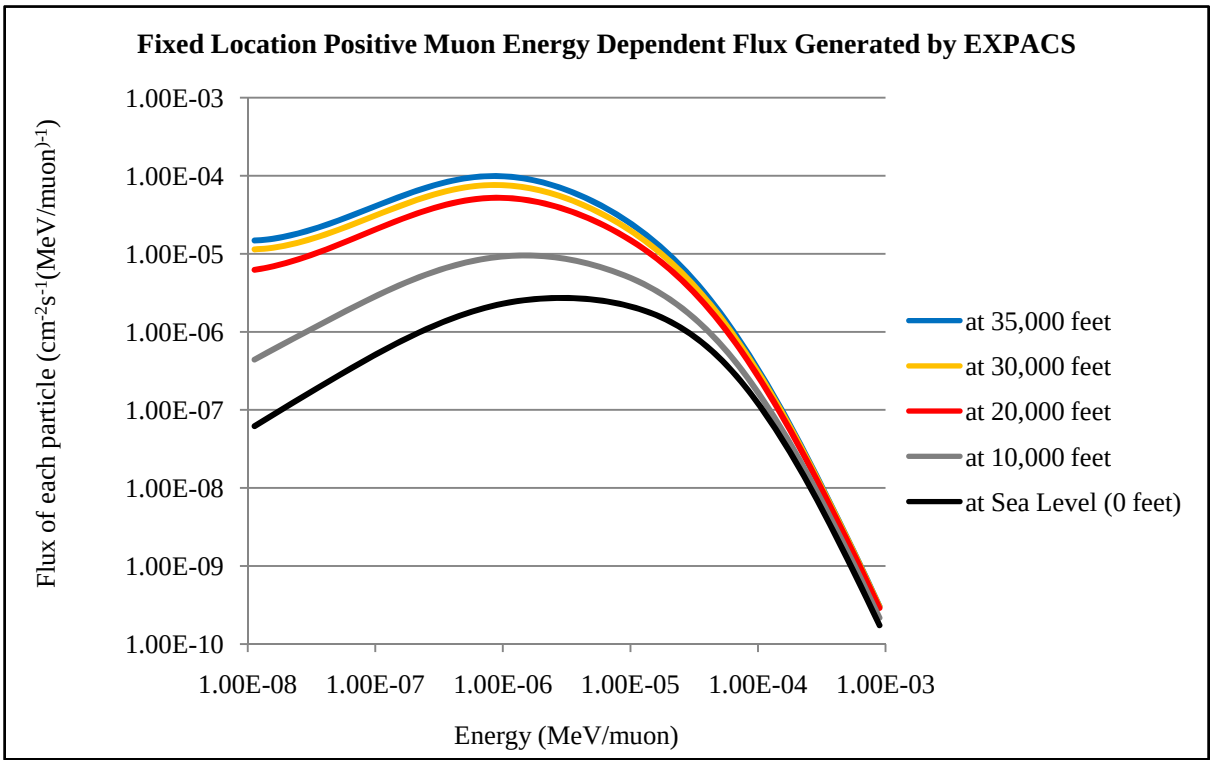

Figure G.4 – Positive Muon Energy Dependent Flux at Various Altitudes

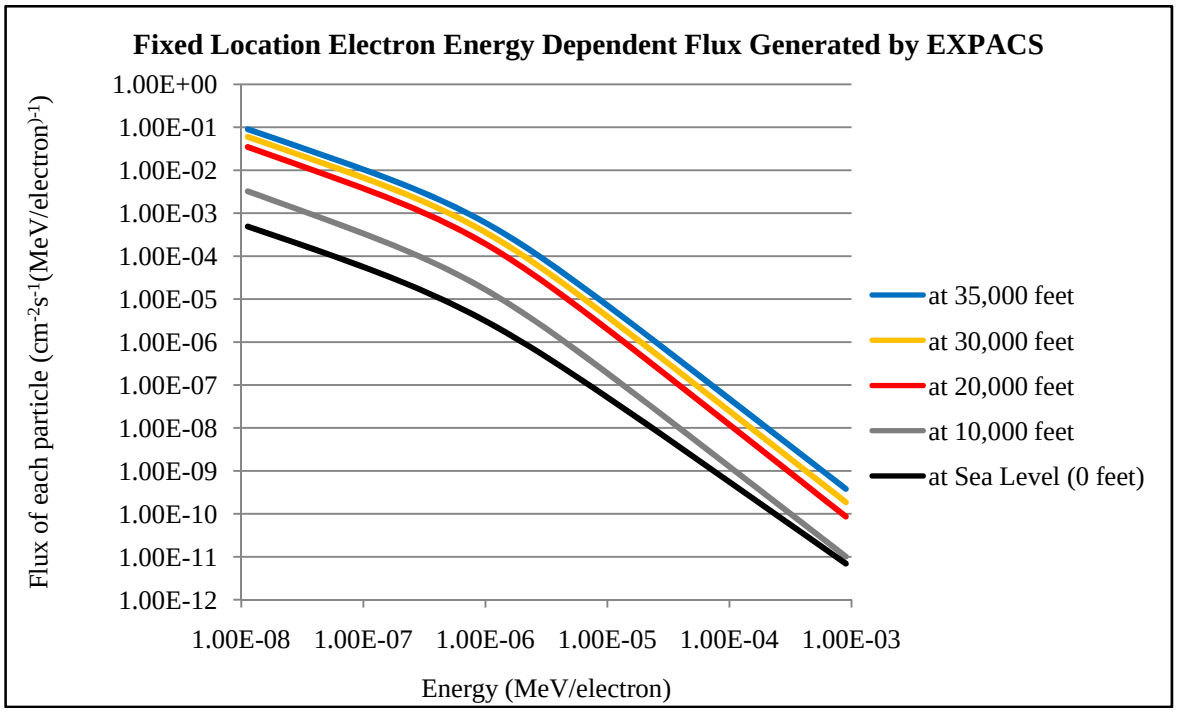

Figure G.5 – Electron Energy Dependent Flux at Various Altitudes